Utrecht University | Deltares

Modelling mud-induced wave damping with Delft3D and SWAN-Mud

A test case at the coast of Suriname

Master thesis

B.M.C Loef

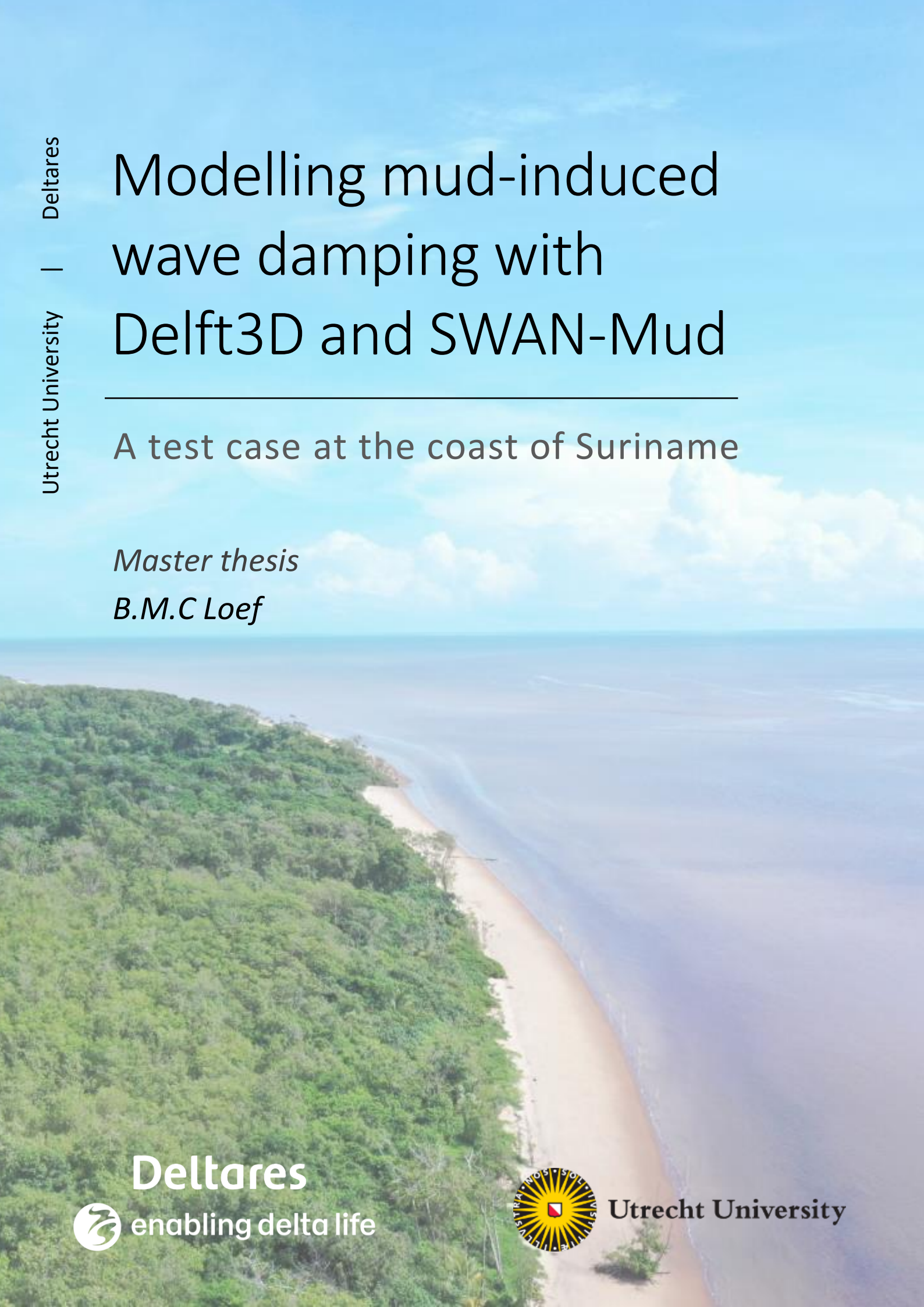

Deltares
enabling delta life

Utrecht University

Modelling mud-induced wave damping with Delft3D and SWAN-Mud

A test case at the coast of Suriname

Bram Martinus Cornelis Loef

5703875

To obtain the degree of Master of Science at the Faculty of Geoscience,

Utrecht University

Supervised by:
Prof. Dr. B.G. Ruessink[1]
B.P. Smits MSc.[2]
Prof. Dr. S.M. de Jong[3]
Prof. Dr. H.E. de Swart[4]

Utrecht University
Department of Physical Geography[1,3]
Institute of Marine and Atmospheric Science, Utrecht[4]

Deltares[2]
Sediment dynamics and ecosystems
Coastal and marine environment

Date:
13-06-2022

Abstract

Fluid mud is suspended cohesive sediment on top of the consolidated bed. The fluid mud is generated by an external force that liquefies the bed sediment. When the water in the overlying layer is in motion, it experiences energy dissipation due to the fluid mud. A large decrease in significant wave height was observed in field experiments for beaches with fluid mud compared to beaches without this mud (Wells & Coleman, 1981). Often this fluid mud forms mudbanks in front of a shore, alternating with areas without mud, the interbank area. These mudbanks are found, for example, in front of the coast of India or on the north coast of South America. This study aims to learn more about mud-induced wave damping as a function of mud and wave characteristics. To reach this aim, various idealized model simulations were set up in which mud and wave characteristics were varied in 1D and 2D; the model was then applied to a case study on the Suriname coast. SWAN-Mud is combined with Delft3D-Wave, an application from Deltares that works around SWAN-Mud and improves the model's usability for more extensive and complicated experiments. Different formulations for dissipation of wave energy due to fluid mud are implemented in the model SWAN-Mud, but experience with these formulations in real-life test cases is limited.

At the onset of this study, we corrected an error in the dispersion relationships embedded in SWAN-Mud. Furthermore, different bugs in the source code have been restored, which improved the model. For the DeWit method, a dissipation term had to be included in SWAN-Mud. In order to test different mud characteristics, experiments for a 1D setting (transects) were performed, based on Kranenburg (2008). A 2D experiment with an idealized mudbank was conducted for different wave heights, periods, and directions at the domain's boundaries and different wind speeds and directions. The same wave characteristics have been tested for the Suriname experiments as in the 2D experiments. These wave and wind characteristics were based on the ERA-5 model data set, representing summer, winter, and storm conditions. However, more practical scenarios have been conducted to find accurate results. For the wave environment, only one parameter, e.g., direction, was changed in these scenarios.

After updating SWAN-Mud, results for the imaginary wavenumber (which measures the rate at which wave height exponentially decreases when the wave propagates through the domain.) correspond to analytical solutions of the dispersion relationships. With the updated model, we could observe the influence of the mudbanks on the incoming waves. Mud dissipation is highest for the waves with the largest wave height. However, a minimal wave period seems necessary for dissipation to happen. Compared to the scenarios without mud, the significant wave height is much smaller when the waves reach the shore. This implies that without these mudbanks, the coast is much more exposed to wave forcing and, e.g. erosion of the coast is more severe. The mud does not only dissipate waves with larger wave periods. Measuring the wave spectra over the mudbanks revealed that the mud dissipates a fraction of high-frequency wind waves generated in the domain. However, a large part of the high-frequency waves still reaches the shore. Nevertheless, the exact morphodynamics and hydrodynamics on and around the mudbanks remain unclear. The influence of the mudbanks on the wave environment and so the coastal morphodynamics is huge. The mudbanks play an essential role in protecting the hinterland of the mudbanks and are related to areas of coastal accretion. In contrast, the interbank areas are related to coastal erosion due to the high waves reaching the shore.

Acknowledgements

Just before the start of my thesis, a major ankle operation put me in a wheelchair for almost two months, followed by two months bound to crutches. This, combined with my master's thesis, was probably the hardest challenge I have ever faced physically and mentally. For this, I would like to thank my family, especially my parents and my little brother Sem for taking care of me. They always made sure I could eat, wash or go to the toilet and made sure I was always able to study. Equal gratitude goes out to my friends, especially Lard, Jesse and the Thomasses, who always made sure I was not alone and were there to have a coffee, lunch or talk during these hard times. All of them made sure I was able to study or even drove me to the Deltares office.

At first, having four supervisors made me nervous as the knowledge in this group of supervisors is impeccable. However, their enthusiasm about the topic and about their own research was something that motivated me. After every meeting, I felt re-energized and ready to take on every challenge. I want to thank all of them separately! Bob, as my daily supervisor, we had much contact, and you always motivated me to get the best out of the project. You always responded enthusiastically, which must have tested your patience as I often asked the obvious questions. Also, you encouraged me to come to the office and meet many new people, trying to make the most out of the COVID situation. Gerben, you were always friendly but had sharp and constructive feedback during our meetings, ensuring every part of my thesis was of essence. I have never been more enthusiastic about a country I have never been to, and this was because of the unlimited enthusiasm of Steven, inviting me for meetings with the Suriname group and was always ready for a talk. Thank you, Gerben and Steven, for being my first two supervisors. Whenever I had problems with the physics in the models or mathematical problems, that felt way out of my league. Huib, you were always happy to help and always responded in a way that helped me out of the problems. So again, I want to thank the four of you for the best supervision I could ever have wished for.

I want to thank Job for all the brainstorming sessions and discussions and for sharing his knowledge about Suriname. Lars, thank you for your help with the Suriname datasets. Joren and Tim were always ready to help with a quick word of advice or some feedback. Furthermore, I would like to thank Qinghua and Bert from Deltares for helping me with the software and debugging. Lastly, I want to thank my study friends and flat mates for the small talk during long study days.

Bram Loef

"Follow your heart, but take your brain with you." – ***2pac Shakur***

Table of Contents

Table of Symbols

Symbol	Description	Unit
H_{w0}	Equilibrium height of water layer	m
H_{m0}	Equilibrium height of mud layer	m
H_{tot0}	Equilibrium height of total system	m
h_w	Height of the water layer	m
h_m	Height of the mud layer	m
h_{tot}	Height of the total system	m
ζ	Displacement of the water surface	m
a	Amplitude of the water surface displacement	m
φ	Phase difference between surface and intersurface displacement	rad
φ'	Phase angle between surface and internal wave	rad
ξ_0	(complex) amplitude of interface displacement m,	m,rad
ξ	Displacement of interface (ref. = eq.)	m
b	Amplitude of interface	m
ρ	Density of water	kg/m^3
ρ	Density of mud	kg/m^3
υ_w	Kinematic viscosity of water	m^2/s
υ_m	Kinematic viscosity of mud	m^2/s
u	Horizontal velocity in x-direction	m/s
w	Vertical velocity in z-direction	m/s
z	Axis in vertical direction, up is positive	
p	Pressure	N/m^2
ω	Wave (angular) frequency ($2\pi/T$)	rad/s
k	Wavenumber	rad/m
k_i	Imaginary part wavenumber	
k_r	Real part wavenumber	rad/m
k_{nm}	Wavenumber when no mud	rad/m
k_c	Complex wavenumber	
H_{sig}	Significant wave height	m
T_p	Peak wave period	s
Dir	Wave direction	degrees
S_i	Dissipation by i	W/m^2
τ	Shear stress	N/m^2
E	Energy	Nm
g	Gravitational acceleration	m/s^2

List of figures and tables

Figures

Tables

LIST OF ABBREVIATIONS

SWAN = Simulating WAves Nearshore

HCMS = High Concentrated Mud Suspension

A-O = Amazon-Orinocco

SPM = Suspended Particle Matter

ITCZ = Intertropical Convergence Zone

1 Introduction

1.1 Introduction

The thought of going to the beach for most will steer towards sun, blue water and coarse sand they can feel between their toes and disregard their muddy variant altogether. Muddy beaches, however provide a plethora of benefits on their own. Muddy beaches are the most abundant type of coastline in the tropics (Toornman et al, 2018). Due to low wave energy affecting tropical coasts, the fine sediments from large rivers are stored in these areas. These mud-rich coastlines provide fruitful areas for the local populations because the shrimp farms thrive on the gentle sloping and vegetation-rich coast. Additionally, the timber from mangroves is also suitable as construction material. The mangrove vegetation helps protecting the coast from flooding due to its buffer function (Borsje, 2019) and its capability to trap sediment. When these muddy ecosystems are healthy, they create positive feedback loops that enhance their resilience. The mudflats, mudbanks and saltmarshes that are formed in front of the coast enable additional flora and fauna to thrive in the intertidal zone. Furthermore, salt marches and mangroves can capture large amounts of CO_2 (Temmink et al., 2022). Nevertheless, these flat, low-lying areas are susceptible to coastal erosion and flooding due to consolidation and rising sea levels. The accumulations of mud in front of the coast can reach up to tens of kilometers in length and width (see Figure 1.1)

Figure 1.1: An image of the mud rich coastline of Suriname with the edge of the mud visible in the right corner. (Image by Job de Vries, 2019)

The mud is accumulated in large sized mudbanks that are separated by areas without mud (the interbank area). The presence of these large mud accumulations in front of the coast has a large influence on the alongshore variability of the wave environment. It is known that mudbanks protect the hinterland as the incoming waves are damped by the mud (Augustinus, 2004). The interbank area where mud is absent is associated with coastal erosion as the waves can travel relatively freely towards the shore. Figure 1.2 illustrates how waves without mud(the clear water) can reach the shore and break, while the muddy water on the left does not show any wave breaking as the waves are damped before they reach the shore. A study by Wells & Kemp (1986) found that 96% of the wave energy was absorbed over 15 km of incoming waves at a mudbank in Suriname. It is known that waves with a more considerable wave period are subject

to more energy dissipation than waves with short periods (Winterwerp et al., 2012). In studies by Sheremet & Stone (2003) and Sheremet et al. (2011) conducted at Atchafalaya Bay in Louisiana, two field sites with different sediment sizes were compared. These sites have a very similar wind climate and wave conditions. For average wind and wave conditions, wave height at the beach with muddy sediments was 70 percent smaller than for the beach with sandy sediments. A later study found a difference of 50 percent under stormy conditions at the same field site (Winterwerp et al., 2007; 2012).

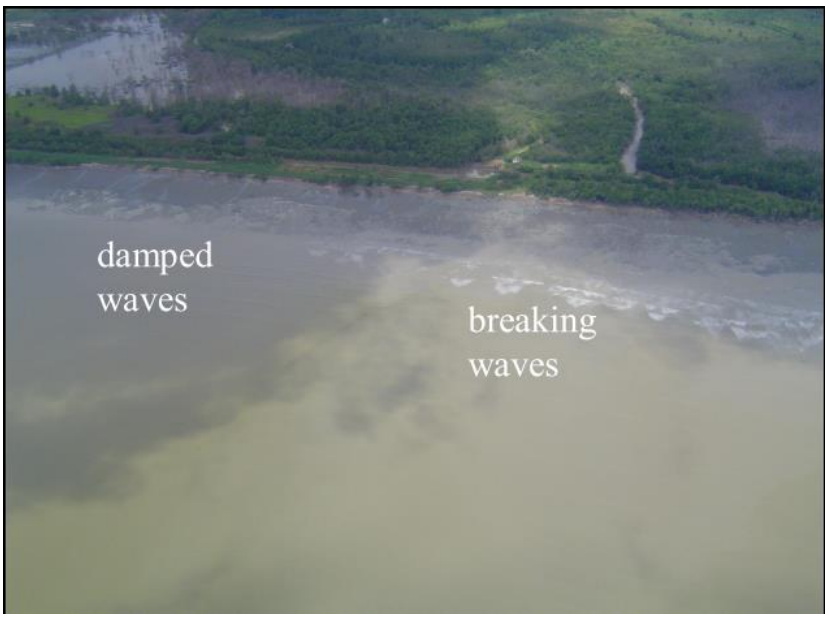

Figure 1.2: An image of the coast at Demara, Suriname. Here is visible how waves are breaking in the clear water. The muddy water does not show any wave breaking due to the damping of the waves (Kranenburg, 2008).

These mudbanks show great variation in concentration, thickness and consistency over the whole bank. Some parts of the mudbank are consolidated, while other parts of the mudbank are in fluid state and in suspension (Chevalier et al., 2008). This mud becomes suspended due to wave forcing or currents flowing over the mudbank. When the concentration of mud in the water column becomes very high, the mud forms a slurry-like layer above the bed. When the mud is in this state, it is referred to as “Fluid Mud” (Winterwerp et al., 2022). However, only parts of the mudbanks become fluidized as this process, as well as suspending the mud, requires constant energy input. Without constant force, the mud will settle again. This causes high variability in mudbank size and thickness. Due to the spatial variability in mud characteristics, it is very complicated to measure and quantify the magnitude of these mudbanks. The mudbanks significantly influence the wave environment and, hence the coast, as the incoming wave energy is damped in an alongshore variable fashion.

When the mud becomes “fluid mud,” the energy input by waves causes an internal wave at the interface between the water and mud layer (Winterwerp et al., 2007;). The thickness of this fluid mud layer depends on the history of sediment input and wave history (Winterwerp et al., 2007). Following Ross et al.(1989), the fluid mud has densities ranging from 10 to 300 g/L, but it is highly variable and shows different consolidation states. This fluid mud behaves like a very dense slurry, capable of absorbing incoming wave energy (Anthony et al., 2010). Mud being present in a water column influences the dissipation of wave energy on the mudbanks. This

energy dissipation is called wave damping or, because the mud triggers it, mud-induced wave damping (Winterwerp et al., 2012). The mud itself has characteristics that influence the energy damping. These mud-layer characteristics have different effects on the energy dissipation of the mud layer. Some of these characteristics are, e.g., the mud's viscosity, the density of the mud and the water, the fluid mud layer's thickness, and its mud concentration (Beyramzade & Siadatmousavi, 2018). Zhao et al. (2006) and Traykovski et al. (2015) conducted different small-scale laboratory experiments, which showed that these parameters influence the dissipation by the mud. These studies were able to find the effects of mud viscosity and density on the rate of dissipation and on their effect on the thickness of the mud layer in small-scale laboratory experiments. However, knowledge about the interaction of these different mud characteristics in numerical models is still limited. Knowing how mud dissipation responds to different mud characteristics is of high importance as the mud dissipation rate is greatly influenced by these characteristics (Traykovski et al., 2015). In the absence of effect reproducibility, the modelling of realistic case studies remains unreliable.

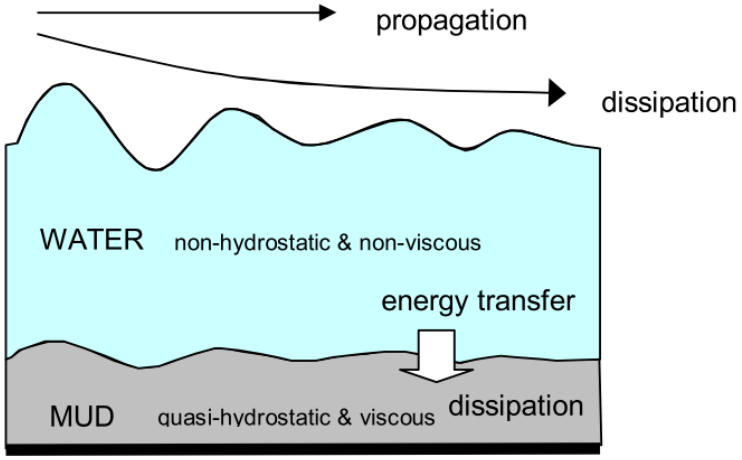

Figure 1.3: A sketch of the fluid mud layer with the overlying waterlayer. The transfer of energy is indicated with the arrow while the waves dissipate (Kranenburg, 2008).

The significance of fluidized mud in coastal and estuarine zones has been a topic of research for decades, which started with research into mudflow followed by mud transport by wave-induced forcing and has been an exasperating topic since then (Einstein 1941; Inglis & Allen 1957; Owen 1976; Nichols 1984-1985). Modelling the energy damping by mud has been an ongoing research topic since Gade derived a dispersion relationship in 1958. This dispersion relationship is necessary as the standard shallow water equation was not applicable due to the complex behavior of the mud. The dispersion relation is combined with an energy dissipation balance to calculate the mud-induced wave damping. After Gade, multiple researchers have attempted to make the most complete and the least limiting model. The work from Gade was reproduced and further improved by De Wit (1995). Followed by the likes of Kranenburg (2008) and Guo (2002). This thesis will discuss four of them (including Gade). Winterwerp et al. (2007, 2012). researched muddy coasts and their interaction with mud. His work was one of the first modelling studies of the fluid mud and was further developed by Beyramzade & Siadatmousavi (2018). The amount of studies focusing on mud-wave interactions however remains minimal. Because of the limited experiments with fluid mud, the exact response of waves over a layer of fluid mud is not exactly known. Only a few experiments by Gade (1958)

and Ng (2000) were used to test their dispersion relation. However, there is a limited amount of experiments that test the interaction between different wave environments and the fluid mud. There is limited knowledge about the effect of different wave characteristics on the rate of the dissipation. Neither is there much experience with modelling this. It is important to have knowledge about the wave environments and their interaction with fluid mud before the model could be applied on a realistic case study.

Research is limited to small idealized test cases and reproductions of measurements. Modelling studies with fluid mud are limited to small and simplified reproductions of laboratory experiments as computations with fluid mud are very complicated. Especially attempts to reproduce realistic scenarios have been unsuccessful. This impairment for modelling was mitigated through the wave energy calculation in SWAN, Different dispersion relations are included in SWAN-Mud, which is used in this thesis. SWAN is a state-of-the-art third-generation, and two-dimensional spectral model which is designed to model wave propagation. SWAN-Mud can predict the mud-wave interaction and was used in previous research by Winterwerp et al.(2007), who looked at the coast of French Guyana, a neighbor of Suriname and used the SWAN-Mud model to reproduce the field measurements from Wells & Coleman (1981). Siadatmousavi et al. (2012) and Beyramzade & Siadatmousavi (2018) used SWAN-Mud as well and tested it on realistic case studies, however this was done without any field measurements. Besides these studies, the knowledge of modelling mud-induced wave damping with SWAN-Mud and successful reproductions of realistic case-studies remain sparse.

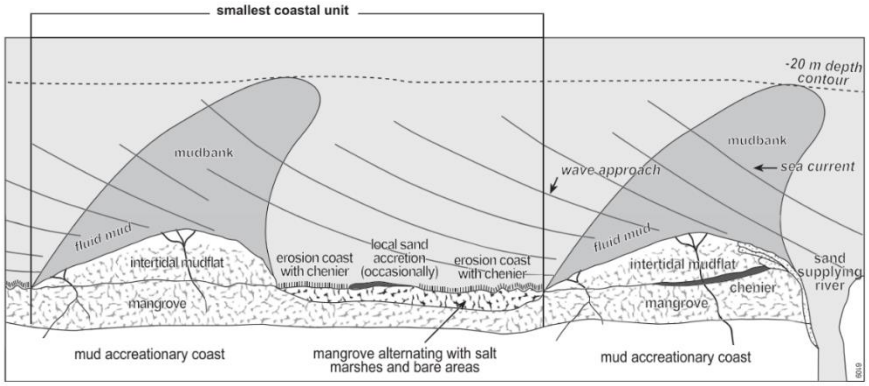

Figure 1.4: A sketched map by Augustinus (2004) of the coastal system for the coast of Suriname including intertidal areas, interbank areas and the mudbanks

For this Master's thesis, a test case is conducted at the Suriname coastline. The coast of Suriname is influenced by a large sediment influx of fine-grained mud originating from the Amazon into the North Atlantic Ocean. These large volumes of sediments, up to 13×10^8 m^3yr^{-1} (Anthony et al., 2010), are transported alongshore from the Amazon delta to the northwest (Tzampazidou, 2020). This sediment transport is driven by a combination of currents generated by the obliquely incident waves and the Guiana current. These large mudbanks form a buffer for the coastline and protect the coastline by mud-induced wave damping (Anthony et al., 2010). The buffer function of the mudbanks against coastal erosion also forms a safe location for mangroves to grow in the low-energy environment. A lot has been written about Suriname and the unique coastline of the Guianas. Augustinus (2004) pioneered research on the Guiana coastline, focusing mainly on the Surinamese coast. Augustinus sketched the mudbank system of Suriname in (Figure 1.4). In this figure is the shape of the mudbank given. This shape is characteristic for the Suriname coast with a gentle sloping edge facing the incoming waves and

a steep edge on the lee side of the mudbank. Nowadays, studies in French Guiana are becoming more abundant, although these studies are more into measuring and calculating the role of trade winds or river input on the mudbanks trajectory and magnitude (Gratiot et al., 2007; Antony et al., 2008). It is also known that these mudbanks migrate alongshore, causing periods of erosion and periods of accretion. However, the exact processes driving this migration are not known. Winterwerp et al. (2022) hypothesizes that this migration is event-driven. Research in Suriname has not been successful yet in quantifying the exact rheology and size of the mudbanks.

1.2 Research questions & Objectives

1.2.1 Research Questions

The overarching aim of this thesis is to learn more about the processes involved in the mud-induced wave damping and to gain expertise about modelling the dissipation of waves by the mud. This is done with the support of two main research questions. Subsequently, these two main research questions have been defined in order to learn more about the modelling of the mud-induced wave damping with Delft3D-Wave and SWAN-Mud. This study is supported by a case study for the coast of Suriname. For this case study, different objectives have been constructed to maintain relevance to the actual situation in Suriname. At the onset of the study, some problems were found in SWAN-Mud and the coupling with Delft3D-Wave. Hence, debugging the model became an objective of this study. The test case and the debugging objectives are introduced in this chapter after introducing the research questions.

Which characteristics of the "fluid mud" are most important for the mud-induced wave damping and why?

The dissipation by fluid mud depends on several mud characteristics. In SWAN-Mud, the mud is homogeneous and static and depends only on four parameters; water depth, mud thickness, mud density and viscosity. The characteristics that can be varied for all grid cells are the water depth and the mud layer thickness. The viscosity and density of the mud layer are constant over the mudbank. The influence of these characteristics on the dissipation rate of the waves by the fluid mud is tested with an idealized 1D experiment. This is done in the stand-alone version of SWAN-Mud without the coupled Delft3D-Wave.

What is the influence of the wave environment on the mud-induced wave damping?

After we learn more about the characteristics of the mud and their effect on wave damping, the focus will be on how wave height, period and angle of these incoming waves influence the mud-induced wave damping. Different scenarios are tested: first, a sensitivity analysis is performed for these wave parameters. Furthermore, different angles of incidence of the waves are tested. The influence of the wind is also part of these scenarios as they it influences the waves by frequency shifts and wave growth. This will be done in idealized 2D experiments, and these will be explained in the method section. The experiments related to this research question are done with Delft3D-Wave

1.2.2 Test Case: Suriname

After answering the main research questions, SWAN-Mud and Delft3D-Wave will be used in a more realistic case study to test the model in more complicated situations. The Suriname coastline will as a test case. Objectives were set up for the Suriname test case to apply the model on realistic scenarios to test and learn more about the influence of the mud-wave interaction on the coast of Suriname. More information about the Suriname coastline is provided in Section 2.3.

Experience with modelling is limited for the coast of Suriname, while the coast is an excellent example of a coastline that is heavily influenced by mud dynamics. The case study will be divided into different research objectives, the results of which will be compared to the results of the more idealized experiments. The influence of the mudbanks on the incoming waves is investigated for the three main scenarios, summer, winter, and winter storms. Furthermore, the influence of different wave environments on mud dissipation is tested, as well as the influence of local winds during summer on the dissipation rate. Lastly, the effect of different wave incidence angles is studied for winter storms.

1.2.3 Other Objectives

In Tzampazidou's study (2020), a couple of problems regarding SWAN-Mud and Delft3D-Wave were encountered. As her thesis was a prequel to this study, these problems had to be solved first. These problems were caused by incongruencies in SWAN-Mud and the communication between SWAN-Mud and Delft3D-Wave. Solving these bugs became a necessity for this thesis at the onset. The DeWit method did not give any energy dissipation outcome in SWAN-Mud. However, it did calculate a wavenumber with both an imaginary and a real part which implied a bug in the dissipation term. This problem was solved during this thesis, which is explained in Subsection 2.2.3 as part of the explanation of the DeWit method. Furthermore, Tzampazidou(2020) concluded that there are errors in the dispersion relationships of DELFT and DeWit, which are included in SWAN-Mud. The debugging steps are included in the methods and results of this study. Another observation by Tzampazidou was that the Ng method did not work for any 2D scenarios. This is not documented in this study, although the problem was solved. More importantly, the interaction between the SWAN-Mud and Delft3D-Wave models was previously not yet developed. The software department of Deltares developed the communication between the models before the start of this thesis. The interaction between these two models was tested and improved at the start of the thesis. This was an ongoing process while writing this thesis.

2 Materials and Methods

2.1 Mud-induced wave damping

2.1.1 Fluid Mud

Mud is defined as a mixture of water, soil, and often a high percentage of organic matter, but still in a consolidated state. The sediment particles are mostly smaller than 63μm and are classified as clay or silt. These clay particles apply electro-chemical forces when they interact in aqueous ecosystems (De Wit & Kranenburg, 1996). The sediment particles are cohesive, and when they collide, they will form flocs when the attractive forces are strong enough to form bonds, a process called aggregation (Geyer et al., 2004). The formation of flocs influences the settling velocity of the sediment in the water column in both a positive as negative matter. In the early stages, the flocs are heavier and cause an increase in settling velocity. Over time, when the flocs become more significant and the concentration of the suspension increases, the flocs start to hamper other particles, and the settling velocity drops (Figure 2.1). In essence, fluid mud is a suspension with a high concentration of these flocs (McAnally et al., 2007). The interface between the waterlayer and the zone where the settling of particles is hindered is marked by a substantial surge in density. This interface is defined as the lutocline (Van Prooijen et al., 2017); the lutocline and the fluid mud are shown in Figure 2.1. In this figure, it is visible that the transition between the cohesive bed and the fluid mud in terms of concentrations (the top X-axis) is rather diffuse instead of a fast shift. Above the fluid mud, it is visible that the concentration drops, but sediment remains in suspension. When the highly concentrated suspension is not under pressure, consolidation will occur. A bed will form when the water drains out between the particles, and the mud skeleton starts to carry the weight (Van Prooijen et al., 2017).

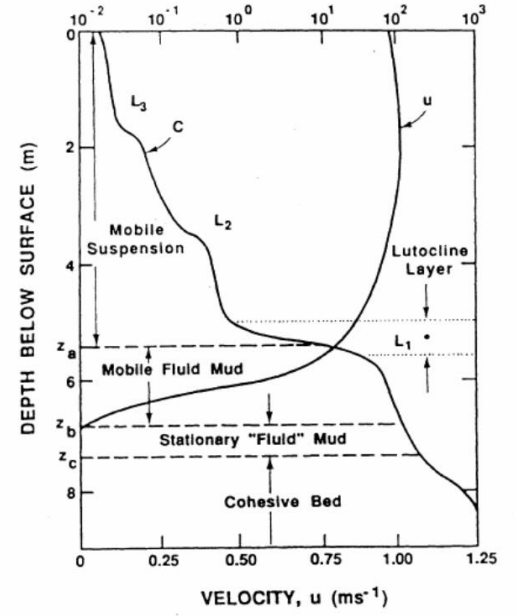

Figure 2.1: Typical concentrations of the water depth and the velocity in very concentrated environments. Indicating the different layers in the water column including the Lutocline and the fluid mud. (Ross and Metha, 1989).

The definition of "fluid mud" has a broad range of variations in the literature. The most common definition of fluid mud is from Winterwerp et al. (2019), who states that fluid mud is: *'a suspension or mixture of cohesive sediment at a concentration point around or larger than the gelling point'*. The sediment concentrations corresponding to this point differ between 10 and 100 g/L (Borsje, 2019). Fluid mud is often stationary and easily mobilized. This is caused by the minimal effective stresses that are often neglected, resulting in non-Newtonian behaviour of the fluid mud (Borsje, 2019). Effective stress is the total stress minus the pore pressure (Lade & De Boer, 1997). Fluid mud is generated by hydrodynamic forcing, for example, waves flowing over a mud bed or a turbulent current from a tidal inlet (Mehta, 1991). These forces that work on the cohesive bed break the bonds between the particles of the upper layer of the bottom and stir the particles into the water column (Doyle, 1973). The location of the fluid mud in the column is visible in Figure 2.2.

Experiments in the field and laboratory experiments observed that waves have the strength to weaken the strong, cohesive bonds in the muddy sediments of the bottom, which results in the formation of a fluid layer above the bed (Ross, 1988; Sakakiyama & Bijker, 1989; Mathew & Baba, 1995). This is a process regarded as liquefaction in literature (De Wit & Kranenburg, 1997). Research by Maa (1986) concluded that the flow-induced pore water pressure induces the liquefaction of the cohesive sediments. Wave-induced liquefaction reduces the effective stress in the bed, and, as the total stress does not change, the porewater pressure increases. Ross (1988) was one of the first researchers who measured these stresses. In his tests, it was observed that liquefaction does not appreciably change the sediment concentration. However, further research into liquefaction is limited. Another process able to liquefy the bottom is fluidization, which is the process of water being pressured into the soil (Maa and Mehta, 1990). The fluid mud can only be stable when an external energy force works on the layer. Often this force is represented as wave energy or horizontal currents (Borsje, 2019). If this energy source is absent, the cohesive sediment will settle on the bottom of the water column and consolidate. Ross (1988) noted that only a small horizontal current is necessary to create horizontal fluid mud transport.

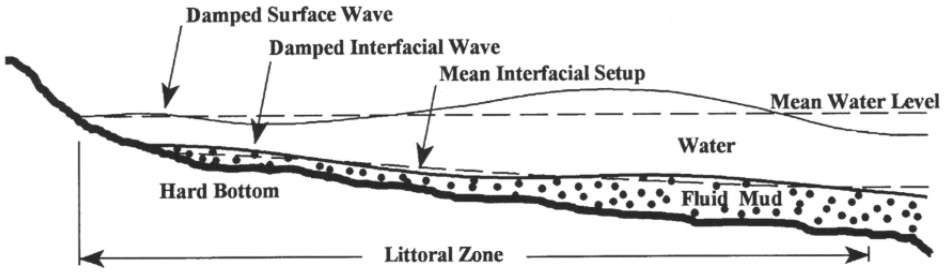

Figure 2.2: A schematic overview of how fluid mud is positioned in the water column with the overlying waterlayer, the hard bottom and the interface (Rodriguez and Mehta, 2001)

McAnally (2007) summarizes the formation of fluid mud in his study, where he assumes the primary process involved is liquefaction, as described above. In this explanation, the force causing liquefaction is assumed to be wave energy. Waves flowing over the bed induce a pressure gradient in the pores of the cohesive bed; this causes a flow of the pore fluid. As a result will the wave-averaged pore pressure built up over this period, while the wave-average effective normal stress in the cohesive bed sediment drops towards zero. When this pore pressure becomes zero, the bottom is fluidized. Fluidized means that the aggregates of the soil are broken, and instead of grain-supported, the sediment becomes fluid-supported. As a result,

the increased pore pressure destroys the soil matrix. The response of the bed is elastic, which means that the liquefaction is reversible. Over time the bed shows plastic behaviour, which means that the soil will not return to its original state. Deposition of sediment can form fluid mud as well, but only when the settling rate of the sediment is slower than its consolidation rate. Local hydrodynamic conditions influence the formation of the fluid mud (Maa and Mehta, 1990). If the local energy is too high, either the sediment flocs cannot settle, or they will be washed away straight after settling. Therefore, fluid mud formation features in lower energy areas, for example, harbours or lagoons (Winterwerp et al., 2012). However, these phenomena are also observed in open water environments like the Suriname coastline (Winterwerp et al., 2020). In this situation, fluid mud occurs when the orbital motion of waves causes a shear flow that is strong enough to erode the top layer of the mud on the seabed. A progression that will endure until the saturation point is touched and surpassed by the large amount of sediment stirred into the column (Borsje, 2019). The fluid mud layer forms on top of the bed deposition in this case. Due to the cohesive behaviour of the mud, the sediment will try to stay together and stay in one layer.

2.1.2 Mud dissipation

As stated before, the fluid mud dissipates wave energy. The rate of this energy dissipation depends most on the characteristics of the mud (Suhayda, 1984), and on the phase and amplitude difference between the wave at the water surface and the wave at the interface (see Figure 2.2). Energy is dissipated when energy is exchanged from the water layer into the mud layer, and a wave at the interface is created (Maa & Mehta, 1990). This process is influenced by many factors, such as the density difference between the layers, the difference in phase of the water surface and the interface (the top of the mud layer), and differences in wavelength and viscosity (Winterwerp et al., 2012). This energy transfer induces an internal wave at the interface. Meanwhile, inside the mud layer is a viscous energy transfer is created, as this mud layer has high viscosity (Traykovski et al., 2015). These energy transfers result in the damping of the waves at the water surface. Field experiments have shown the impact of fluid mud on the significant wave height (Jaramillo et al., 2009; Rogers and Holland, 2009; Traykovski et al., 2015; Winterwerp et al., 2007). Although the change of wave height at the water surface is easy to measure, the height of the internal waves at the interface is difficult to quantify. This process is sketched in Figure 2.3; for further detailed explanation of the phase difference between the free surface and the interface and the amplitude of the interface, see Appendix B. A more elaborate description of Figure 2.3 and the supporting physics can be found in Deng et al.(2017) as mud-wave calculations are a complicated topic, and most of the involved equations are out of the scope of this thesis.

Jaramillo et al. (2009) and Traykovski et al. (2015) measured the height of the lutocline and the movement of the interface waves using acoustic backscatter. Traykovski et al. (2015) measured the velocities in the fluid mud layer. They found internal waves with an amplitude between 1 and 10 cm and orbital velocities in the order of 0.1 m/s in the mud layer. Winterwerp et al. (2012) hypothesized that most wave damping occurs just after high wave events. This is when the sediment stirred into the column starts to settle into a mud layer. In the same study,

Winterwerp et al. (2012) found that most of the energy dissipation by the mud happens in lower frequency waves.

All these different factors are included in mud dissipations models, which generally contain a dispersion relationship to define the wavenumber (both imaginary and real) and an energy dissipation equation to define the mud dissipation. A new dispersion relation is necessary as the standard shallow water equations are not applicable anymore due to the second layer. An elaborated explanation of the different models and methods used in this thesis is explained the following sections, however, the fluid mud plays an important role in the formation of mudbanks and their dynamics. This is first explained in the next subsection.

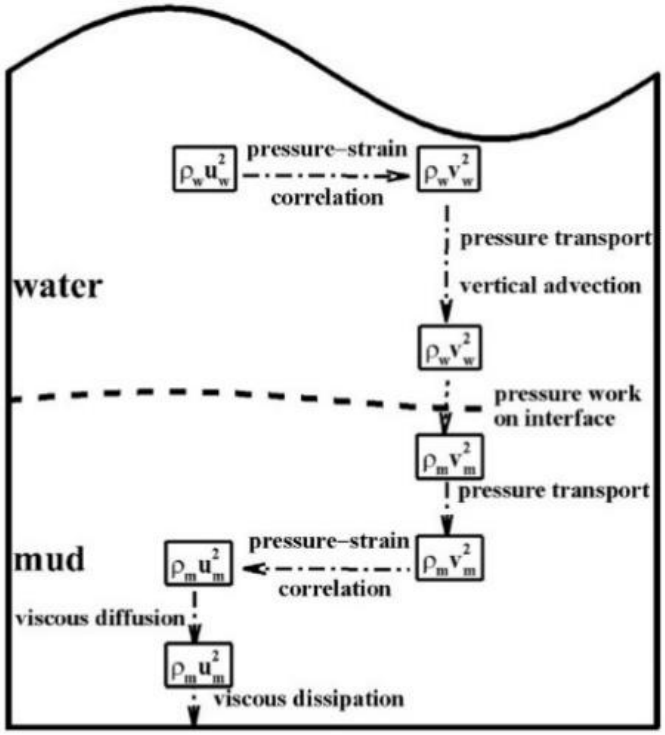

Figure 2.3: A schematic overview of how energy is transferred from the top layer into the bottom layer Deng et al.(2017)

2.1.3 Mudbanks and mudbank dynamics

Mud is often stored in mudbanks in front of the shoreline. However, only parts of the mudbanks are in the "fluid mud" state, while some parts will be more consolidated. The exact dimensions and state of mudbanks are a complicated study, and knowledge here is limited. Winterwerp et al. (2020) sketched the interaction between the mudbanks and waves and the dynamics of these mudbanks for a situation in Guyana. The influence of the tide and the Guiana current are also accounted for in Figure 2.4a. Although these figures are focused on Guyana, however, the main theory and assumptions apply to most mud-rich coastlines, including Suriname.

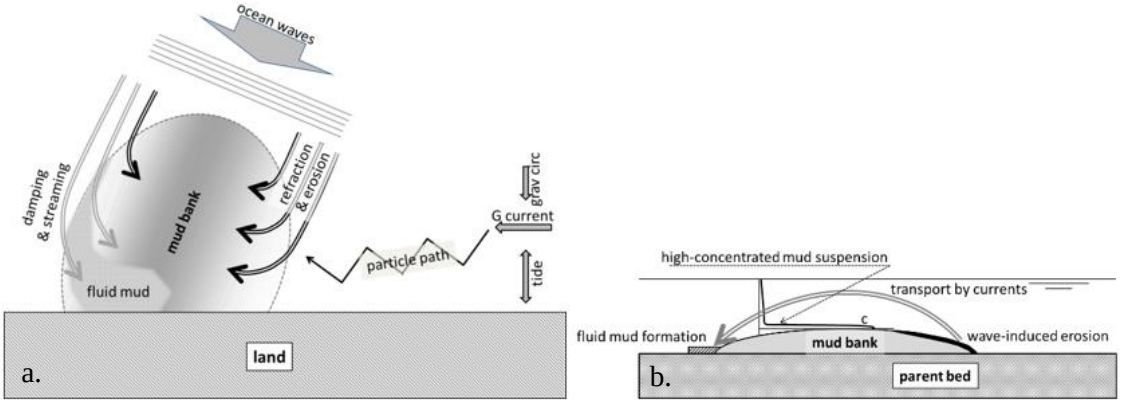

Figure 2.4: Schematic flow of the processes involved in the mudbank/wave interaction from above and as transect. Including: Guiana current, tidal, wave refraction and streaming and damping. This figure cannot be complete as it does not explain how the mudbanks remain their shape during migration (Winterwerp et al., 2022). Figure a. shows the system from above, while b. shows a transect of the mudbank from an alongshore angle.

The incoming waves refract when they start to interact with the shallower mudbanks. Together with the tide and the Guiana current, they cause the sediment to travel in a 'zigzag' pattern (see Figure 2.4a). The incoming tide causes sediment transport toward the coast through flow-induced advection (Winterwerp et al., 2022).

The sediment then flows over the crest of the mudbank (Figure 2.4b). The flow decelerates as it reaches calmer water and mixes with the fine sediment stirred from the lee side and transported by the waves that are refracted by the crest of the mudbank in the alongshore direction (Figure 2.4a). When the flow velocity reduces, the suspension becomes stratified, and when this happens, a High-Concentrated Mud Suspension (HCMS) is formed (Figure 2.4b) (Deng et al., 2017). This suspension is characterized by its lack of vertical mixing of the suspended material (e.g., Winterwerp, 2001; Winterwerp et al., 2020). The HCMS is still in a Newtonian state and prone to transport by turbulent flow. If the SPM-concentrations are large enough, the mud becomes too thick to be transported by this turbulent flow (Winterwerp et al., 2019). At this moment, the fluid mud state is reached. This fluid mud dampens the energy of incoming waves by dissipation within its mud layer.

Waves induce significant stress on the mud in the direction of the wave damping. This stress, also regarded as radiation stress, works on its own as a force in the direction of the waves (see Figure 2.5). This process is called streaming (Winterwerp et al., 2020). Stresses induced by this streaming in the water column are proven to be more significant than the stresses in the fluid

mud layer (e.g., Gade, 1958; Winterwerp et al., 2022). Forces in the water column can be up to several Pascal, while stress in the fluid mud remains around 0.1 Pa. High stresses in the water column could induce a setup, although these cannot be maintained because the layers are laterally confined.

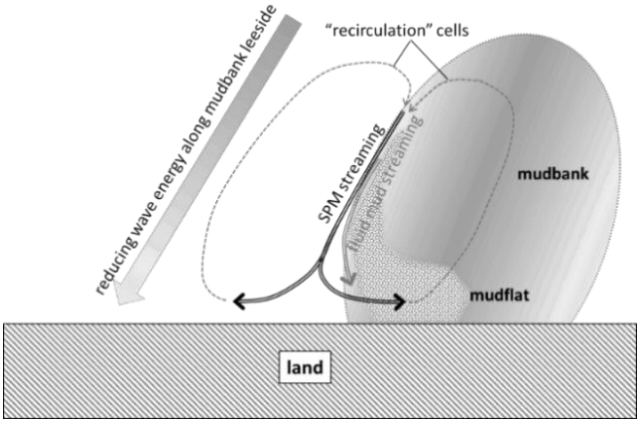

Figure 2.5: A schematic sketch of the recirculation cells described in Winterwerp et al. 2022 powered by wave-damping-induced streaming and resulting onshore flux of suspended fine sediment (SPM).

Because this pressure cannot be maintained, and the layers are laterally confined, streaming triggers a water flow parallel to the shore and away from the mudbank. This flow is compensated by sediment-rich water flowing towards the coast. This induces a horizontal circulation cell similar to rip currents at sand-rich beaches (see Figure 2.5). The circulation process brings large amounts of fine sediment towards the coast and helps form the fluid mud layer behind the crest of the mudbank resulting in its known shape as illustrated in Figure 1.4. The sediment flows towards the coast can even be so large that it exceeds the flow of sediment offshore by the tide going out (Winterwerp et al., 2020). Although stress caused by the streaming process is smaller in order of magnitude than stress in the water column, sediment flux can remain very large. The fluid mud is sheared vertically during streaming because of the bottom friction. This causes the fluid mud to over-consolidate, meaning that the fluid mud densifies too much, soft mud starts to settle, and sedimentation takes place. This sedimentation is where mudflats are starting to form, just behind the mudbank between the shoreline and the mudbank (see Figure 2.5). This happens during more significant wave events, and the sediment is pushed in by these events (Winterwerp et al., 2020).

When these depositions are high enough, mangroves can colonize them and settle. When the waves are not strong enough to erode the trailing edge of the coast, there is no forming of fluid mud, and waves are lesser damped. The stirring of the waves causes the negligible effect of wave damping. These low energy waves are not able to transport the fluid mud, although, they are strong enough to keep the sediment in suspension. Ultimately, the incoming flow of the rising tide remains the primary transporter of sediment. However, due to the formation of mudflats, the net effect of the process results in no addition to mudbank migration (Winterwerp et al., 2022).

2.2 Modelling mud-wave interaction

This thesis makes use of three different models. The main model is SWAN, which is a spectral wave model that will be introduced in the next subsection. Mud-wave calculations are not included in SWAN, and an extension is needed to make this possible. These calculations can be done with different models. For SWAN, one extension is made available: The two-layered viscous model. This model includes a new dispersion relation and a dissipation term for calculations when a mud layer is present in the water column. This extension of SWAN is named SWAN-Mud. Delft3D-Wave is a model from Deltares that works around SWAN-Mud to improve the workability of both input as output. It also includes two programs the make more complicated grids and locations of the mud layer. The Delft3D software also includes programs to export the output into files which can easily be postprocessed. This interaction of the different models and the new dispersion relations, as they are used in this study, are given in the workflow in Figure 2.6.

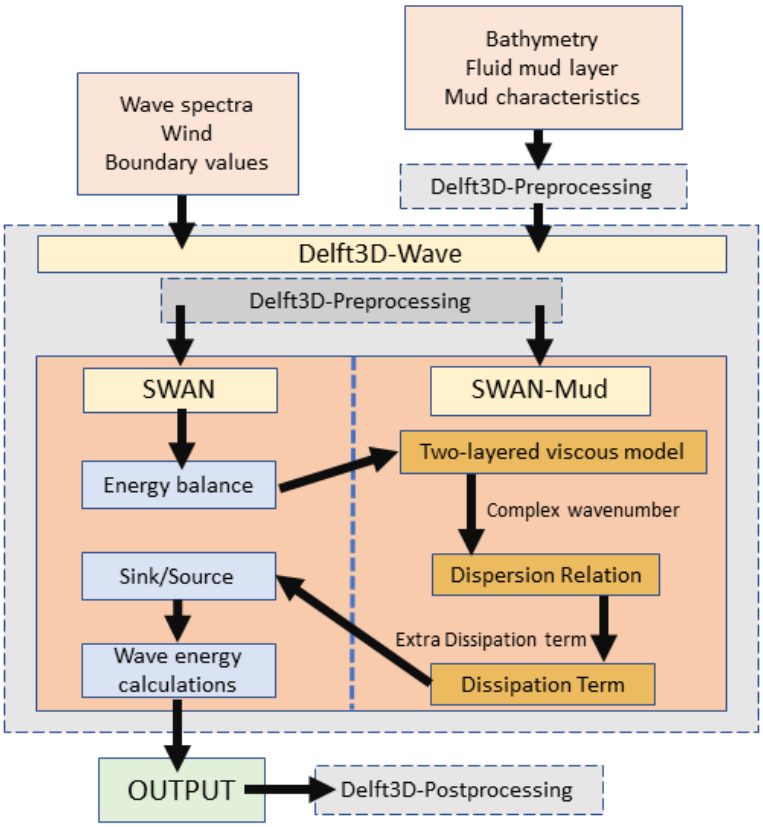

Figure 2.6: Workflow between the models used in this thesis and involved in modelling of the mud-wave interaction

2.2.1 SWAN

SWAN (Simulating WAves Nearshore), a commonly used model, is a state-of-the-art third-generation model which has as its primary goal to solve the spectral action balance equation for wave propagation from the open ocean to the surf zone nearshore(SWAN, 2009). Refraction, propagation, shoaling, dissipation, generation, and wave-wave interaction are all included in the model. SWAN is fully spectral, which means it can operate in all directions and frequencies. It can compute wind, ice, mud, and bottom friction influence. The Delft University of Technology developed SWAN, which is an open-source model.

In SWAN, waves and wave generation are assumed to be wind-generated, and the assumptions and equations involved are described in this subsection. Wind-generated waves are built up of a spectrum of frequencies (Holthuijsen, 2007). At any time and location, the elevation of the water surface of open oceans is the sum of many harmonic waves (SWAN, 2009). The wave energy is distributed over the wave frequency in SWAN as the energy density is a function of the frequency. In SWAN, this spectra is also distributed over the wave direction. This makes the energy denoted as $E(f,\theta)$, given with Equation 1, in which the wave energy is distributed over both the direction as the frequency of the spectra.

$$E(f) = \int_0^{2\pi} E(f,\theta)d\theta \tag{1}$$

Modelling open-ocean waves and their propagation to the shore includes different processes in different parts of the coast or at different parts of the wave's path to the coast. It involves many equations that can be found in the manual of SWAN (SWAN 2009; 2014), as most of them are out of the scope of this study. Only the fundamental equations regarding the wave energy and dissipation terms will be discussed.

$$E_{tot} = \frac{1}{8}\rho_w g H_{rms}^2 \tag{2}$$

The wave energy is defined by Holthuisen (2007), as shown in Equation 3. The wave energy is proportional to the root-mean-square of the wave height. In Equation 3, H_{rms} is the root mean squared wave height (Holthuisen, 2007). This equation includes the water density (ρ_w) and the gravitational acceleration (g).

$$\frac{\partial N}{\partial t} + \frac{\partial c_x N}{\partial x} + \frac{\partial c_y N}{\partial y} + \frac{\partial c_\sigma N}{\partial \sigma} + \frac{\partial c_\theta N}{\partial \theta} = \frac{S_{tot}}{\sigma} \tag{3}$$

One of the fundamental functions of SWAN is the wave action density balance (Eq.3). The action density $N(\vec{x},t;\sigma,\theta)$. is determined in SWAN-Mud as it is preserved during wave propagation along its direction when there are ambient currents present. This is not the case for wave energy (Whitham, 1974). The wave action density can be derived from the wave energy as $N = E/\sigma$. Here is $E\ (\sigma, \theta)$ the energy density, and σ represents the wave radial frequencies. The wave action density is used in SWAN to define energy changes for one location in time and space ($\vec{x},t;\ \sigma,\ \theta$). Time is introduced in the first term of the equation. The second term includes c_x and ∂x where c_x is the factor representing propagation velocity on the x-axis of the spectrum and ∂x the distance in the x-direction. The third term is similar to the second term but for the y-axis instead. The fourth and fifth terms include c_σ and c_θ which are propagation

velocities in spectral space (σ, θ) (e.g., Mei, 1983; Komen et al., 1994). The terms on the left side represent an in-or outgoing flux for a point in time and space. The right side of the balance covers S_{tot}: a source/sink that includes all physical processes involved in generating or dissipating energy. The term S_{tot} in Eq (3) can be defined with an energy balance, containing both generators of waves and thus energy (the source) and dissipators of energy (the sinks) (SWAN, 2009). Every term is spectral as they are all dependent on frequency and direction. The energy balance is given as:

$$S_{tot} = S_{wind} + S_{wc} + S_b + S_{br} + S_{mud} + S_{nl} \quad (4)$$

S_{tot} = The total accumulation of all the sources and sinks

S_{wind} = Wind generation

S_{wc} = The energy dissipation by whitecapping: steepness induced wave breaking

S_b = The energy dissipation by bottom friction.

S_{br} = The depth-induced wave breaking.

S_{mud} = Energy dissipation by the (fluid) mud layer.

S_{nl} = accounts for non-linear wave interactions causing energy transfer between wave frequencies.

All dissipation terms are shortly described in Appendix A, and the standard equations and processes are explained. Further and more in-depth explanations can be found in SWAN (2009). In this study, the focus is on the mud application of SWAN, which will be explained more in-depth in the next subsections.

2.2.2 Different types of models

As SWAN stand-alone is not proficient in calculations that include mud-wave interaction. An extra model extension had to be included in SWAN. De Wit (1995) categorizes the models capable of modelling the interaction between waves and a muddy environment into five groups that are divided based on their implementation of the mud layer rheology. Borsje, 2019 summarizes this models as:

- Ideal elastic models
- Poro-elastic models
- Viscous models
- Visco-plastic models
- Visco-elastic models

The Ideal and Poro-elastic models assume the bed to be ideal elastic where viscous behaviour is not considered. For the poro-elastic models, the pore water and the effect on the elastic bed are integrated into the model. Because there is no incorporation of viscous effects in these models, the dissipation of the wave energy by the fluid mud is not accounted for, which results in no damping of the waves. This limits the use of these elastic models to cohesive beds that are non-fluid and consolidated; nevertheless, the second group can still be used for thin fluid mud layers(Borsje, 2019).

In Section 2.1, the characteristics of the fluid mud have been explained. De Wit (1995) argues that the visco-plastic models do not represent the response of fluid mud to forces and orbital motion of waves that can be observed in field experiments (Borsje, 2019). This response shows viscoelastic behaviour, indicating that viscoelastic models are more appropriate for wave-mud interaction. The visco-elastic model depends non-linearly on the depth, consolidation time, the oscillatory strain amplitude, and different measurement methods of mud properties, making this approach very complicated compared to the latter (De Wit, 1995). In the viscous models, due to the assumption that the mud is a highly viscous Newtonian fluid, the rheological properties of the mud are only partly accounted for. However, these models can still calculate wave-induced velocities in the mud layer and estimate wave damping. De Wit (1995) shows that the estimations made with the viscous models for the fluid mud are suitable for considerable strain amplitudes when the fluid mud is assumed to be viscous. The viscous models are also more beneficial than the other models as they are relatively easy to implement. The viscous models used in this thesis, described above, are built of two layers, hence the name: two-layer viscous model. In SWAN-Mud, the methods for mud-wave interaction are all considering two-layer viscous models.

2.2.3 SWAN-Mud: Two-Layer viscous model

As introduced before, SWAN-Mud is an extension of the SWAN model. The mud dissipation is added to the energy balance (see Eq.4). SWAN-Mud uses a two-layered viscous model (Figure 2.7). This concept was first used by Gade (1958), who described the bottom layer as a high density and viscous layer overlying a non-ridged consolidated bed; this describes the mud layer. On top of this mud layer lies a viscous waterlayer. Figure 2.7 shows this two-layered model, including all parameters necessary, which are all given in the table of symbols. These parameters are the same throughout this thesis except when stated otherwise explicitly. Gade made assumptions that are important for the reliability of this model (Gade, 1958). Kranenburg (2008) summarized these assumptions:

1. Viscosity and density are constant for each layer.
2. Fluids are incompressible, and the mud is a Newtonian fluid.
3. No interfacial mixing, stable interface.
4. The waves cannot liquify the consolidated bed.
5. The waves are plane and sinusoidal.
6. The layers are assumed to have an infinite horizontal length.
7. The wave amplitude is relatively small compared to the water depth
8. The waves working on the mud are free waves with no direct association with driving or dissipating shear forces.
9. Surface pressure is constant, and variations are neglected.
10. There are no effects of earth rotation
11. The mean current is zero
12. The motion of the fluids in both layers is free of divergence

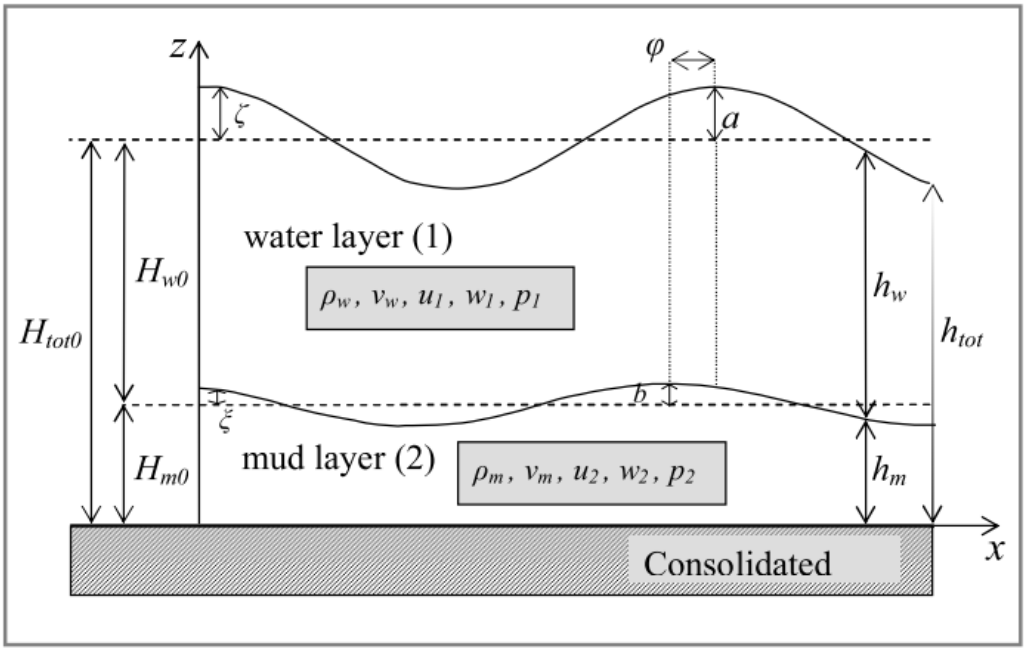

Figure 2.7: The two-layer viscous model as designed by Gade(1958), figure from Kranenburg(2008). The figure includes different parameters, these are explained in table of units included in the beginning of the report.

When these assumptions are implied, the effects of turbulence, Coriolis effect, and advection are neglected. The continuity equation can be combined with both layers' linearized momentum equations. These are given as:

$$\frac{\partial u_i}{\partial x} + \frac{\partial w_i}{\partial z} = 0 \tag{5}$$

$$\frac{\partial u_i}{\partial t} + \frac{1}{\rho_i}\frac{\partial p_i}{\partial x} - \nu_{x,i}\frac{\partial^2 u_i}{\partial x^2} - \nu_{z,i}\frac{\partial^2 u_i}{\partial z^2} = 0 \tag{6}$$

$$\frac{\partial w_i}{\partial t} + \frac{1}{\rho_i}\frac{\partial p_i}{\partial z} - \nu_{x,i}\frac{\partial^2 w_i}{\partial x^2} - \nu_{z,i}\frac{\partial^2 w_i}{\partial z^2} = 0 \tag{7}$$

Here is Equation 5 the continuity equation, Equation 6, the horizontal momentum balance and Equation 7 is the vertical momentum balance, all for layer *i*, *u* represents the horizontal orbital velocity and *z* vertical axis, positive is upwards. The *w* indicates the orbital velocity along the z-axis. The density of layer *i* is given with ρ and the time is given by *t*. They are all also given in the table of symbols.

p_i represents the total pressure in these equations and can be divided into three terms (as in Equations 8 and 9). In Equation 8 is visible that the first term represents the orbital motion. The second term represents the hydrostatic part. This can be explained as the length to the surface or interface equilibrium, both described in Figure 2.7(Kranenburg, 2008). The third term is the pressure at the interface caused by the water surface or the pressure at the water surface: the ambient pressure, which is zero for the waterlayer (Equation 8) and equal to the pressure induced by the weight of the waterlayer at the interface (Equation 9).

$$p_1 = p_1^{orb} + \rho_1 g(H_{tot0} - z) + 0 \tag{8}$$

$$p_2 = p_2^{orb} + \rho_2 g(H_{m0} - z) + \rho_1 g H_{w0} \tag{9}$$

Displacements of the surfaces of both layers are given in Equations (10) and (11), which are dependent on layer *i*. In these equations is $\zeta(x,t)$ representing the displacement at the water surface, while $\xi(x,t)$ represents the displacement of the interface, these are given Figure 2.7 and the table of symbols. The amplitude of the water surface displacement is given with a, and b indicates the amplitude of the interface. The wave angular frequency (ω) is included in both equations. Equation (11) also includes the phase difference between the layers (φ). Displacement at the interface is complex because the imaginary part of the wavenumber is complex when the phase shifts between the displacement of the surface and inter-surface. This complex amplitude is unknown before calculation. Important to note that the phase angle becomes negative over time as *t* grows. This is the same for all viscous models used in this thesis, and these are also included SWAN-Mud in this way. This negative phase shift would imply that the interface elevation propagates further than the surface elevation, which is not possible.

$$\zeta(x,t) = ae^{i(kx-\omega t)} \tag{10}$$

$$\xi(x,t) = \xi_0 e^{i(kx-\omega t)} = be^{i\varphi}e^{i(kx-\omega t)} \tag{11}$$

Boundary conditions in the SWAN model are the same for all the different methods. However, all methods have their limits. This is because they all simplify the boundaries discussed below. All their limits are based on the assumptions made in their derivation; these are explained later in this study. These boundaries follow from earlier assumptions.

At *z = 0:* penetration and slip are not allowed on the fixed and rigid bed.

$$u_2(x, 0, t) = 0 \tag{12}$$

$$w_2(x, 0, t) = 0 \tag{13}$$

The location at the interface: $z=h_m$ is characterized by continuous velocities and stresses over the interface. Particles on the interface are always following the interface, making it easier to derive the vertical velocities. These are all given or described in:

$$u_1(x, h_m, t) = u_2(x, h_m, t) \tag{14}$$

$$w_2(x, h_m, t) = w_1(x, h_m, t) = \frac{D\xi(x,t)}{Dt} \tag{15}$$

$$\sigma_{zz2}(x, h_m, t) = \sigma_{zz1}(x, h_m, t) \tag{16}$$

$$\sigma_{xz2}(x, h_m, t) = \sigma_{xz1}(x, h_m, t) \tag{17}$$

$$w_2(x, h_m, t) = \frac{\partial\xi(x,t)}{\partial t} \tag{18}$$

Here, $\sigma_{zz} = -p + 2\rho_i v\frac{\partial w}{\partial z}$ represents the normal component of stress at the interface while $\sigma_{xz} = \rho_i(v\frac{\partial w}{\partial z} + v\frac{\partial u}{\partial z})$ is the tangential component of this same stress at the interface.

The assumptions are the same for the free surface location ($z = h_{tot}$) as the particles follow this free surface. This gives an extra set of boundaries as the dynamic boundary conditions that are favorite need normal and tangential stresses are equal to zero. All symbols included in the equations explained in this chapter are given in the table of symbols.

$$w_1(x, h_{tot}, t) = \frac{\partial\zeta(x,t)}{\delta t} \tag{19}$$

$$\sigma_{zz1}(x, h_{tot}, t) = 0 \tag{20}$$

$$\sigma_{xz1}(x, h_{tot}, t) = 0 \tag{21}$$

$$k = k_r + ik_i \tag{22}$$

From this wavenumber (k), the complex part represents the energy damping by the mud, while the real part represents the wavelength. The standard dispersion relationship does not give an accurate result for muddy situations as it does not apply to the presence of fluid mud. Hence, a new dispersion relation is necessary as stated before.

As stated before, all the different methods introduced later simplify these boundaries in different ways and add additional assumptions applying to the corresponding model. To calculate the energy dissipation, multiple different methods are derived over time. These authors derived their dispersion relationship to define a wavenumber (Kranenburg, 2008). In the SWAN-Mud model are six different dispersion relationships included that can be used for calculating the wavenumber: Gade(1958), DeWit(1996), Guo(2002), Dalrymple(1978), Ng(2000), and DELFT(2008). In this study, only Gade, DeWit, Ng, and DELFT are used because these methods are known to be the most accurate or most robust.

Gade (1958)

Gade was a pioneer in mud dissipation calculations; he was the first to use the two-layered viscous model described above. He studied different effects of the non-rigid and impervious bottom on external waves that are also assumed in the two-layered model. The water depth is assumed to be shallow for these layers, implying the shallow water equations. Vertical accelerations are neglected in the Gade dispersion relation, while the pressure in the layers is assumed to be hydrostatic. For this dispersion relation, the horizontal velocities are independent of depth. All the assumptions that are made simplify the model to a certain extent, resulting in simplified boundary conditions and differential conditions that restrict this model to shallow water depth and mud thickness. Gade derived this dispersion relationship by substituting the assumed harmonic solutions in each variable. In different pieces of literature, the Gade dispersion is criticized for its limited range and lack of accuracy. In Kranenburg(2008), some of these restrictions of the Gade method are discussed. Although this dispersion relationship is limited in real scenarios, it is straightforward and trustworthy.

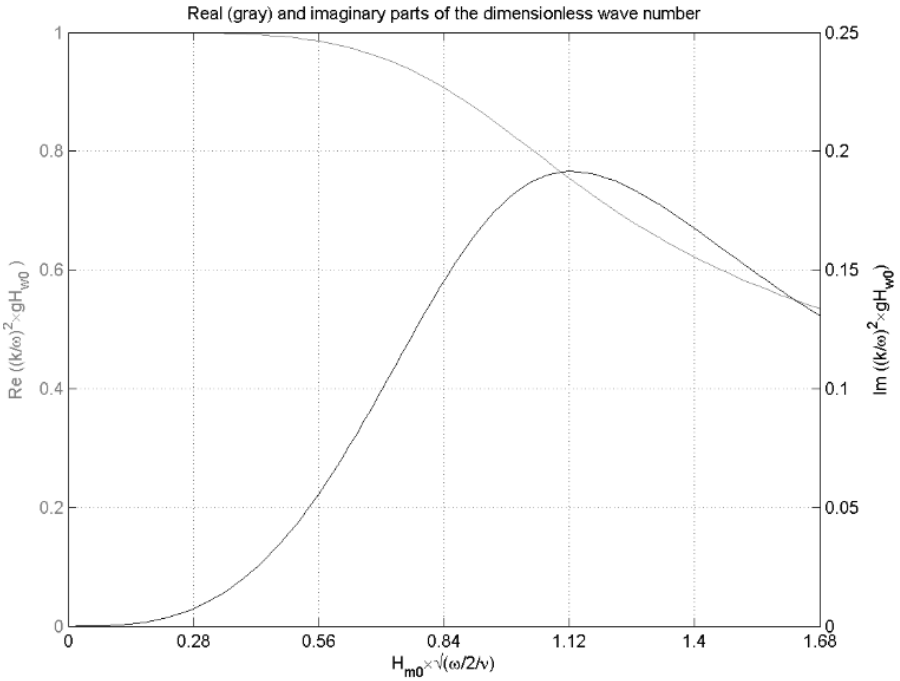

Figure 2.8: Results of the dispersion relation as in Gade(1958) for different mud layer thicknesses. All axes are made dimensionless. The left Y-axis shows the real part of the wavenumber, which corresponds with the grey colored line and the right Y-axis shows the imaginary wavenumber.

Figure 2.8 illustrates the original results for the wavenumber by Gade (1958). The imaginary wavenumber shows an optimum around 1.12, which corresponds to mud layer thickness that is equal to what is described in the literature as the Stokes boundary layer (De Wit, 1995). The real part of the wavenumber represents the wavelength. This declines more gradual with increasing mud layer thickness. This relation between the Stokes boundary layer and dissipation is further explained in Appendix B.

The dispersion relationship is given as:

$$k = \pm\omega \left\{ \frac{\left(1+\Gamma\frac{H_{m0}}{H_{w0}}\right) \pm \sqrt{\left(1+\Gamma\frac{H_{m0}}{H_{w0}}\right)^2 - 4\gamma\Gamma\frac{H_{m0}}{H_{w0}}}}{2\gamma g\Gamma H_{m0}} \right\}^{1/2} \tag{23}$$

H_{m0} and H_{w0} indicate the equilibrium heights of the mud and water layer, respectively. Furthermore, in Equation 24 represents Γ an auxiliary parameter used in the dispersion relation, and this is further explained in Winterwerp et al. (2012). In Equation 25, is ω the wave angular frequency which is a parameter given by: ($2\pi/T$).

The wavenumber becomes complex because m (which is another auxiliary parameter), explained in Kranenburg (2008) is complex (Equation 23), this means the wavenumber has an imaginary and real part. In Equation 26 is γ the ratio between the mud and waterlayer density. All the units used in this thesis are described in the table of units at the beginning of this report.

$$\Gamma = 1 - \frac{\tanh(mH_{m0})}{mH_{m0}} \tag{24}$$

$$m = (1-i)\sqrt{\frac{\omega}{2\nu}} \tag{25}$$

$$\gamma = \frac{\rho_2 - \rho_1}{\rho_2} \tag{26}$$

Gade's dispersion relation leads to four solutions, of which only the solution with waves in the positive direction is relevant. This solution has a positive first root and a negative second root. A small wavenumber results in a high propagation speed representing the external wave (Kranenburg, 2008). This dispersion relationship developed by Gade gives an explicit expression for the wavenumber. Shallow water approximations are used to solve wave velocity. The limit of Gade is given in Equation 30, mainly caused by the shallow water assumptions. Gade used Equations 27,28, and 29 to normalize his results and represented his results as non-dimensional values.

$$Re\left(\frac{k^2}{\omega^2}H_{w0}g\right) \tag{27}$$

$$Im\left(\frac{k^2}{\omega^2}H_{w0}g\right) \tag{28}$$

$$H_{m0}\left(\sqrt{\frac{\omega}{2\nu}}\right) \tag{29}$$

$$H_{m0}\left(\sqrt{\frac{\omega}{2\nu}}\right) \leq 1.6815 \tag{30}$$

An important finding by Gade is the decay of the wave height over a constant mud layer. When the imaginary wavenumber stays constant, the wavenumber's decay is exponential. Gade designed an energy dissipation term for this imaginary wavenumber given in Equation 31. ϕ represents the phase difference between the surface and interface displacement. While ϕ' is the phase angle of this difference. Equations 32 and 33 are used to define the variables in the dissipation term (Equation 31). This dissipation term includes the phase and amplitude differences between the mud and waterlayer, explained with Equations 32 and 33. In these equations is, the R representing the amplitude while β is the argument of $(\frac{k}{\sigma})^2$. The limits of Gade are plotted in Figure 2.9 and these are for waves with a significant wave height of 0.9 meters and a peak period of 6.6 seconds. The cross-section is from the coast of Suriname that will be used later in this study. The figure gives a good impression of the usability of the Gade method for a realistic scenario.

$$\frac{S_{b,m}}{E} = -\alpha\omega g H_{w0} R \frac{b}{a}\sin(\phi - \phi') \tag{31}$$

$$R * e^{i\beta} = \left(\frac{k}{\omega}\right)^2 \tag{32}$$

$$\frac{b}{a} = \sqrt{\left(1 - gH_{w0}R\cos(\phi)\right)^2 + \left(gH_{w0}R\sin(\phi)\right)^2} \tag{33}$$

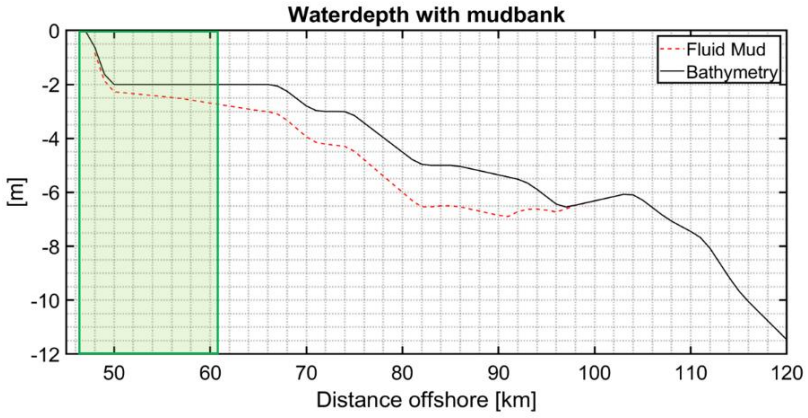

Figure 2.9: the limits of the Gade method given in green for the coast of Suriname for waves with H_s = 0.9 m and T_p = 6.6 sec. Here is visible that Gade is only applicable in shallow water.

DeWit (1995)

The "DeWit" method is a modification of Gade (1953) made by De Wit (1995) at Delft Hydraulics. This method is designed to make the dispersion relationship of Gade less limited and more complete. This includes the vertical accelerations in the vertical momentum equations. For the mud layer, this is not included as the situation in the mud layer is still quasi-hydrostatic. The momentum equations to calculate these vertical velocities are included in the continuity equation. The parameters used are similar to the ones in Gade(1958) and displayed in the Table of Symbols

This dispersion relation defined by DeWit is given as:

$$DeWit = \left(-1 + \frac{\left(1-\frac{\rho_1}{\rho_2}\right)gk\left(kH_{m0} - \frac{k\tanh(mH_{m0})}{m}\right)}{\omega^2}\right)\left(\frac{gk\tanh(kH_{w0})}{\omega^2} - 1\right) - \left(\frac{\rho_1\left(kH_{m0} - \frac{k\tanh(mH_{m0})}{m}\right)\left(\frac{gk}{\omega^2} - \tanh(kH_{w0})\right)}{\rho_2}\right) = 0 \quad (34)$$

In the DeWit dispersion relation, different variables are replaced with separable assumptions over time and direction; this is similarly done as in Gade by using the differential equations. Gade (1958) neglected the variables in the z-direction for his dispersion relation. De Wit(1995) included these in his method, which resulted in an expression of the variables that can be implemented in the boundary conditions of this dispersion relation (Kranenburg, 2008). This new formulation can then be derived as a matrix equation. Non-trivial solutions can only be obtained when this matrix equation is singular and homogeneous. This is solved by setting the coefficient to zero; this way, only the wavenumber *k* is unknown, which is solved with the Newton-Muller iteration method in SWAN-Mud (Beyramzade & Siadatmousavi, 2018). The DeWit computations are very complicated, and although his methods are explained very elaborated, some errors were made. In his paper, some errors and typos were found that made reproduction complicated. While attempting to reproduce the work of DeWit, a new dispersion relation was accidentally derived, resulting in the DELFT dispersion method, which will be explained later (Kranenburg, 2008). The method by DeWit is applicable in most situations, and this was why this method was often preferred to use Winterwerp et al. (2007). The DeWit method is limited for relatively thin mud layers compared to the water column ($kH_{m0} << 1$), these limits are given in a realistic scenario as Suriname in Figure 2.10. The longer applicability compared to the Gade method is obvious.

In order to improve the DeWit method, the dispersion relationship has been updated by Siadatmousavi et al. (2012). This was done to improve the calculation speed in SWAN. The result is given with Equation 35, the outcome of the different dispersion relationships should be similar. In this equation, k_c represents the complex wavenumber and not H_{m0} and H_{w0} are used, but h_w and h_m are used instead. All other variables are similar to the old DeWit and Gade method and are explained in the table of symbols.

$$\sigma^4\left(\frac{1}{k_c}-\frac{\rho_w}{\rho_m}\frac{\tanh(k_c h_w)\tanh(mh_m)}{m}+h_m\frac{\rho_w}{\rho_m}\tanh(k_c h_w)\right)$$
$$+\sigma^2 g\left(\frac{k_c}{m}\tanh(mh_m)-k_c h_m-\tanh(k_c h_w)\right)$$
$$+g^2k_c^2\tanh(k_c h_w)\left(1-\frac{\rho_w}{\rho_m}\right)\left(h_m-\frac{\tanh(mh_m)}{m}\right)=0 \quad (35)$$

As the dissipation term by DeWit was not introduced, it had to be reproduced from De Wit (1995), which was complicated as multiple typos were found in this method. The energy dissipation term was split up into two important parts, the $F1_k$ and $F2_k$,(Equations 39 and 40) in order to find the energy dissipation; these two are necessary to find β, which is used in the calculations of the energy dissipation (Eq.36). These were not included in SWAN, as stated before. As this study was also focused on improving SWAN-Mud, this energy dissipation was added together with solving multiple bugs limiting the model to make the DeWit method working

The new energy dissipation term is given as:

$$S_{mud}=\beta*\omega*E \quad (36)$$

All parameters below have been explained more elaborate in De Wit (1995).

$$\omega=2\pi f \quad (37)$$

$$\beta=Im[F1_k]*Conjugate[F2_k] \quad (38)$$

$$F1_k=\cosh(kH_{w0})(1-\left(\frac{gk}{\omega^2}\right)\tanh(kH_{w0})) \quad (39)$$

$$F2_k=\cosh(kH_{w0})(1-\left(\frac{\omega^2}{gk}\right)\tanh(kH_{w0})) \quad (40)$$

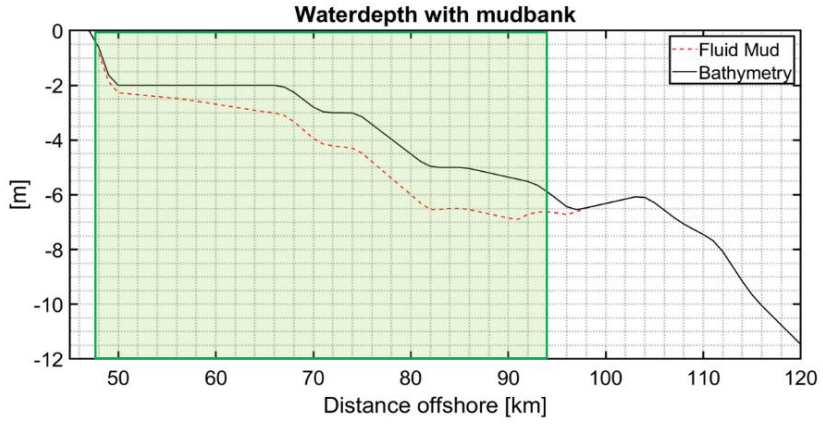

Figure 2.10: The limits of the DeWit method given in green for the coast of Suriname for waves with H_s = 0.9 m and T_p = 6.6 sec. Here is visible that the DeWit method is applicable in a broader range compared to Gade. It is only not applicable when the mud becomes relatively thin compared to the waterdepth.

Ng (2000)

The method designed by Ng in 2000 differs from the other methods as it focuses more on the Stokes boundary layer. DELFT and DeWit were based on solving the wavenumber iteratively by using a solver. Ng searches for an approach to the Stokes boundary layer as he assumes that the optimal thickness of the mud layer is found around the thickness of the Stokes boundary layer. This was visible in the method by Gade in Figure 2.8. Instead of using a solver, the solution searches for a value close to the Stokes boundary layer.

Ng (2000) did not continue with the model of DeWit but continued with the model of Dalrymple (1978) and added limits to the model of Dalrymple by trying to approach the thickness of the Stokes boundary layer. The main assumption in the Ng model is that the thickness of the mud layer and the incoming wave amplitude are of the same order of magnitude as the boundary layer. The wave amplitude is much smaller than the wavelength. This resulted in an ordening parameter ε, given in Equation 41.

$$\varepsilon \equiv ka \sim kH_{m0} \sim k\delta_{BL} \ll 1 \tag{41}$$

As the water is very shallow, the fluid mud's viscosity dominates the mud's wave-induced motion (Kranenburg, 2008). This leads the boundary layer equations to become the governing equations for the mud layer and part of the water layer close to the interface/ This is where the ordering parameter of Ng is used to determine which of the terms are neglectable. All these terms are explained in Ng(2000) elaborately.

For the water layer, formulations for velocities regarding the inside of the boundary layer and near to the interface are determined by Ng. Close to the surface inside the boundary layer is damping assumed to be very small when compared to the rest of the boundary layer, this is part of the solution. These two equations for the two layers are matched asymptotically. This results in a complex determination of an eigenvalue for the wavenumber *k*. Here are Equations 42 and 43 used to solve for *k*.

This dispersion relationship by Ng is:

$$\frac{\omega^2}{gk} = \frac{\tanh(kH_{w0}) + B}{1 + B\tanh(kH_{w0})} \tag{42}$$

B is the result of the asymptotical matching and is a complex parameter. Wavenumber k_1 is a real number, and k_2 is complex and can be calculated with Equation 43. These relate together as given in Equation 22.

$$k_2 = -\frac{Bk_1}{\sinh(k_1H_{w0}) + \cosh(k_1H_{w0}) + k_1H_{w0}} \tag{43}$$

The imaginary part in this formulation represents the dissipation by the fluid mud, this term is the rate of the wave attenuation. The exact wave damping can be calculated directly if *k1* and *B* are known. There are multiple different equations used to calculate the *B*, *k1*, and *k2*, all of these can be found in his paper. Ng concluded that: 1) Higher viscosity of the mud results in higher energy dissipation, 2) an optimum in the mud dissipation is found when the mud layer is around one and a half times the thickness of the Stokes Boundary layer. 3) The mud density

induces the largest dissipation when close to the water density (Ng, 2000, p.229). The limits are given in Figure 2.11. Here is visible that when the mud becomes relatively thick compared to the water depth, the model is not applicable. This results in the method only being valid at the edges of the mudbank, for this figure is 0.01 used as the limit for <<1. The applicability will be larger when a larger value is used.

Rogers and Holland (2009) define the energy dissipation term as corresponding to the Ng method. Their dissipation term is implemented in SWAN-Mud. This energy dissipation term includes the wave action density and the wave group velocity. This method is simplified by substituting it into the action density balance. An advantage is the possibility of calculating the energy dissipation for each value in the $E(\omega, \sigma)$ spectrum. This new term is given as:

$$\frac{S_{b,m}}{E} = -2C_{g,x}k_i \tag{44}$$

In this equation is the C_g the group velocity of the waves in the x-direction.

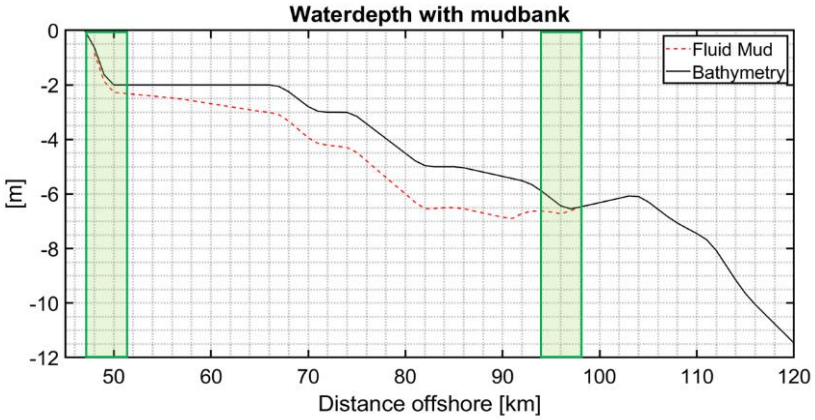

Figure 2.11: The limits of the Ng method given in green for the coast of Suriname for waves with H_s = 0.9 m and T_p = 6.6 s. This method is applicable for deep waters with relative thin mud layers. So very close to the coast the water is relatively deep compared to the very thin mud

DELFT (2008)

The DELFT method, set up by Kranenburg in 2008, was an attempt to reach the same results as De Wit (1995) but became an improvement as the same results could not be reached, pointing to restrictions in the DeWit method (1995). The DELFT method also contains more variables than the DeWit method, making it potentially more accurate and complicated.

The DELFT dispersion relation is given as:

$$\begin{aligned}
&\omega^4\left(\frac{\cosh(kH_{w0})\cosh(mH_{m0})}{k}-\frac{\rho_w}{\rho_m}\frac{\sinh(kH_{w0})\sinh(mH_{m0})}{m}+h_{m0}\frac{\rho_w}{\rho_m}\sinh(kH_{w0})\cosh(mH_{m0})\right)\\
&+\omega^3 2ik\nu_m\cosh(kH_{w0})(\cosh(mH_{m0})-1)\\
&+\omega^2 g\left(\frac{k}{m}\cosh(kH_{w0})\sin(H_{m0})-kH_{m0}\cosh(kH_{w0})\cosh(mh_{m0})-\sinh(kH_{w0})\cosh(mH_{m0})\right)\\
&+\omega^2 gk^2\nu_m\sinh(kH_{w0})(1-\cosh(mH_{m0}))\\
&+g^2k^2\left(H_{m0}\frac{\rho_2-\rho_1}{\rho_2}\sinh(kH_{w0})\cosh(mH_{m0})-\frac{\rho_m-\rho_w}{\rho_m}\frac{\sinh(kH_{w0})\sinh(mH_{m0})}{m}\right)=0.
\end{aligned} \tag{45}$$

The expression defined by Kranenburg includes phase and amplitude differences between surface and interface, similar to DeWit, but also includes the amplitude of pressure fluctuations for the whole domain, so all water depths and mud thicknesses. The DELFT method assumes that the energy transport through the interface is equal to the energy dissipation in the mud layer. This energy transfer over the interface is related to the pressure applied to the fluctuating interface (Kranenburg, 2008). DELFT is also solved as an implicit function that can be solved analytically. In SWAN-Mud, this is done with the DZANLY routine.

For shallow water, the calculation of the energy dissipation is similar to the method by Gade, while in deeper water, Gade is not reliable anymore. The DELFT method includes multiple pressure equations to make it possible to model deeper waters. All these depth pressures can be added to Equation 49. For the deeper waters, the energy dissipation equation is given in Equation 48, including the pressure terms. Furthermore, the DELFT method reproduces similar results to Ng for deep waters with relatively thin layers of mud. For the small water depths, the energy dissipation is given with Equation 47. This is mathematically equivalent to the Gade method.

Kranenburg (2008) used more general assumptions than the previous described two-layer models. He assumed that the primary mechanism for energy dissipation in the mud layer is caused by viscous dissipation, and elasticity and plasticity effect are neglected in the method. Kranenburg proved that the model can reproduce results by Gade (1958) for shallow waters, Ng (2000) for thin mud layers and Dalrymple and Liu (1978) for relatively thick mud layers.

For kH_{w0}"1 then:

$$RelDiss1 = \frac{\omega \cosh(H_{w0}k_r)\cos(H_{w0}k_i)b\sin(\varphi)}{a} \tag{46}$$

$$RelDiss = -\omega\frac{b}{a}\sin(\varphi) \tag{47}$$

For other depths:

$$\frac{S_{mud}}{E} = -\sigma\frac{Re\{p_{1(z=H_{m0})}\}}{\rho_1 g\alpha}\frac{b}{\alpha}\sin\varphi \tag{48}$$

$$P_1(depth) = \rho_1 ag\cosh(k_r * depth) - \frac{\rho_1 a\omega^2\sinh(k_r * depth)}{MODk} \tag{49}$$

In Siadatmousavi et al.(2012), the DELFT method was updated and improved for application in SWAN-Mud. The new dispersion relation is given with Equation 50. These changes make the calculations of DELFT faster with equal results. Furthermore, a different solver is used to solve the wavenumber iteratively. The DZANLY routine is replaced by the Newton-Muller routine. Ng's wavenumber is used as the solver's starting point when h_m/h_w <0.05. When the mud layer is relatively thicker, the starting point is based on Gade(1958) and Guo(2002) (Siadatmousavi et al., 2012). It can be seen in Figure 2.12 that the DELFT method is applicable for the whole mudbank, making it the most suitable method for this study.

$$\begin{aligned}
&\sigma^4\left(\frac{1}{k_c} - \frac{\rho_w}{\rho_m}\frac{\tanh(k_c h_w)\tanh(mh_m)}{m} + h_m\frac{\rho_w}{\rho_m}\tanh(k_c h_w)\right)\\
&+\sigma^3 2ik_c v_m\left(1 - \frac{1}{\cosh(mh_m)}\right)\\
&+\sigma^2 g\left(\frac{k_c}{m}\tanh(mh_m) - k_c h_m - \tanh(k_c h_w)\right)\\
&+\sigma 2igk_c^2 v_m\tanh(k_c h_w)\left(\frac{1}{\cosh(mh_m)} - 1\right)\\
&+g^2k_c^2\tanh(k_c h_w)\left(1 - \frac{\rho_w}{\rho_m}\right)\left(h_m - \frac{\tanh(mh_m)}{m}\right) = 0
\end{aligned} \tag{50}$$

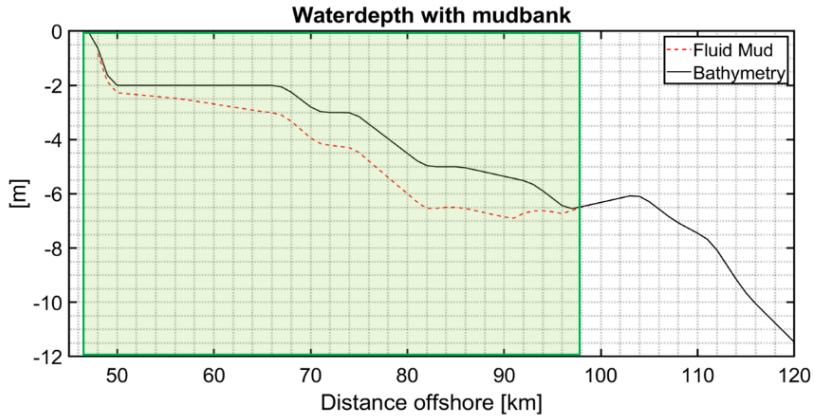

Figure 2.12: The limits of the DELFT method given in green for the coast of Suriname for waves with H_s = 0.9 m and T_p = 6.6 s. This method is applicable for the whole domain, so the green area covers the total mud layer

2.2.4 Delft3D-Wave

Delft3D-Wave is a module of the Delft3D program developed by Deltares. It simulates wind-generated waves in coastal areas, tidal inlets, and estuaries and focuses on the propagation of these waves (Deltares, 2021, p4.). The Delft3D-Waves uses the basis of SWAN and works as a user-friendly interface around it to model the interaction of waves with the shore. The SWAN model considers the propagation caused by currents and depths. It represents different processes that interact with the waves, such as generation by wind or dissipation by wave breaking. Further information about the standard SWAN model can be found in the previous sections and in the manuals of SWAN (SWAN, 2009).

Fully implicit propagation schemes are implemented in SWAN and Delft3D to reduce computation time (Deltares, 2021, p5.). Furthermore, these propagation schemes keep the model stable when running computations. This gives a more robust model that is easier to work with for practical applications than the SWAN stand-alone. Output for the SWAN model has been verified in different field cases or laboratory experiments.

For mud dissipation, an extension of SWAN is used, SWAN-Mud. The interaction between SWAN-Mud and Delft3D-Wave is made possible after the study by Tzampazidou (2020) by Deltares. Although the development of this connection between the models was not an objective of this study, multiple tests and improvements have been conducted during this study. The output has been made available in QUICKPLOT, an extension of the Delft3D program built for postprocessing of results. Not all output has been made available for this study as it is still a work in progress. Hence, for some functions of SWAN-Mud, the stand-alone version of SWAN-Mud is used. The preprocessing to make grids and bathymetry and the postprocessing tools as QUICKPLOT are also indicated in the workflow in Figure 2.6.

2.3 Test case: Suriname

2.3.1 Research area

The Guiana coastline stretches from the Amazon delta in the North of Brazil to the Orinoco delta further to the northwest in Venezuela, and this coast is often referred to as the A-O coast in literature (Anthony et al., 2014). This coastline has a length of approximately 1500 kilometres and crosses the borders of; Brazil, French Guiana, Suriname, Guyana, and Venezuela. This coastline is heavily influenced by a large sediment influx of fine-grained mud with an estimated volume of $13 \times 10^8 m^3 yr^{-1}$ and with considerable temporal variation, originating from the Andes and the Amazon basin and transported by the Amazon into the Atlantic Ocean (Anthony et al., 2010). Only 20% of the sediment is transported in the alongshore direction from the delta to the northwest in suspension (Figure 2.13) and 40% of this part accumulates in large mudbanks all around the coast. The dimensions of these mudbanks are variable; their lengths can raise up to 60 km long and 30 km wide with a thickness of maximal 10 m. Mudbanks do not reach deep water and are not found past the 12m isobath (Augustinus, 2004). The interbank areas indicate the areas between the banks. These interbank areas range up to 25km long and are known for strong erosion processes at the coast (Figure 2.14). These mudbanks have an alongshore migration velocity of approximately 1 up to 5km per year (Anthony et al., 2008) and are driven by ocean waves and coastal currents.

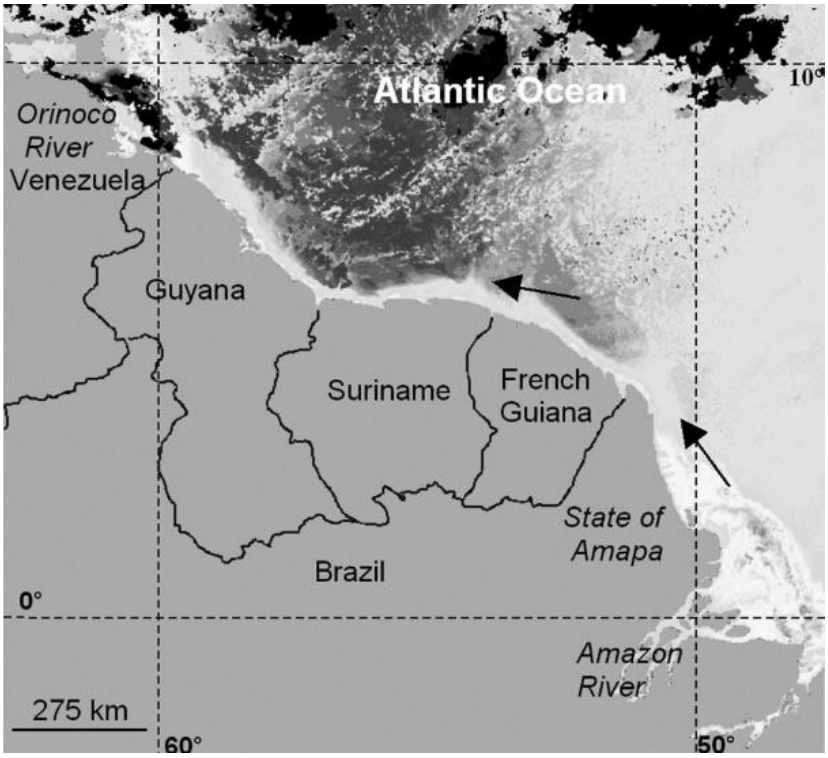

Figure 2.13: Sediment transport along the Guiana coastline given in arrows. The mud is visible as a white colored band around the coastline (Gardel et al., 2005).

This coastline is known for its large number of mangroves protecting the shore from erosion (Toorman et al., 2018). The Suriname coastline and its mangrove-rich shoreline are disrupted by multiple smaller rivers, including the Suriname river flowing through to the capital of

Suriname, Paramaribo. For all countries along the A-O coastline, its circumstances as wave environment, sediment, geology, and climate are very similar; hence, most researchers assume the system to be one overarching system: the Guiana's. The only apparent difference between the Suriname coastline and Guyana and French-Guiana is its west-east orientation compared to the northwest-southeast orientation of the latter (Anthony et al., 2014).

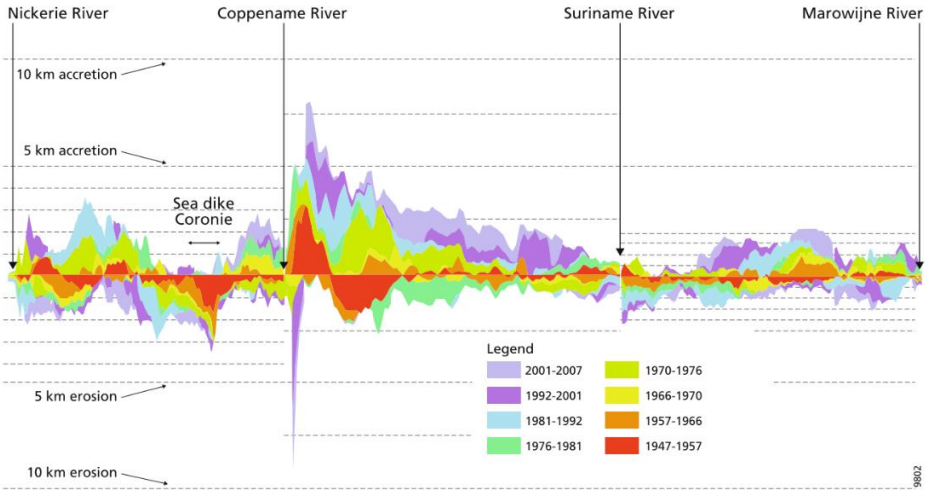

Figure 2.14: Periods of erosion and accretion for the coast of Suriname. The amount of erosion is given on the Y-axis. Periodicity in the accretion/erosion is very visible alongshore (De Jong et al., 2021)

Since the beginning of the Holocene, the Guiana basin has been an accretion belt of fine mud, and these sediments are overlying the crystalline Guiana shield (Augustinus, 1978). Because of the movement of the banks, the coastline is prone to periods of erosions and accretion. Gratiot et al. (2007) calculated a sediment deficit, which means erosion, for the French Guiana coast in the period 1988-1999, this trend reversed after 2000, and a period of accretion occurred. This trend is visible in Figure 2.14, where the periods of coastline change are measured. In Suriname, there has been net accretion of the coast for the last 60 years, except for Paramaribo at the mouth of the Suriname River. Here is, of course, dredging going on to ensure access of ships to the harbour of Paramaribo, combined with much traffic disturbing the natural settings. Augustinus (2004) observed a similar cycle of accretion and erosion of approximately 18 years, corresponding to the mudbanks' travel speed (Wong et al., 2017).

2.3.2 Hydrodynamics

Different processes influence the hydrodynamics of the Suriname coast and thus influence the alongshore morpho-dynamics of the coast. There is the influence of the trade winds, local winds, tides, local rivers, and the Amazon river and different swells with different angles of incidence (Augustinus, 1978). This makes modelling wave behaviour for the Suriname coast a challenge. The Guiana Current, which flows northwest, follows the Guiana coastline as an extension of the North Brazilian Current. This North-Brazilian current is a product of the trade winds that dominate with a NE to SW direction (Augustinus, 2004). The wind direction is seasonal but has an average NE direction. However, during November-March, the winds are stronger, leading to increased wave height and possibly an increase in mudbank migration.

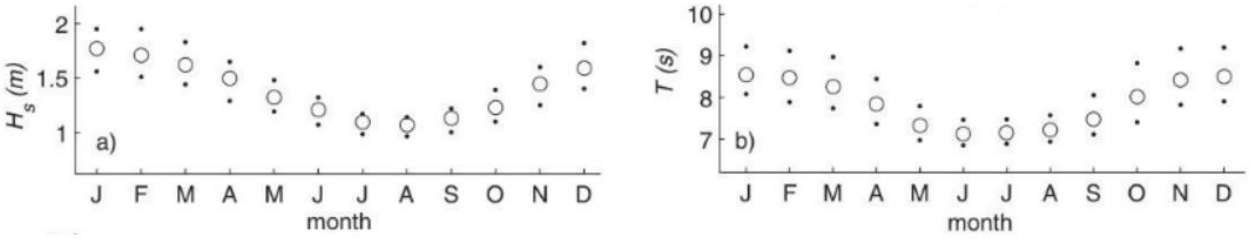

Figure 2.15: ERA-40 wave data. On the left the significant wave height and on the right the wave period. The ERA-40 data is from a 44-year record (Gensac et al., 2016). The large rounds are the averaged values and the dotes indicate one time the standard deviation

Trade winds cause a constant wave input from the same direction (Augustinus, 1978). These waves have an average significant wave height of 1.5 m and a wave period between 6 and 8 s. Figure 2.15 illustrates that the wave height is highest between November and March with a height of 2.0 m which coincides with the strongest trade winds. These waves have periods between 8 and 9 s. Larger waves originate from storms in the North Atlantic or hurricanes from the Mid-Atlantic/Caribbean region, having a more significant period (>10s) and wave heights exceeding 2 m. These waves come from a different direction than those generated by the trade winds and can differ from NW to NE (Van Ledden et al., 2009).

The tides at the Guiana coast are semidiurnal, and spring tides can reach up to 2.8 m intervals, while the neap tides only have a 1 m interval. The tidal currents operate perpendicular to the coast (Tzampazidou, 2020). The alongshore current gives a zigzag pattern of particles moving alongshore towards the west (Augustinus, 1978), driven by both the tide and the dominant wave direction. This pattern is illustrated in Figure 2.16.

The mangrove coast of Suriname has multiple relatively small rivers compared to the Amazon. The largest is the Suriname river, close to Paramaribo, with a discharge of 426 m^3/s. These smaller rivers bring fresh water and sediment into the system. This sediment is coarser (300-600 μm (Augustinus, 1978)) than the fine Andes sediments brought into the system by the Amazon river (Anthony et al., 2014). These sandy sediments support the formation of the so-called cheniers (sandy and shelly beach ridges), but their interaction with the mudbanks is not known. (Augustinus, 1978).

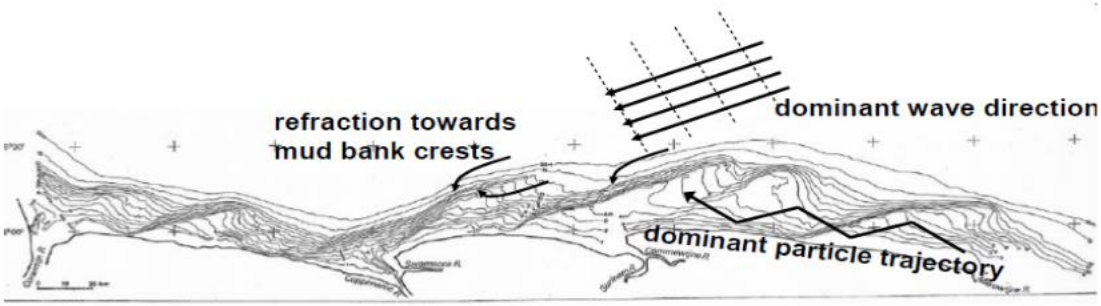

Figure 2.16: Sketch by Augustinus (1978) of the mudbanks for the coast of Suriname. In this sketch the bathymetry of the mudbanks is visible and the dominant wave direction and particle trajectory are included

2.3.3 Morphology

The migrating mudbanks play a significant role in the morphodynamics of the Guiana coastline. The prevailing trade winds force the Guiana current towards the coast, preventing the sediment from flowing into the deep ocean (Augustinus, 2004) and causing the mud to stay close to the shore in a band of 30km. Shorelines protected by a mudbank have net accretion and provide a suitable environment for pioneer mangroves to settle. Shorelines in the interbank zone are not sheltered by a mudbank and experience erosion of the shoreline and the previously settled pioneer mangroves (Froidefont et al., 1988). These mudbanks travel westward and have a variable but estimated return period of 30 years (Augustinus, 2004). These mudbanks are triangular shaped and attached to the shore by a mudflat (Figure 2.17). These mudbanks contain the equivalent of one year's supply of the Amazon river, 8 x 10^9 kg (Anthony et al., 2010). As illustrated in Figure 2.17, the banks have a trailing edge on the east which is exposed to erosion by the incoming waves from the NE. The impact of the wave will mobilize the mud and bring it into suspension. This fluid mud is transported by the waves and the alongshore current (a combination of wind and the Guiana current). The crest of the mudbank has a direction perpendicular to the incoming wavefield. This means that the mudbanks are not perpendicular to the coastline itself and can differ over the length of the coast, as can be seen in Figure 2.18 (Nedeco, 1972).

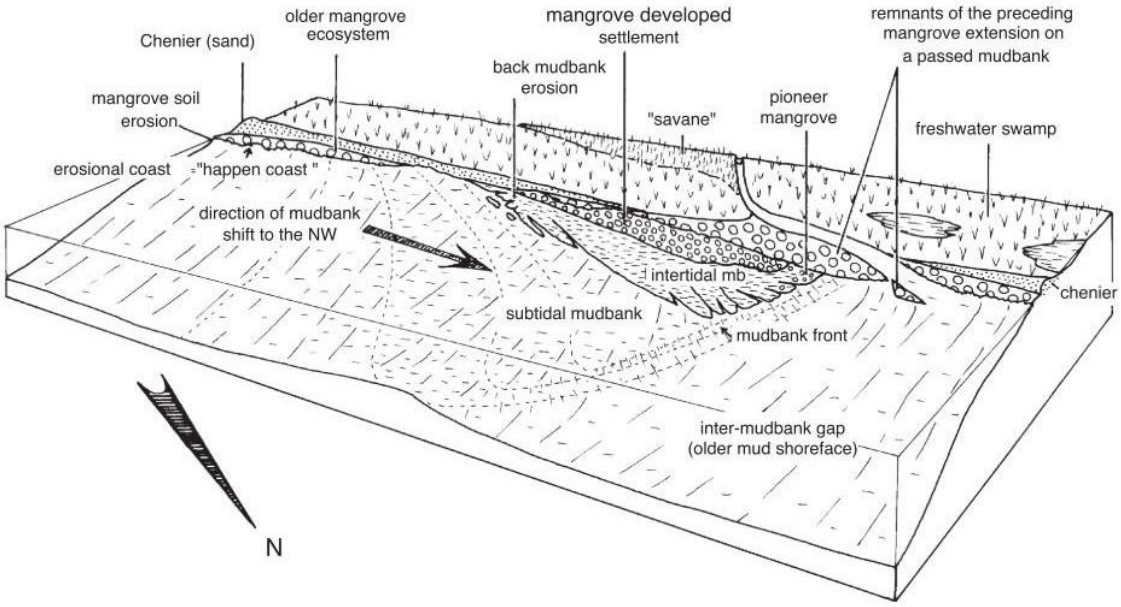

Figure 2.17: Outline of a mudbank with mudflat for the Guiana coastline (Augustinus, 2004). Showing the sloping side of the mudbank and the steeper mudbank front. The interbank is included with cheniers.

The mud thickness can be up to 10 m, but the fluid mud that plays an essential role in the wave damping is only up to 2 m thick. The rest of the mud is consolidated as the bed (Toorman et al., 2018). The formation of cheniers takes place at some regions of the coasts where coarser sandy sediments are found. Cheniers are crest-formed ridges formed by sandy deposits (Figure 2.17). These sands come from existing deposits or are transported by the smaller rivers. These ridges are abundant in places with higher wave energy and eroding coastlines. Because they are more resistant to wave energy and erosion, these circumstances characterize interbank areas, and cheniers are present in these areas (Augustinus, 1978).

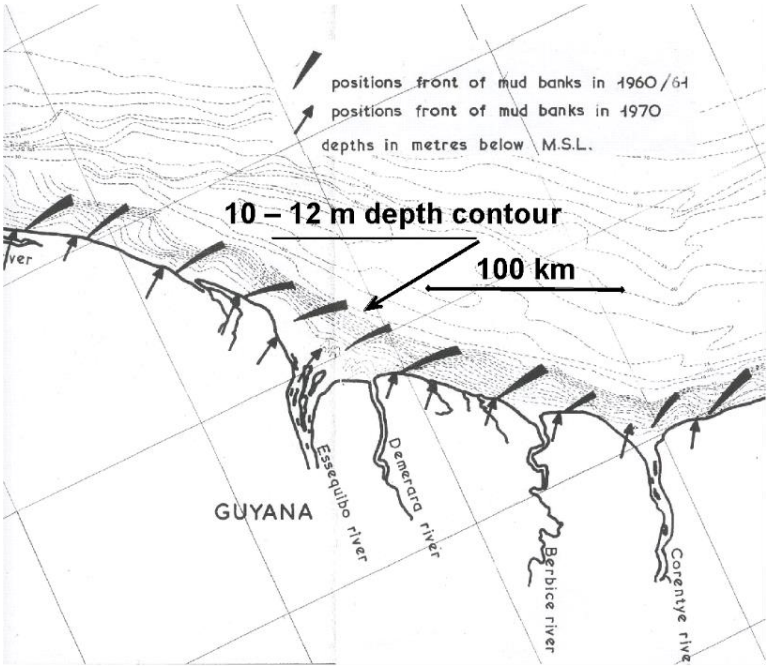

Figure 2.18: The position of the crest of the mudbanks and their relation to the bottom contours and the orientation of the coastline. Also, the older location of the banks is included (Nedeco, 1972).

2.3.4 Coastal threats

The Suriname coastline is a relatively low-lying land, making it prone to sea-level rise, marine flooding and erosion. Mangroves forests are capable of energy dissipation, this way, they protect the land lying behind them (Toornman et al., 2018). During the last decades, the mangrove forest has been cut down to change the land into shrimp/fish ponds or polders for farming. The mangroves trap sediment and stimulate wave damping in areas not protected by mudbanks. Without these mangroves, coastal erosion will significantly increase, and rigid structures are necessary to reinforce the coast. In some places in Suriname, the coastline is reinforced with dikes. Some 'Building with Nature' projects have been launched to replant mangroves in the area without significant results (Wetlands international, 2016). The rigid structures will protect the land lying behind but will stop the sediment influx inland and so stop the land from keeping up with sea-level rise (Nedeco, 1968).

Oil was first found in the Guiana region, making Suriname an exciting location for large oil companies. However, no significant environmental impacts have been observed caused by these activities. The impact on the mangroves is immense as they have to be cut down to make room for waterways for ships and pipelines and for the drilling islands. Recently more oil was found in front of the coast of Paramaribo. Simpson et al. (2012) studied the sea-level rise and climate change in Suriname. This study found an accelerated sea-level rise which increases the risk of flooding and an increased chance of salt intrusion, which is also correlated to the hard-coastal protection. Following Simson, who also investigated the results of climate change on tourism, infrastructure, and GDP, the country is already vulnerable to an enormous impact on these sectors because of the low-lying shoreline. For example, salt intrusion could influence the agricultural sector, mainly found in the polders. It is expected that the sea-level will rise by 3.1 mm/year on the Suriname coast, which is close to the global average (Simpson et al., 2009).

2.4 Methods

2.4.1 Debugging SWAN-Mud

This section discusses the model setup for the three different experiments. But before, the debugging steps for SWAN-Mud are explained, which is important as some calculation errors were found in the process of this study. The most important calculation error found in this study is explained below. For each experiment, different model components are discussed: computational grid, bathymetry, physical processes, and boundary conditions for the experiments. Most of these components of the experiments differ for the three model set-ups. They will be discussed separately in the subsections following the debugging section.

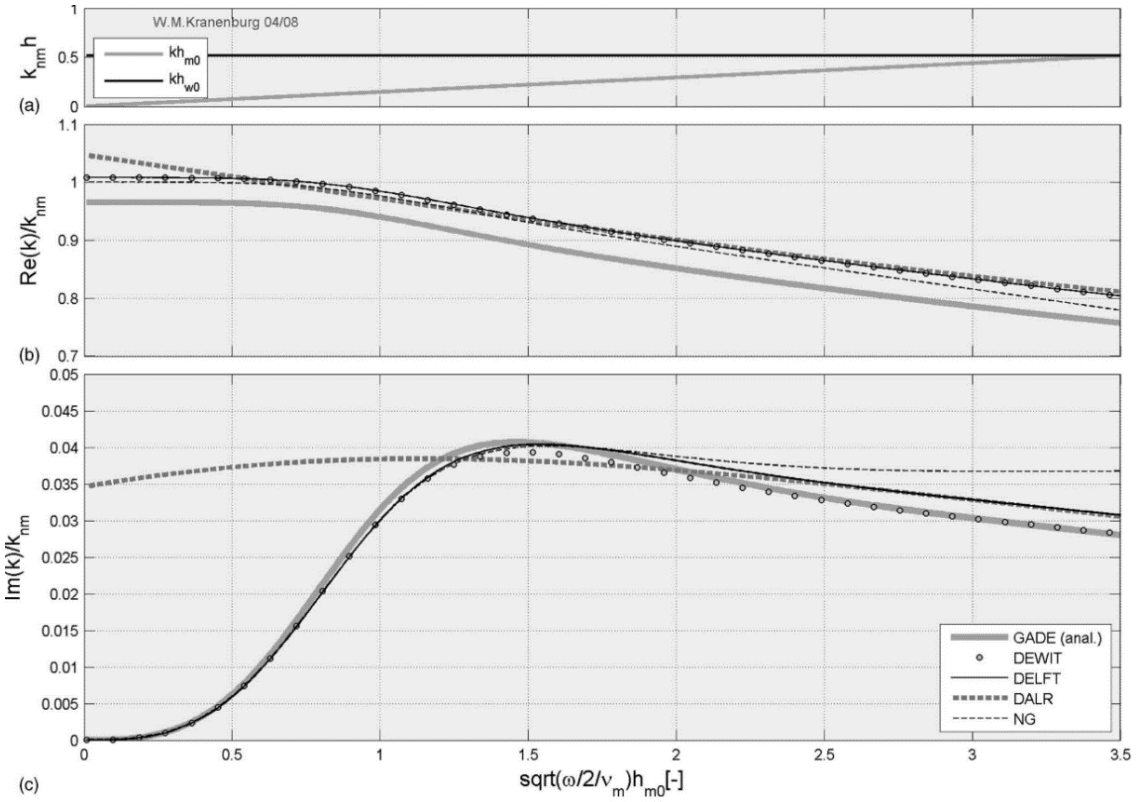

Figure 2.19: The optimal mud layer height test done by Kranenburg (2011). The upper figure shows the thickness of the mud layer, the middle shows the real wavenumber and the bottom figure shows the imaginary part of the wavenumber. Note that this is not a transect but a graph with single point calculations for different mud thicknesses. Model inputs: H_s= 4 m, T_p=8s,ρ_m= 1750kg/m^3 and ν_m = 0.5 m^2/s. The x-axis is scaled with the boundary layer thickness $\delta_{bl} = \sqrt{\frac{2\nu}{\sigma}}$and the y-axis is scaled with the wavenumber for situations without fluid mud.

Tzampazidou reproduced an experiment done by De Wit in 1995 to compare the new DeWit method with the older Gade method ("Optimal Mud Layer Height Test" in Tzampazidou, 2020). Kranenburg conducted this same experiment in 2011 to compare his new Delft method with the Gade, Ng, DeWit, and Dalrymple methods. The experiment seeks an optimum in the wave damping for different mud layer thicknesses. The mud layer in this experiment is flat and homogeneous in thickness and concentration.

This test is 1D (Figure 2.19); essential to note is that this is not a transect but rather a summation of multiple tests with a variating mud layer. This test is conducted for an increasing mud thicknesses, ranging from 0.01 to 3.5 meters. When visualizing this data graphically, an optimum for the imaginary wavenumber is found; this is almost similar for all methods. The real part of the wavenumber decreases when the mud thickness increases. Simultaneously, the imaginary wavenumber increases and reaches an optimum when the mud is approximately 1.3 times the Stokes boundary layer (Gade (1958), Ng (2000) and Kranenburg (2008)) and after it decreases slightly.

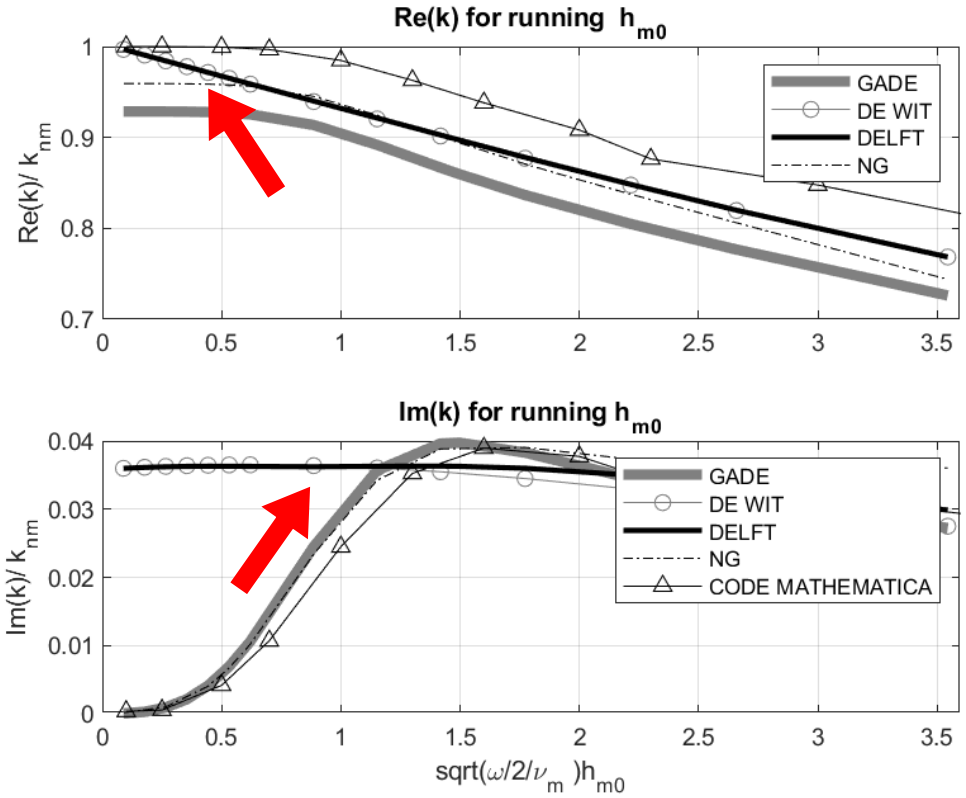

Figure 2.20: The Optimal mud layer height test done with the SWAN-Mud version of Tzampazidou (2020). The same parameters are used as in Kranenburg (2011). The difference in the pattern is indicated in the top panel where the red arrow indicates the lack of change in pattern for the real wavenumber. The red arrow in the second panel shows the lack of optimum in the imaginary wavenumber. Model inputs: Hsig= 4m, Tp=8s,ρ_m= 1750kg/m^3 and v_m = 0.5m^2/s. These axes are not scaled (Tzampazidou, 2020)

The results obtained by Kranenburg (2008) are provided in Figure 2.19. Interestingly, Tzampazidou's (Figure 2.20) results did not correspond for the DELFT and DeWit method with Kranenburg's (2008) results. For these methods, no optimum in imaginary wavenumber was received while the real part did not correspond either; these results are provided in (Figure 2.20). Noteworthy is that both studies used a different version of SWAN-Mud. The version used in this thesis is the most recent (September 2021), and before updating, the same results as Tzampazidou(2020) were obtained. Preliminary to the mud characteristics and wave environment experiments, this "bug" in the methods had to be solved. By comparing the methods to the analytically solved solutions in Wolfram Mathematica, mathematical errors in the different methods could be excluded.

The energy dissipation relationship for the DeWit method was not included in SWAN-Mud. Instead, it is proposed to use the dissipation relationship by Gade (Kranenburg, 2008). This method must be switched on manually, which is not an option in the Delft3D as was designed in this thesis. The output will only contain zeros when using this option. This problem was solved by adding a dissipation term in the source code of SWAN-Mud. This function was first tested in Wolfram Mathematica and then included in the source code. The results of the debugged DELFT and DeWit method will be discussed in the results section. Smaller debugging attempts and small changes in the code will not be discussed in further detail.

For this study, there are three groups of experiments. The first two are idealized experiments in order to answer the research questions. The first experiment is in 1D and the second in 2D. The third experiment is designed to test the research questions and the model for a realistic case study. In these three experiments, different variations are tested, and different parameters are used. These are all discussed in the next sections.

2.4.2 Research Question 1

After SWAN-Mud is debugged, the new version of the model can be used to answer the first research question. This experiment can be performed in SWAN-Mud as a stand-alone model. The first research question is: **Which characteristics of the "fluid mud" are most important for the mud-induced wave damping and why?**

To answer the research question, the sensitivity of the model for the following characteristics is tested: mud viscosity, mud density, mud layer thickness, and water layer thickness. The focus will be on the DELFT and DeWit methods as they are the most complete and least limited. Since Gade and Ng were known to be working correctly in SWAN-Mud, they were used as a verification method for DELFT and DeWit. Earlier research by Winterwerp et al. (2012) and Kranenburg (2008) focused on the mud layer thickness, and Winterwerp also researched the mud viscosity. But, besides the influence of the mud layer thickness and the mud viscosity, the density of the mud and the thickness of the overlying water layer are of interest. This experiment is a sensitivity analysis for all different mud characteristics for which different point calculations have been done. These experiments are performed for different water depths and mud layer thicknesses.

Computational grid & bathymetry

This experiment is separated into three series of experiments, all of them in 1D. These are divided in: One series of tests for the water layer thickness, one series for the mud layer thickness, and one to test the mud viscosity and density. For this experiment, the domain has a length of 4000 m. Except for the water depth test, the water layer is varied between 1.0 m and 4 m. For most of the experiments, the mud thickness is varied between 0.01 m and 3.5 m, while for the experiment concerning the water layer, the mud thickness is kept constant at 0.5 m. For these experiments, the domain has a constant water depth of 4 m. All parameters used in this set of experiments are summarized in Table 2-1: Parameters for the 1D-experiments

Boundary conditions

The significant wave height is 0.5 m, and the wave peak period is 8 s. All waves enter the domain from the West. There is no wind in these experiments; this means that Quadruplets and triads are also switched off in Delft3D-Wave. A commonly used JONSWAP spectrum was applied with a peak enhancement of 3.3.

Physical processes

Winterwerp et al. (2007) tested different viscosities for the mud layer, and it was found that a higher viscosity results in more wave damping. The influence of the viscosity of the mud layer will be tested in this study by using the "Optimal mud layer height test.". For these tests, the water viscosity is set to $1.0*10^{-6}$ m^2/s, while the mud viscosities range from 0.0001 to 1 m^2/s (based on Kranenburg et al., 2011). Similar results are expected for the present study.

Intuitively, mud-damping would increase with increasing density (McAnally, 2007). The same test as for the viscosity is conducted. For this test, the mud viscosity is kept constant at 0.00276 m^2/s as it is the default setting of SWAN-Mud (Winterwerp et al., 2012). At the same time, the water density is constant at $1010kg/m^3$. The tested mud density ranges from 800 to 2000 kg/m^3. All dissipation factors are accounted for (e.g., Wave breaking, bottom friction, whitecapping). However, the domain is very small and homogeneous, so no influence of these is expected. The incoming waves are also not high enough for depth-induced breaking at a water depth of 4 m.

Table 2-1: Parameters for the 1D-experiments

	Experiment 1 Mud density	**Experiment 2** Mud viscosity	**Experiment 3** Waterlayer thickness
Used Method	DELFT	DELFT	DELFT
Domain lenght [m]	4000	4000	4000
Wave height [m]	0.5	0.5	0.5
Wave period [s]	8	8	8
Water depth [m]	4.0	4.0	1.0 - 4.0
Mud thickness [m]	0.1 - 3.5	0.1 - 3.5	0.5
Water density [kg/m^3]	1010	1010	1010
Water Viscosity [m^2/s]	$1*10^{-6}$	$1*10^{-6}$	$1*10^{-6}$
Mud density [kg/m^3]	800 - 2000	1400	1400
Mud Viscosity [m^2/s]	0.00276	0.0001 - 10	0.00276

2.4.3 Research question 2

The second research question is defined as: **What is the influence of the wave environment on the mud-induced wave damping?** The sensitivity of the model results to the following wave characteristics is tested here: wave height, wave period, and wave direction. Furthermore, the influence of the wind is tested for both the wind direction and the wind speed. Noteworthy is that this test is only conducted for the DELFT method.

Computational grid & bathymetry

A rectangular grid is used with 500 by 200 grid cells and a cell size of 50x50m. The boundary effects are limited by using a large grid extent on the east side of the mudbank. Consequently, the waves at the boundary that have an unrealistic height compared to their distance from shore will not reach the mudbank or interfere with calculations. The water depth is constant at 6m over the whole experiment. The mud layer is positioned in the south of the grid with increasing thickness and rectangular shape; the mud thickness increases up to 2.0 m. The design of the mud layer is provided in Figure 2.21. The right panel shows a sketch of the implementation of the mud layer in the bathymetry. Important to note is that the mud for this test is implemented as is the standard in SWAN, which means the water column stays constant, and the mud becomes part of the bathymetry. For the 2D experiment, the mud is implemented as a mudpatch instead of a mudbank.

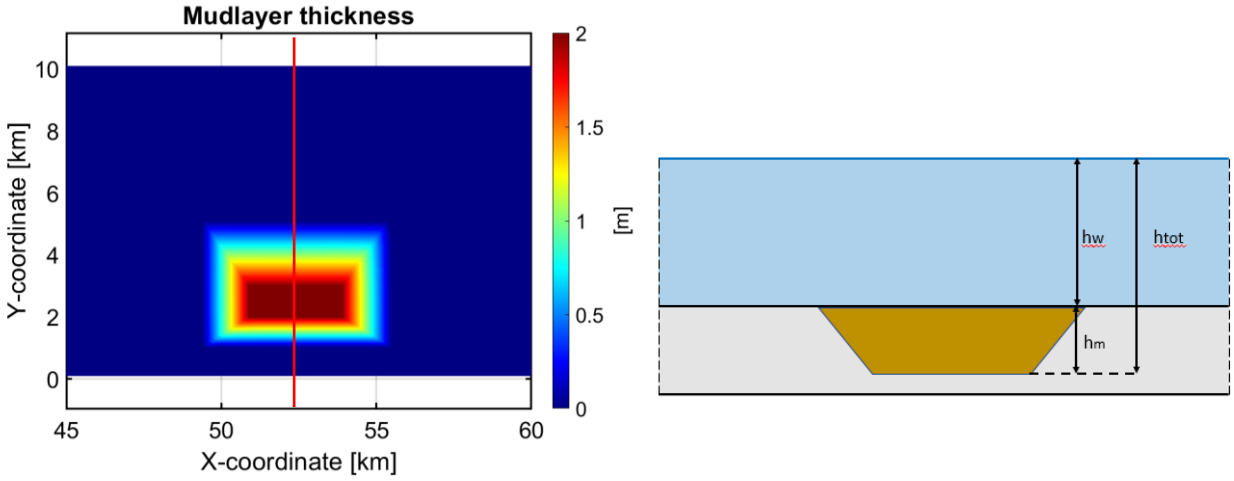

Figure 2.21: The mud thickness for the domain used in the 2D experiments, the grid extends further to the right, but this part is not of interest for this study (left). Conceptual sketch of the implementation of the mud in SWAN-Mud (underneath the water column) (right).

Boundary conditions

The focus was on the wave period to test the different wave characteristics. The wave height was tested based on the wave steepness, and if this is too high, waves will dissipate due to whitecapping. This steepness was calculated with Equation 55 and was limited between 0.01 and 0.04. Due to depth-induced breaking, the wave height cannot surpass 3 meters at a water depth of 6 meters. When the waves surpass this height, the waves will break due to depth-induced breaking. Three sets of experiments focused on the influence of the wave height and period on the rate of dissipation. The parameters for all experiments are given in Table 2-2.

$$Steepness = \frac{Hsig * 2\pi}{g * {T_p}^2} \tag{55}$$

The influence of mud on wave direction is tested for constant height and period (H_s = 1.0m and T_p= 8s). This is done in combination with researching the influence of the waves' direction on the rate of mud dissipation. The incoming wave direction is varied between the north (0 degrees) and east (90 degrees); the wave direction can be plotted as an output of Delft3D-Wave; here are different options for output; all of the outputs are in radials. These can be converted to degrees from the north so that the refraction can be visualized. Expected is that the mud layer has a similar effect on refraction as a sandbank would have, which means refraction towards the thickest part of the mud layer.

For the experiments regarding the wave height, wave period and wave direction, there was no wind included in the model (see Table 2-2). Two more experiments have been conducted to find the influence of the wind on the mud dissipation. The influence of wind on mud dissipation is discussed in multiple papers (Winterwerp et al., 2007). A similar experiment in Tzampazidou (2020) showed that total wave height over the mudbank is different for situations with or without wind. This is caused by wave generation by the wind, which adds to the energy balance. In these studies, wind-generated waves in higher frequencies were observed at the mudbank. It is expected to receive more dissipation by the mud as the wind causes the wave energy to increase. The wind will vary from onshore to offshore in 8 steps for the wind experiments. The wind force will be varied for an angle of 45 degrees with speed between no wind and 10 m/s. For these scenarios, the summer wave parameters are used.

Besides calculating the significant wave height and mud dissipation over the transect, the wave energy density over different frequencies of the wave spectra can be modelled. This indicates in which wave frequency most dissipation will happen. These points are offshore, at the beginning of the mud layer and the thickest part of the mud. These frequencies can be measured for wind angle and wind power experiments. Furthermore, a similar plot can be made for a whole transect perpendicular to the coast and visualized in a Hovmöller plot, which is often used to plot a certain output over the wave frequency along a transect. These plots show the wave energy density for the wave spectra along a transect.

Physical processes

The density of the water is similar to the other experiments 1010 kg/m^3 with a viscosity of 1*10^{-6} m^2/s. The mud viscosity is constant, with 0.00276 m^2/s over the whole mud patch and a density of 1400 kg/m^3. There is also wind growth and frequency shift of wind-generated waves with the wind switched on. All processes causing dissipation are switched on for these experiments to make the situation as realistic as possible.

Table 2-2: Table with parameters for all different experiments that have been tested for the 2D-idealized experiments

	Experiment 1 Wave height	**Experiment 2** Wave period	**Experiment 3** Wave direction	**Experiment 4** Wind
Used Method	DELFT	DELFT	DELFT	DELFT
Grid size [m]	250x100	250x100	250x100	250x100
Water depth [m]	6	6	6	6
Wave height [m]	0.1-4	1	1	1
Wave period [s]	8	3-14	8	8
Wave Direction [dgrs]	0	0	0-90	0
Wind speed [m/s]	x	x	x	1-12
Wind Direction [dgrs]	x	x	x	0-180
Water Density [kg/m^3]	1010	1010	1010	1010
Water Viscosity [m^2/s]	1*10^{-6}	1*10^{-6}	1*10^{-6}	1*10^{-6}
Mud Density[kg/m^3]	1400	1400	1400	1400
Mud Viscosity [m^2/s]	0.00276	0.00276	0.00276	0.00276

2.4.4 Test case: Suriname

The experiments in the case study for Suriname are similar to the idealized 2D experiments. As introduced in Section 2.3, the mudbanks play an important role in coastal accretion and erosion, and modelling studies in this area are limited. By providing more context for the test case, this thesis will contribute to the knowledge of the study area. Rather than only the reproduction of the idealized experiments and testing of SWAN-Mud and Delft3D-Wave.

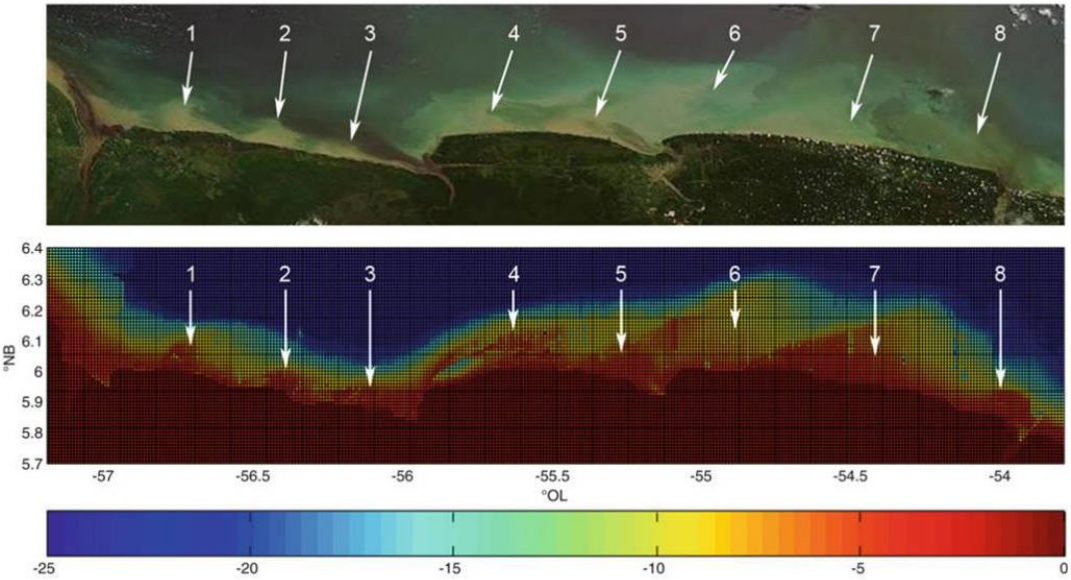

Figure 2.22: Top panel shows a satellite image from 2006, while the lower panel is a bathymetry image of Suriname in 2005 (Dewaelheyns and Emeo, 2007) with in both figures the mudbanks indicated with arrows.

The focus of the case study is divided into four topics. This will be the results of these experiments are analyzed and discussed. The first focus will be on the influence of the mudbanks in front of the coast for situations with and without mud, but also on the bank and interbank areas. Furthermore, wave scenarios will be tested with different energy levels, with variations in wave height and period but with constant direction. Local winds are thought to

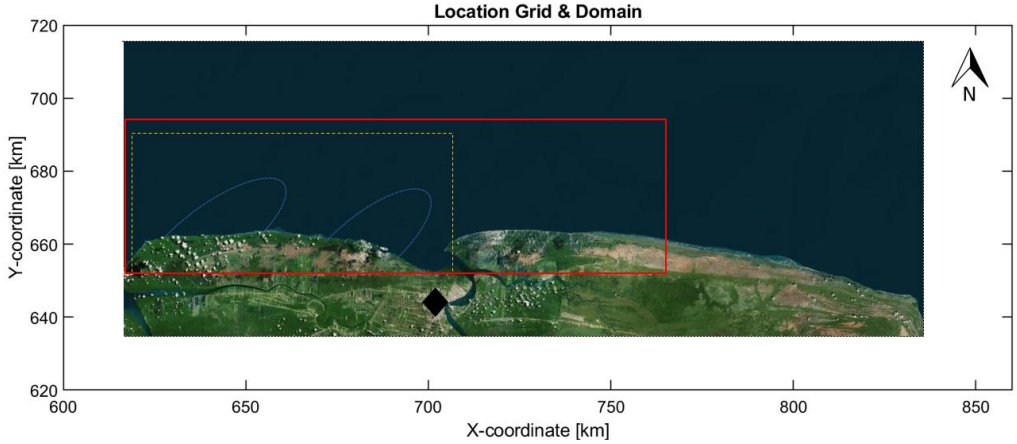

Figure 2.23: Computational grid, the domain and the estimated location of two realistic mudbanks. The yellow dashed box is the domain used for all the calculations. An estimation of two current mudbanks is given with the blue dotted areas; Paramaribo is indicated with the black square.

influence the wave environment when the ITCZ shifts over Suriname, mainly during summer (Solaun et al., 2021). This is analyzed separately as well. Lastly, the impact of storms with different angles is analyzed. In Figure 2.22 is visible where the mudbanks were positioned in 2005 and 2006 (Dewaelheyns and Emeo, 2007). Mudbank 4 and 5 from this figure were inspiration for the design of the mudbanks in this test case.

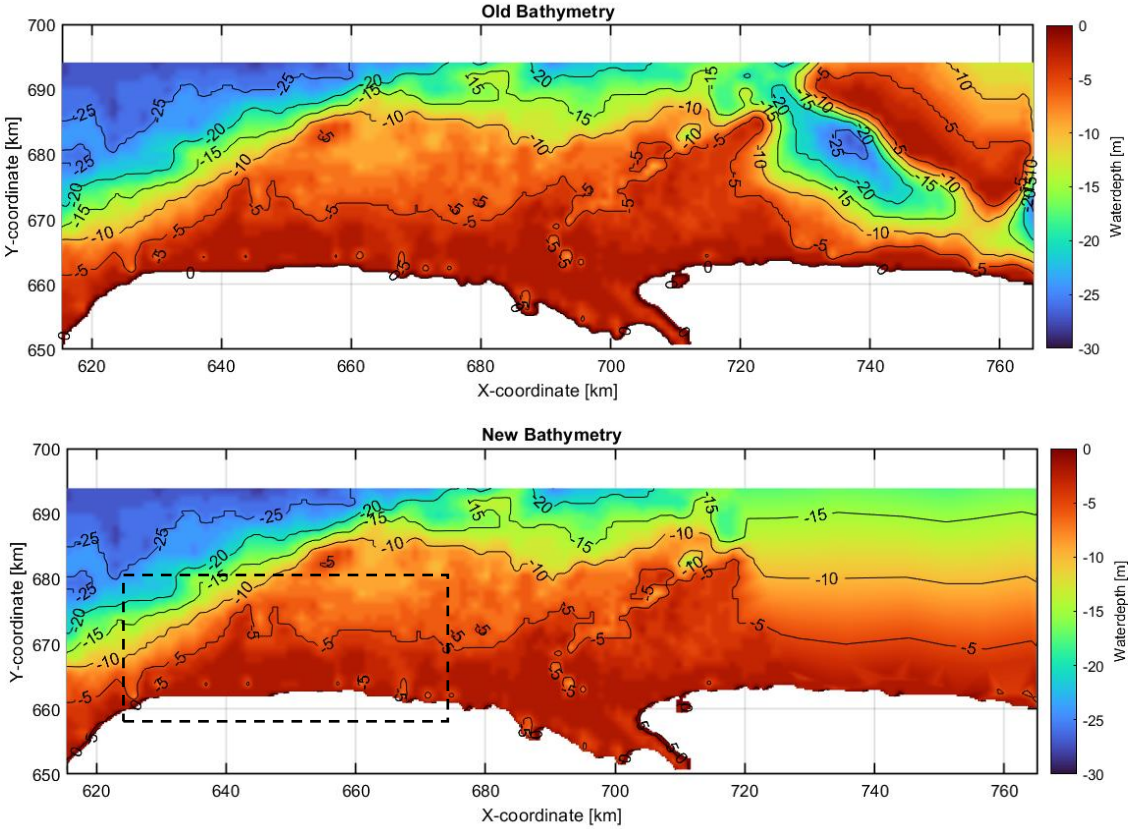

Figure 2.24: The old bathymetry with the deep section in the east part of the domain (top figure), the bottom figure shows the bathymetry where the deep section is replaced by a sloping bathymetry. The used domain is shown with the dotted box. The contours of the mudbanks is recognizable with the dark red colours.

Computational grid

For the Suriname test case, a grid was made using the open-source Delft Dashboard designed by Deltares. This application made it possible to draw a grid on a location of choice. The size of one grid cell is 250x250m to get the most detailed sketch of the actual situation. The grid is made more extensive on the north and east boundary to avoid boundary effects, especially on the east boundary, so waves do not have an unrealistic large wave height when reaching shore (see; this grid extension is used when the waves reach the shore with an angle. The total grid is provided with the red box in Figure 2.23. The yellow dashed box is the domain used for all analyzes. An estimation of two current mudbanks is given with the blue dotted areas, these are also visible in Figure 2.22, indicated with number 4 and 5, Paramaribo is indicated with the black square.

Bathymetry & Mud layer

The bathymetry was retrieved from the same Delft Dashboard, which uses GEBCO 2018 dataset. Discussion with experts helped confirm the accuracy of the bathymetry or its errors (De Vries, personal communications, 2022). For example, a very deep area in front of the coast of Paramaribo was found in the bathymetry, which is unlikely to be realistic. The bathymetry is provided in Figure 2.24, where the trough is found in the east. This deep part in the ocean interfered with the research results, so it was filtered out in RGFGRID (a preprocessing tool of Delft3D) and made of equal depth with the surrounding areas (see bottom Figure 2.24). In this way, there is no influence of unrealistic bathymetry on the computations over the mudbanks.

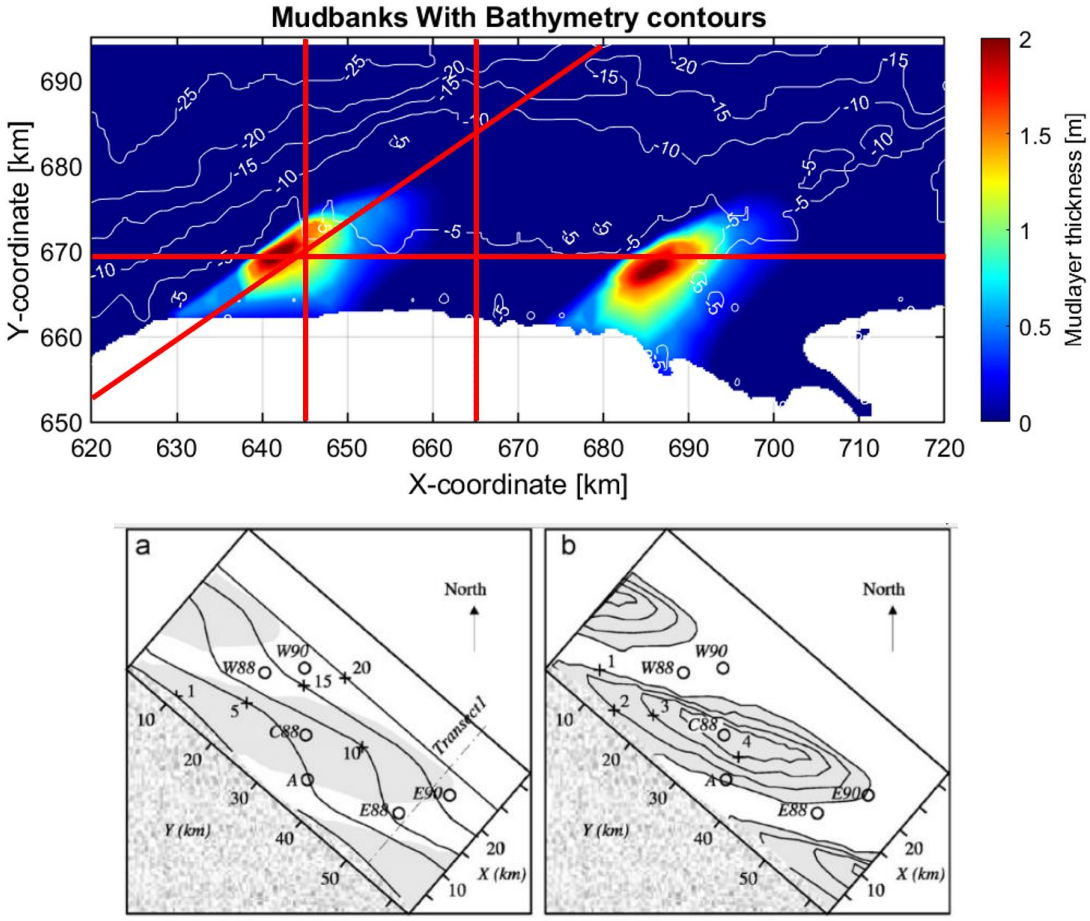

Figure 2.25: Thickness of the mudbanks shown with the isobath lines of the bathymetry. The dotted lines indicate transects used to analyze the results. The bottom figures show the mudbanks on the bathymetry contours and vice versa as designed in Chevalier et al. (2008).

The mudbanks (Figure 2.25) were designed after discussion with experts from the WOTRO group from Utrecht University (De Vries, personal communications, 2022) and on literature (Chevalier et al., 2008; Anthony et al., 2008). The location corresponds with two mudbanks currently located in reality at the given location, which are also recognizable in Figure 2.22. Also, satellite images are used, although similar problems as with the sonar are encountered, and a lot is still unknown about the intertidal part of the mudbanks due to the lack of measurements. The mud depth is indicated by contour lines of the bathymetry; here, it can be seen that the mudbanks stay inside the 10-meter depth isobath as described earlier in Figure

2.18, and the mudbanks point towards the incoming waves from the northeast. The thickest part of the mud is not shore-attached as described in Winterwerp et al. (2022).

Physical processes

Similar to the 1D and 2D experiments is, the viscosity of the mud 0.00276 m^2/s as it is the default value in SWAN-Mud, but also representative for the coast of Suriname (Anthony et al.,2010). The density of the mud is taken as 1400 kg/m^3, while the density of the water is 1010 kg/m^3. All variables used in the different scenarios are given in Table 2-3. The wind is switched on in all experiments, which means that in all these experiments, the wind-induced processes need to be taken into account (e.g., Quadruplets, Triads, Wind growth, and frequency shifts). All different dissipation processes are also considered (Whitecapping, Bottom friction, and wave breaking).

Boundary conditions

Wave data is taken from the ERA-5 model gathered for an offshore location in front of the Suriname coast (ERA-5, 2022). A worldwide model is used to project the wave data for the Suriname coastline at approximal 30km offshore. In this dataset, the seasonality of the trade winds is recognizable, and the data coincides with the few available field observations reasonably well (Hersbach et al., 2019). This data is visualized in multiple wind and wave roses for winter and summer (an example is shown in Figure 2.26). From this dataset, it can be concluded that the waves in the winter period are significantly larger in wave height (between 1 and 1.5m) and period (between 8 and 10s) (see Appendix D). The wave angle for the summer is more NNE than the NE/ENE direction of the waves in the winter (Winterwerp et al., 2007).

The wind is modelled by ERA-5 as well, also revealing seasonal variations. The wind data from ERA-5 is provided in roses to find trends (see Figure 2.26) (ERA-5, 2022), so can it be observed that the wind is incredibly stable in direction for the winter, and so are the waves. This wind is modelled at a distance from the coastline, so the local land wind does not influence the outcome. The Delft3D model, constructed as part of this study, as the grid only reaches 30km out of the coast and contains the part of the coast that is also influenced by local winds, different from the trade winds (Anthony et al. 2010). These offshore winds are often a lot smaller than the trade winds. Changing the wind over the whole domain is advanced and complex, this is not used in this study, and the wind is kept constant over every experiment. For most of the scenarios, the trade winds will be used over the whole domain, and only for two scenarios will the local wind be used. An example of the wind rose during the summer is provided in Figure 2.26. All the other wave and wind roses are given in Appendix C.

Different scenarios

Different scenarios are run to make realistic representations of the Suriname coastline to compare these results to literature and the 2D experiments conducted before. These scenarios are based on literature, the ERA-5 data, and expert experience. The main two scenarios are based on the main seasons in Suriname: Summer and Winter. These will be built up from the averaged data from ERA-5 and will be the foundation of the scenarios. All scenarios are tested with and without mud. So, the impact of the mudbanks is tested directly. Augustinus (2004) hypothesizes that the movement of these mudbanks is event-driven. Therefore, we will focus

mainly on winter because the summer is relatively calm, so all the other scenarios are based on the winter data. The winter scenarios are divided into strong winters for this study, with larger wave periods and wave heights than the average winter data. The same is done for mild winters with lower wave heights and periods. For both scenarios, there are two variants; one where only the wave height is altered from the average winter scenario, and one where only the wave period is changed.

Different storm scenarios are tested as storms influence the mud and the coast (Augustinus, 2004). These storms are constant in size and differ in direction to investigate the response of the mud in waves from different directions and the effect of refraction. These parameters are based on a storm in 2005 hitting the Guyana coast (van Ledden et al., 2009). Lastly, there are three summer scenarios with different wind angles to reproduce the effect of local winds in the model; one of these three has no wind. These scenarios can be found in Table 2-3, where all the different parameters of the scenarios are displayed.

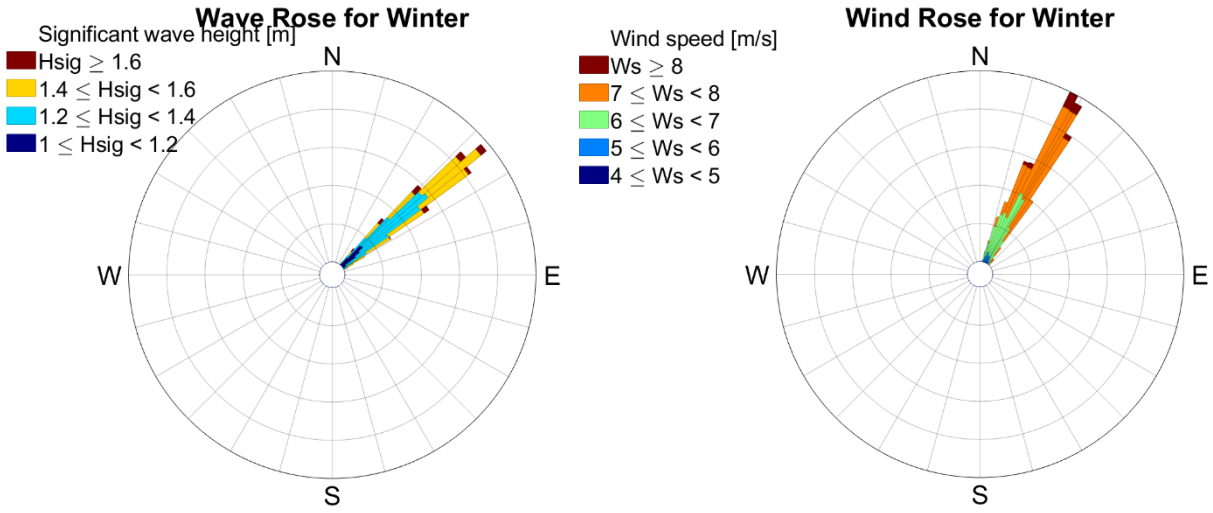

Figure 2.26: Wave and wind rose for Suriname during surmmer with ERA-5 data

Table 2-3: All parameters for the different scenarios. All scenarios are based on three main scenarios: Summer, winter and winter storm.

	Significant Wave Height [m]	**Wave Period** [s]	**Wave Direction** [degrees]	**Wind speed** [m/s]	**Wind Direction** [degrees]
Winter	1.4	7.5	46	7.0	60
Summer	0.9	6.6	40	5.5	78
Winter storm #1	1.8	10	60	7.0	60
Winter storm #2	1.8	10	10	7.0	60
Winter storm #3	1.8	10	40	7.0	60
Strong Winter #1	1.8	7.5	40	7.0	60
Strong Winter #2	1.4	10	40	7.0	60
Mild Winter #1	0.9	7.5	40	7.0	60
Mild Winter #2	1.4	6.6	40	7.0	60
Local Wind #1	0.9	6.6	46	5.5	120
Local Wind #2	0.9	6.6	46	5.5	180
Local Wind #3	0.9	6.6	46	x	x

3 Results

3.1 Debugging SWAN-Mud

3.1.1 Dispersion relation

This chapter is divided into a section discussing the dispersion relations for DeWit and DELFT. The results of the dissipation term added for DeWit are analyzed in the next section.

After coding errors in the dispersion relation for DeWit and DELFT were found and corrected, and inconsistencies in the source code of SWAN-Mud were removed, both the real and the imaginary part of the wavenumber seem to show correct results in line with the methods of Gade and Ng. Compared to the analytical solution of the methods, the results seem correct, and the dispersion relations are restored. The analytical solution is shown in Appendix C, with the SWAN output given with dots on top of the analytical solution. This shows that the correlation between the model and the analytical solution is very high. For the real part of the wavenumber, the difference between the debugged version and the old version can be found for non-dimensional mud thicknesses smaller than 0.7. The older versions do not decline between 0.5 and 1 (Figure3.1a), and their line remains linear over the whole domain. The other working methods bend around one and remain linear for a thicker mud layer. The results from DELFT are slightly lower than all the other methods.

The difference between the old and the debugged version is more profound for the imaginary part of the wavenumber. The debugged methods show an increasing pattern in the beginning until the maximum in imaginary wavenumber around 1.3 (dimensionless)(Figure3.1b). The old DeWit and DELFT methods have a more horizontal distribution. They show a high value when the mud layer thickness reaches zero, which is unrealistic as wave damping will then be very high when mud is almost zero. All dispersion relations show very similar results in the new version. These optima are about 1.2 to 1.4 times larger than the Stokes boundary layer. This is also described in the corresponding papers of each method (Gade, 1958; De Wit, 1995; Ng, 2000; Kranenburg, 2008).

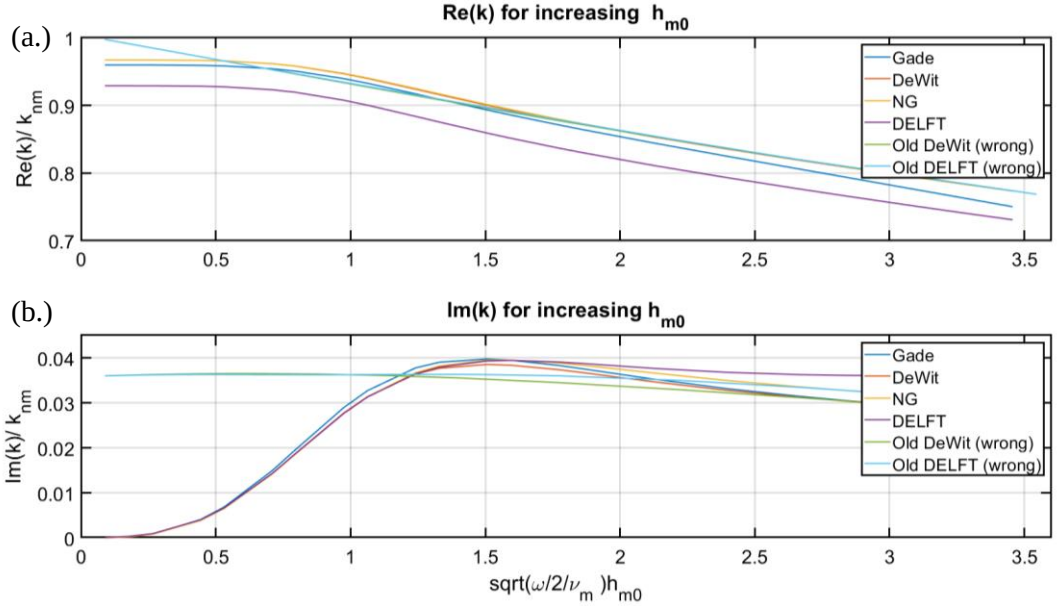

Figure 3.1: The "Optimal mud layer thickness test" (Tzampazidou, 2020) for the debugged DELFT and DeWit model compared to the other dispersion relations and the old versions of DELFT and DeWit as found in Tzampazidou (2020).

3.1.2 Dissipation term

In Figure 3.2, the maximum dissipation by mud is plotted against the non-dimensional thickness of the mud layer for all methods. This is done in the same way as in Figure3.1 but with mud dissipation on the vertical axis instead of the imaginary wavenumber. The figure shows that the trend similar for all different methods in the first half of the plot, which has the same characteristic incline and optimum as Figure 3.1. The Gade method does not decline after the optimum but stays more or less horizontal. For the other methods, the trend is the same, although the peak height is different. DeWit gives the lowest mud dissipation, followed by DELFT, while Ng gives almost double the mud dissipation of DeWit for the same conditions. The method by DeWit shows low results, which is unexpected as the results by DeWit should be similar to the DELFT method. However, the range on the vertical axis is very small, and so is the difference. The methods by Gade and Ng are very limited. Gade is only applicable for half of the domain, and Ng does not reach further than 0.6 of the dimensionless mud thickness. DeWit is applicable for almost the whole domain. In comparison, DELFT is known to have no limits in water depth or mud layer thickness.

Main findings:

1. The old methods do not show a maximum in the imaginary part and maintain an unrealistic high value when the non-dimensional mud thickness is almost zero.
2. The real part of the wavenumber shows differences between the new and old methods and a linear decrease for the bugged versions.
3. The new dispersion relations show an optimum for the imaginary part of the wavenumber corresponding to the Ng and Gade method.
4. The dissipation term of DeWit shows smaller values than DELFT as a function of the mud thickness, although the pattern is very similar.

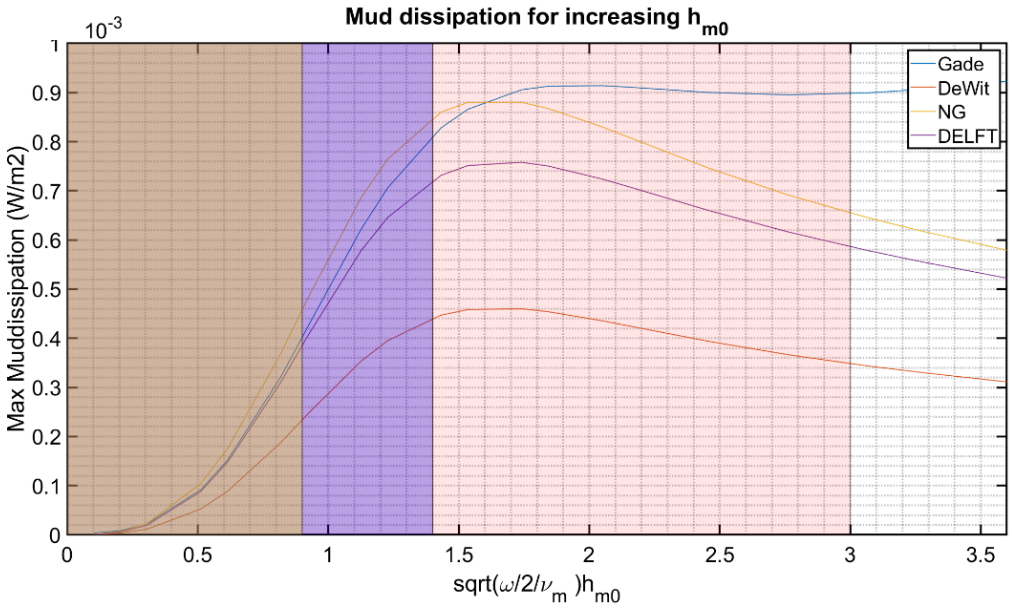

Figure 3.2: The Mud dissipation for the optimal mud layer height as given in the previous figure. The limits of the different methods are given in the same colors as their line.

3.2 1D- Experiments

3.2.1 Water and mud layer thickness

Figure 3.3a visualizes the wavenumber's imaginary part for all methods against the dimensionless mud layer thickness, with an overlying water column of 4 meters. A peak between 1.5 and 2 of the dimensionless mud thickness is shown for all methods. The peaks for the different methods are just slightly different, where DELFT has its peak more towards 1.5, followed closely by DeWit, and Gade and Ng show a peak more towards 2. After the maxima, the methods all follow a different trajectory, but all methods decline (and thus rate of mud dissipation) when the mudlayer becomes to thick. Gade remains high at around 0.035. DELFT drops towards 0.032, slightly higher than DeWit and Ng. These values are dependent on the extend of the horizontal axis, nevertheless they indicate that Ng and DeWit seem to reach each other for thicker dimensionless mudlayers. While Gade and DELFT both deviate slightly in this part of the graph. This indicates a difference in the rate of the decrease in the imaginary wavenumber as a function of the mudlayer thickness.

Figure 3.3b shows the k_i for a decreasing waterlayer thickness. This plot looks different from the test for the mud layer thickness (left). In the first place, the results are almost identical for all methods. Furthermore, the imaginary part of the wavenumber increases exponentially with the water level decreasing.

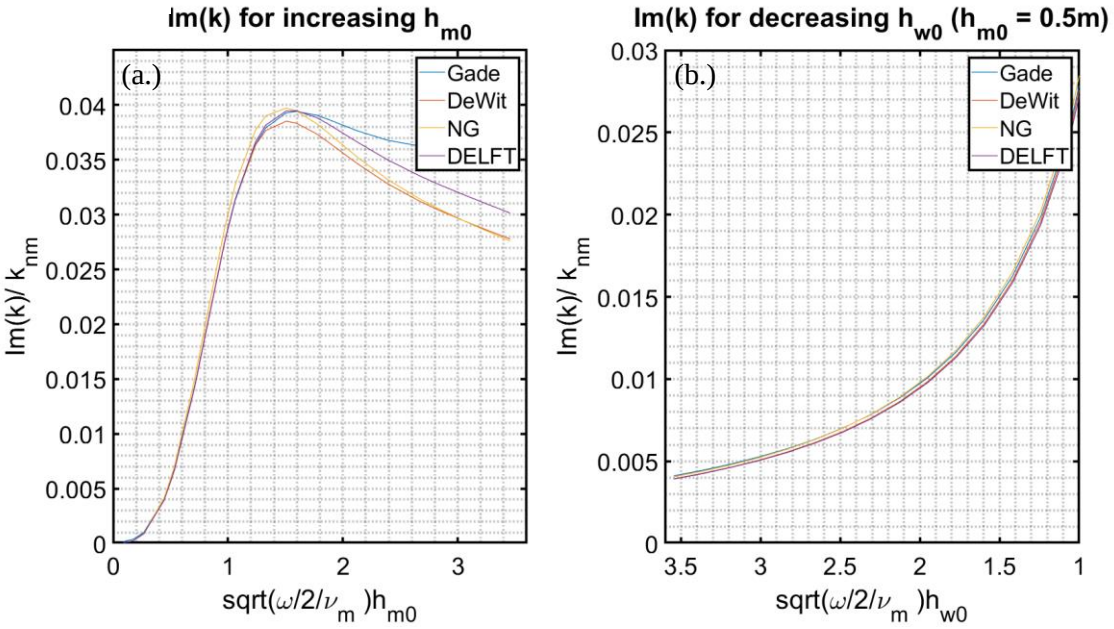

Figure 3.3: a: The optimal mud layer thickness for an increasing mud thickness. Both figures are dimensionless. b: The normalized imaginary wavenumber for a decreasing waterlayer with a constant mud layer

3.2.2 Viscosity and Density

Figure 3.4a shows the optimal mud layer height test with the DELFT method for different mud viscosities. Higher viscosities correlate with a higher peak for the wavenumber's imaginary part, representing the mud dissipation. The maximum imaginary wavenumber (i.e., maximum dissipation) is found at the same mud thickness for all different viscosities. The increase in the imaginary wavenumber is not linear with the increase in viscosity. Instead, the wavenumber increases almost exponentially with the viscosity.

It is visible in Figure 3.4b that the lower densities result in a higher k_i for the thinner mud layers. This changes around approximately 2.8 m, from this point, the k_i is higher for the higher densities. The imaginary wavenumber peak for each mud density shifts to thicker mud layers with increased density. The peak of the imaginary wavenumber is found for the smallest density (1000 kg/m^3) at a mud thickness of 1.1 m, while the peak for the largest density (2000 kg/m^3) is around 1.4 m.

Main findings:

1. The mud layer thickness shows an optimum thickness close to the Stokes boundary layer. There are small variations in the location of this optimum for all methods.
2. The thinner the overlying waterlayer, the higher the imaginary wavenumber. This increase is exponential and similar for all methods.
3. Increasing mud viscosity evokes an increase in the imaginary wavenumber.
4. An increase in the mud density causes a lower imaginary wavenumber up to a mud thickness of 2.5. Above this, a higher mud density results in a higher imaginary wavenumber.

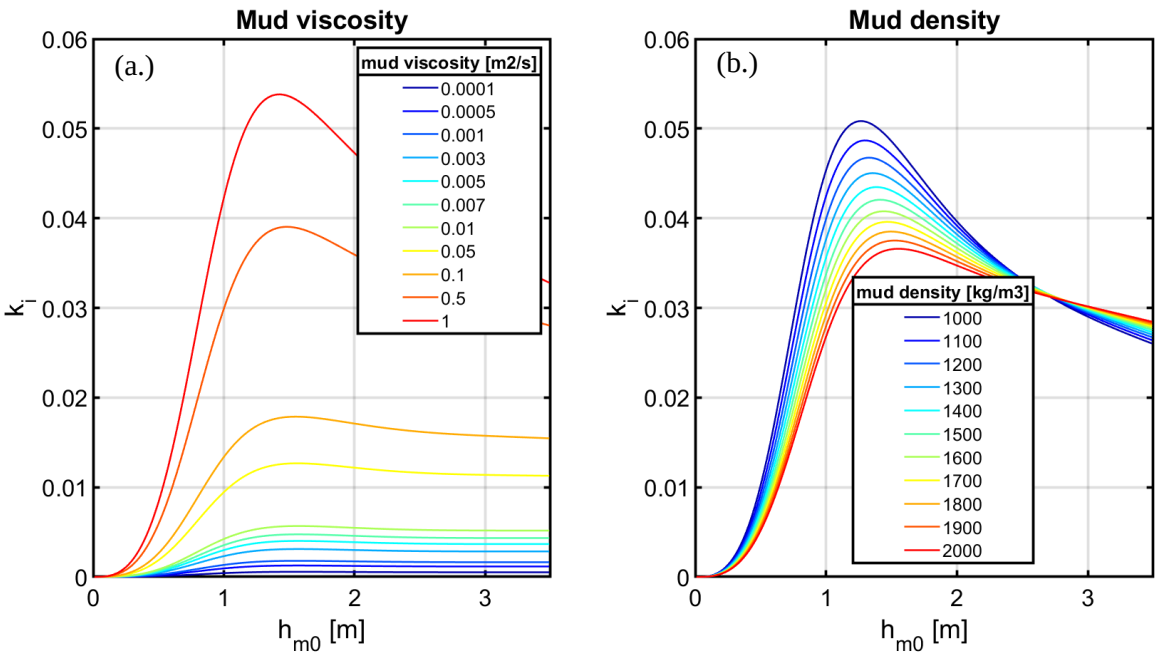

Figure 3.4: The optimal mud layer height test for on the left different mud viscosities and on the right different mud densities. Note that these axes are not dimensionless. The density used for the viscosity tests is 1300 kg/m^3 and the viscosity used for the density tests is 0.00276m^2/s. These are both the default settings of SWAN-Mud

3.3 2D – Experiments

3.3.1 Wave height and period

The mud dissipation for the transect over the mud layer is given in Figure 3.5a and d. For all transects is the offshore location given in the right side of the plot. The waves propagate to the left, which is the shore (this is with exception of the alongshore transect). Scenarios with a constant wave peak period (8 s) are tested with different significant wave heights. The mud dissipation is zero when there is no mud present. As soon as the waves reach the seaward edge of the mud, the dissipation shows a very large peak, which gradually declines until the landward edge of the mud. From this point, the mud dissipation goes to zero. With an increase in wave height, the mud dissipation seems to increase to almost 3 W/m^2, which is more than ten times the height of the peak for the smallest wave height (less than 0.1). After reaching this high peak, the dissipation follows the same trend for all scenarios; they decrease gradually over the transect but will not reach zero until the edge of the mud. The increase in wave height causes a direct increase in mud dissipation.

Figure 3.5b illustrates that the highest waves drop the most in height. Nevertheless, they also remain the highest at the end of the mud. Thus, the largest waves remain most of their height at the end of the mud. The effect of the mud on the wave period (Figure 3.5c) is similar for all situations, a steep drop where the mud is present from 4.8 s to 3.5 s. Except for; the scenario with a wave height of 1.4 m drops slightly more to 3.3 s. This extra drop in wave period is minor. The 1.0-m scenario experiences less of a decline to 3.6 s. Both these differences are around 0.1 s.

Figure 3.5d shows the mud dissipation waves with a constant wave height but variating wave periods. With increasing wave period, the mud dissipation does not seem to increase with the same amount as the increasing wave height. The mud dissipation only increases for the different scenarios until the scenario with a wave period of 10 s. This is when the increase in dissipation seems to reach a limit, and the peak of the mud dissipation only moves offshore slightly for the larger wave periods (>10). Furthermore, this peak seems to be as large or even slightly smaller for very large wave periods larger than 12 s compared to the periods of 10 and 11 s. The vertical axis scale is much smaller for the experiments with different wave periods compared to the experiment with different wave heights (Figure 3.5a).

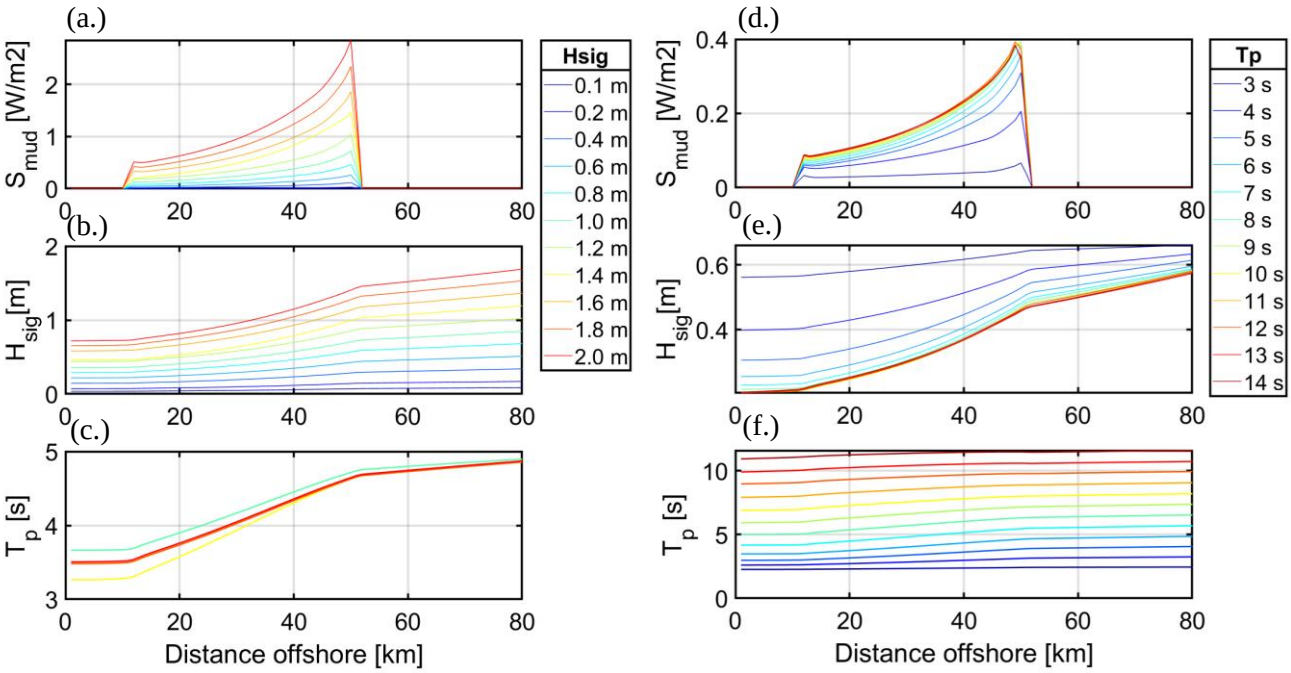

Figure 3.5: Transects of different experiments with the same wave period but, with different wave heights (a-c) and different wave periods for different wave periods (d-f). The dissipation by mud given in (a & d), wave height in (b & e) and wave period in (c & f).

Figure 3.5e illustrates that the waves with the small wave periods remain most of their height and only drop a little in wave height. Here is also visible that when waves have longer periods than 8 seconds, the wave height drops at the same rate, no matter the wave period. This corresponds to the dissipation by fluid mud. Figure 3.5f visualizes different wave periods. Here is visible that there is a different trend for the different wave heights. The waves with periods smaller than 8 s decline in wave period when travelling over the mud. Waves of over 8 s first increase slightly (less than 0.2 s) before declining. For all scenarios, a wave period drop between the seaward edge and the nearshore edge is visible.

The patterns are very similar for all different experiments; a large peak at the beginning of the mud followed by this gradual decline until the end of the mud. Here it drops to zero as no mud is present in this part of the transect. In Figure 3.6, all wave parameters are tested with different peak wave periods and corresponding significant wave heights. The two black lines indicate a steepness of 0.01 and 0.04. A similar transect in Figure 3.5 is used by averaging the mud dissipation over the mudbank's length to indicate the average mud dissipation for different periods and heights. As can be seen, the lowest values are found for the small periods and heights, while the highest values correspond with high periods and heights. Noteworthy is that

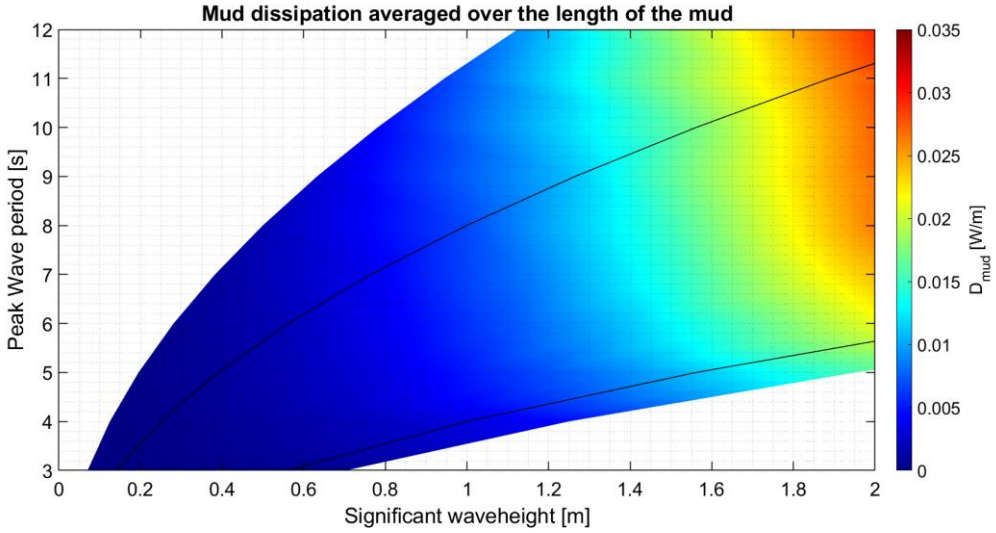

Figure 3.6: This plot indicates the integral of the mud dissipation for waves with different wave periods and their corresponding wave height that is calculated in view of the steepness, which does not surpass 0.05. The integral is calculated for the whole length of the mudbank.

the increase in dissipation is limited in the vertical direction. This means that the dissipation does not increase (significantly) when the wave period increases (from bottom to top) for a certain wave height. When looking horizontally at this graph, the increase is very steep. So, the mud dissipation increases for each wave period when the wave height increases (left to right). This result corresponds with the earlier findings from Figure 3.5, indicating that a change in wave height affects dissipation more than a change in wave period.

3.3.2 Wave angle of incidence

Waves with different angles of incidence have been plotted over the idealized mud layer (Figure 3.7). Panel a shows waves coming from the north (0 degrees), and the right panel shows incoming waves from 30 degrees from the north. The angle of incidence is in both plots given in green. It can be observed that the figures both show higher angles than the angle of incidence on the west side of the mud and lower angles on the east side of the mud. This means that waves refract away from the mud, which contradicts what was discussed in the method section.

Over mudbanks, the effect is the opposite, and waves bend towards the mud. This is caused by the decrease in wavenumber (which is real when there is no mud presence), causing the waves to slow down and move slower over the sandbank compared to the surroundings. The greenish colour found in the first two plots indicates the angle of incidence. For all scenarios, refraction starts when the waves pass a corner of the mud. Over the thickest part of the mud, there does not seem to be a large change of direction. For all experiments, the refraction remains between 5 degrees in both on- and offshore directions, which is rather small.

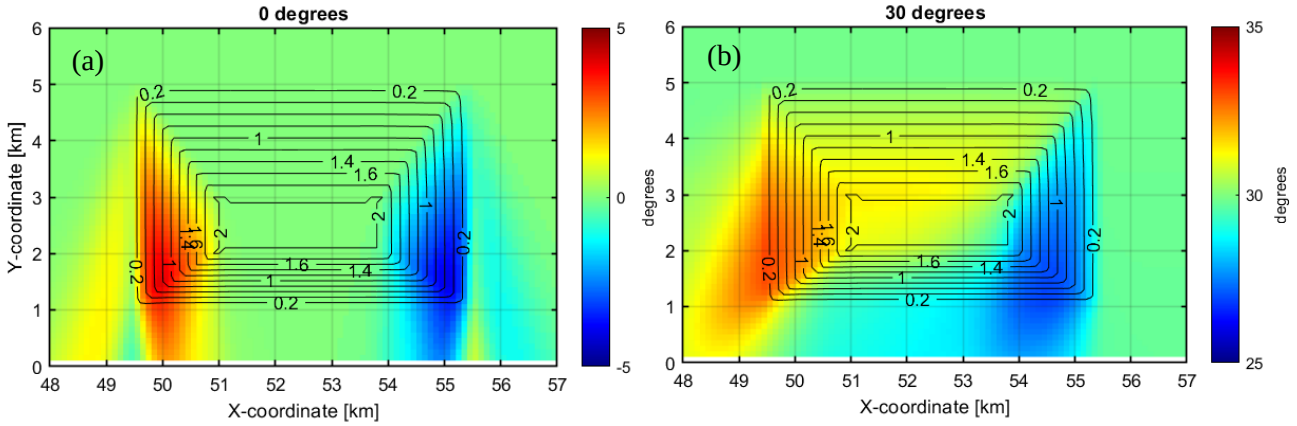

Figure 3.7: The wave angle is indicated with the colors, two different scenarios are plotted, both with different angles of incidence of the incoming waves. The angle of incidence is indicated with the green color, an increase is indicated with red and a decrease with blue.

3.3.3 Wind speed and direction

Figure 3.9 illustrates the wave density spectra for three locations marked in Figure 3.8. The waves are all influenced by a different wind direction. The wind has the same speed in all experiments (7 m/s). The wave energy is measured offshore (1), at the beginning of the mudbank (2), and at the top of the mudbank (3) (see Figure 3.8). Locally generated waves are found at frequencies larger than 0.25Hz (< 4s) in the present case.

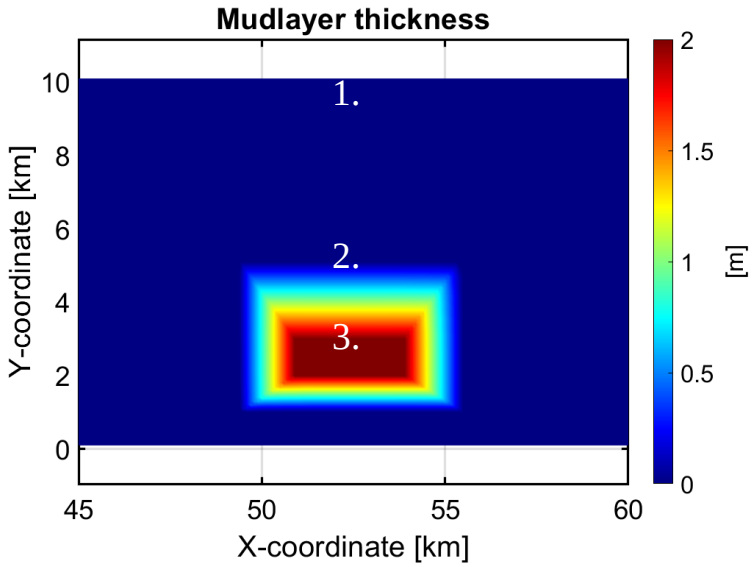

Figure 3.8: The location of the three points of which the energy density spectra is calculated. These are named: offshore (1.), beginning of the mudbank (2.) and top of the mudbank (3.).

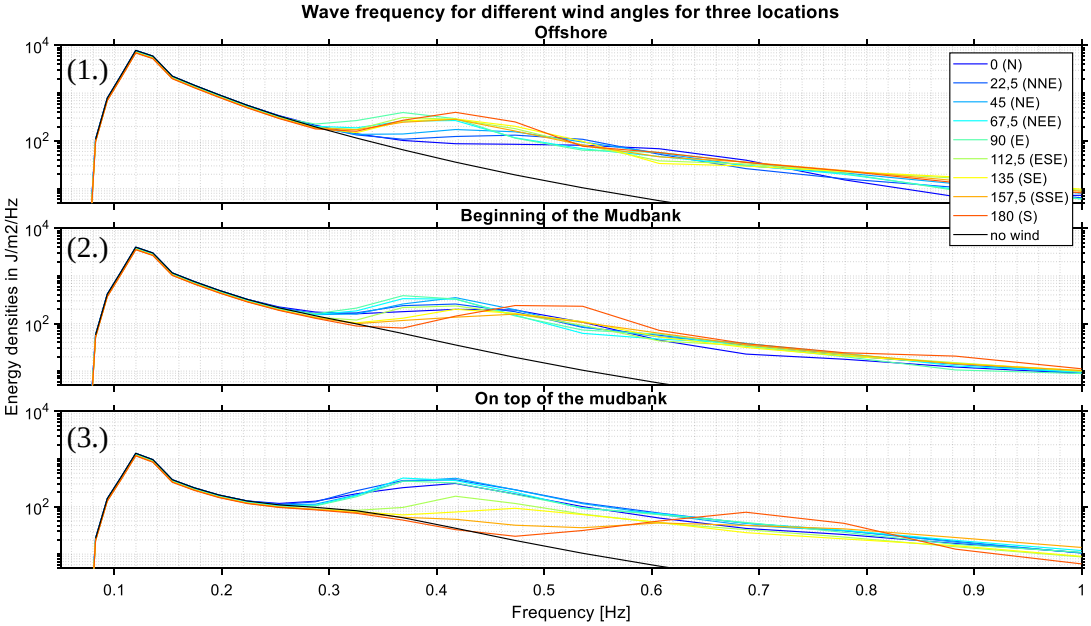

Figure 3.9: The energy density plotted for waves influenced by wind from different angles, the wind speed is constant at 7m/s. The waves have a H_s of 1.0 m and T_p of 8 s coming from the North. The location of the three points are indicated in Figure 3.8.

At the first location (1), the energy in the larger wave period is equal for all scenarios and found at 0.135Hz, corresponding with the waves used for this experiment. The offshore winds generate more high-frequency waves in this part of the domain than the onshore winds, which is caused by the longer fetch for these winds as this location is in the north part of the domain. At the beginning of the mudbank (2), larger periodic waves have lost some energy, which is similar for all different scenarios. No decline was observed in wave energy for the high frequency and wind-generated waves. There has been a frequency shift: the onshore winds are more profound around 0.4 Hz, and the offshore winds are in the 0.6Hz range more present. When reaching the top of the mudbank (3), the large swell waves lost a large part of their energy, while the wind waves did not experience a lot of mud dissipation. The different effects on the wave generation are caused by the different fetch lengths of the different scenarios.

3.3.4 Wave energy density

Four different Hovmöller diagrams (Figure 3.10) have been made for a cross-section over the mudbank. Each diagram represents a scenario in which the waves have a height of 1 m and a period of 8 sec. The scenarios differ in the presence of mud and wind: A situation with a mudbank and the presence of wind (b), a mudbank without this wind (a), a situation without a mudbank but with the wind (d), and lastly, a scenario without mud and wind (c). Without mud, there is little energy dissipating from the waves in this experiment with horizontal bottom due to the negligible influence of other dissipation mechanisms (e.g. wave breaking, bed friction and whitecapping). Similar results are found when mud is absent, but the wind is present. In this situation, the energy of the wind-generated waves is visible in the higher frequencies (0.3-0.7 Hz).

When mud is present, the influence is similar to the situation with and without wind. The energy dissipates mainly in the range between 0.1 and 0.35 Hz. The energy is initially very high, around 0.125 Hz. The mud is present around 3500 meters from the southern border, which is recognizable by the large drop in energy. When the wind is present, there is more wave energy over the whole plot, but the dissipation mostly happens around 3500 from the coast in the 0.1-0.35 Hz range. More energy remains when reaching the shore when the wind is present, which correlates with findings from Figure 3.9.

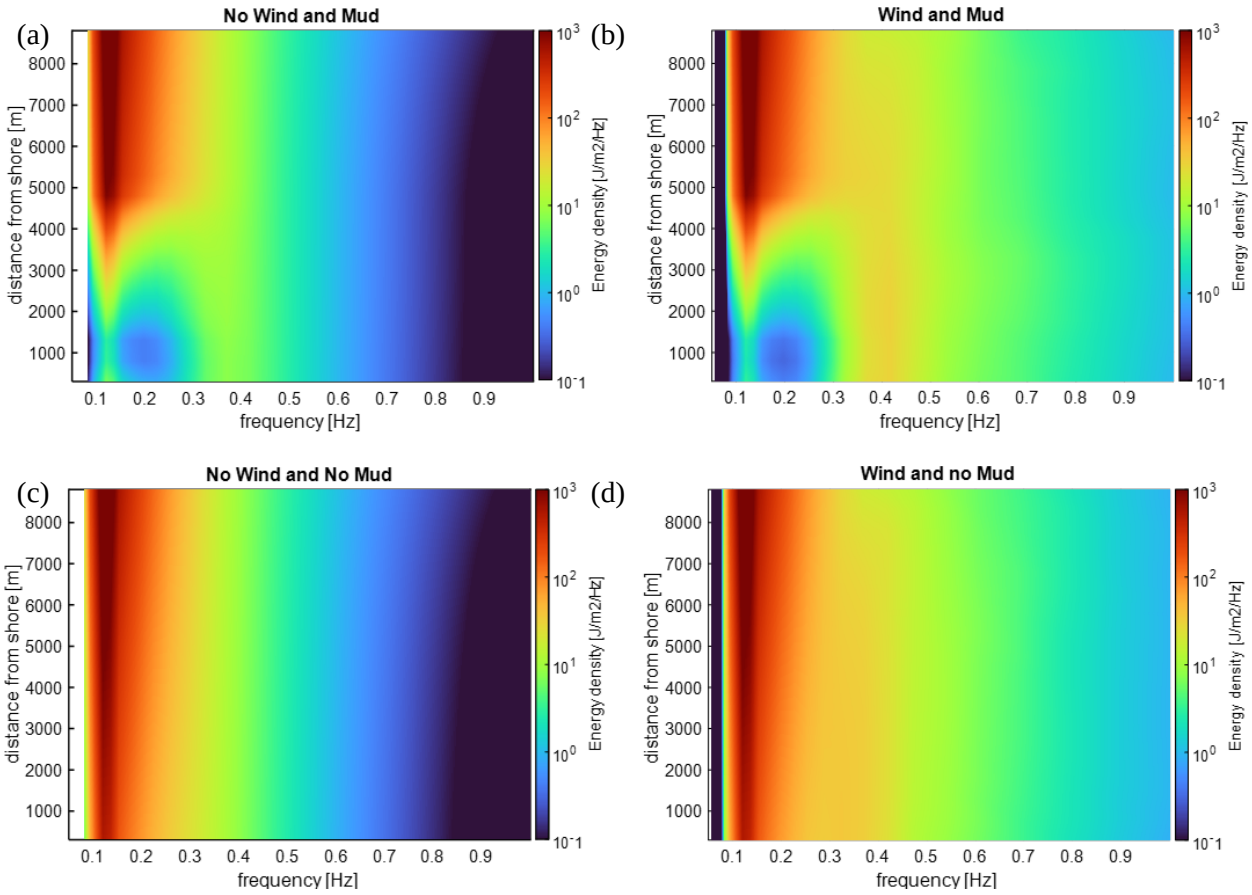

Figure 3.10: The energy density for the wave spectra measured for the transect over the length of the mudbank crossing all three locations (the wave input was: H_s of 1.0 m and T_p of 8 s and when wind was used it was coming from 45 degrees with 7 m/s)

Main findings:

1. An increase in wave height induces a strong increase in the dissipation of mud
2. An increase in wave period reaches a certain optimum in mud dissipation and has a much smaller effect on the rate of dissipation
3. Waves bend away from the mud when travelling over the mud
4. Dissipation mainly focuses on the lower frequency swell waves (0.1-0.2 Hz) and barely on the higher frequencies

3.4 Test case: Suriname

3.4.1 Influence of mudbanks in front of the coast

Figure 3.11 provides the total dissipation for the three scenarios (summer, winter, and winter storm), with and without the presence of mudbanks. These mudbanks are recognizable by very high dissipation, mainly around the edges of the mud. The total dissipation is very high for the higher energetic scenarios, while the dissipation is relatively low for the summer. The different bathymetry features can be distinguished. Very shallow parts are recognizable with high dissipation caused by bottom friction. Contours in dissipation mark the edges of the mudbanks. After the high dissipation peak at the edges of the mud, the dissipation decreases towards the middle of the mudbanks. The dissipation at the centre of the bank is lower for the situations with mud compared to similar scenarios without mud. This could be caused by the strong decline in wave height due to the peak in dissipation at the beginning of the mud. The large peak in dissipation corresponds to the results of the 2D experiments, shown in Section 3.3.

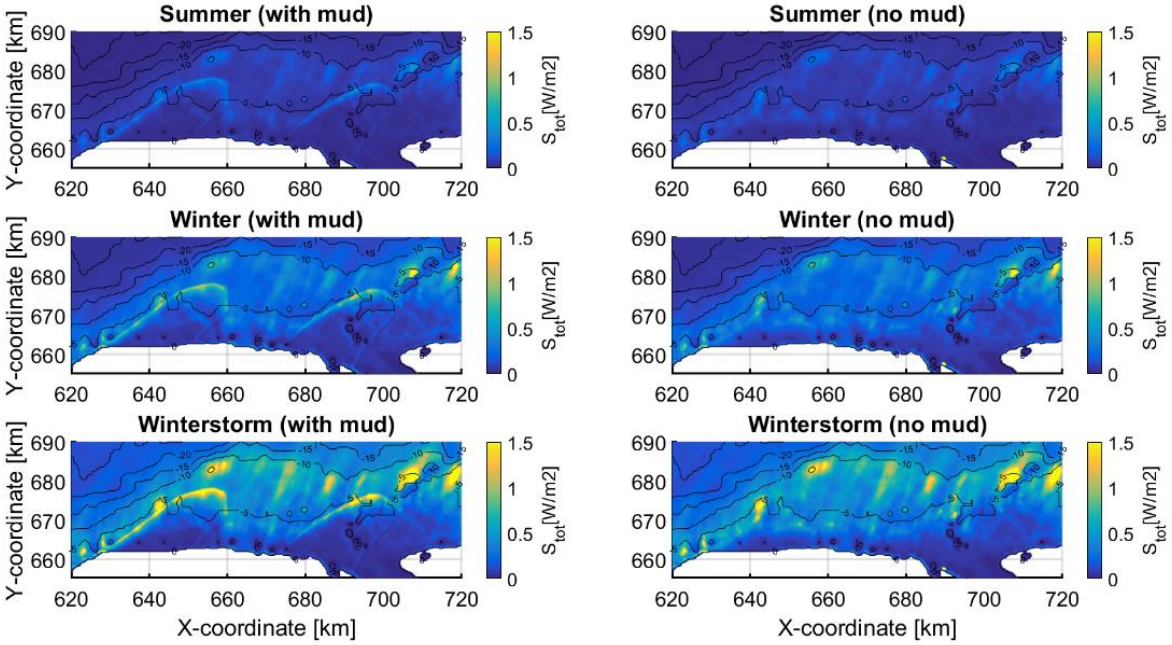

Figure 3.11: The total dissipation for Summer, winter and a winter storm. For all these scenarios is the situation with mud given on the left and the situation without mud on the right. The contours of the bathymetry are included in all panels

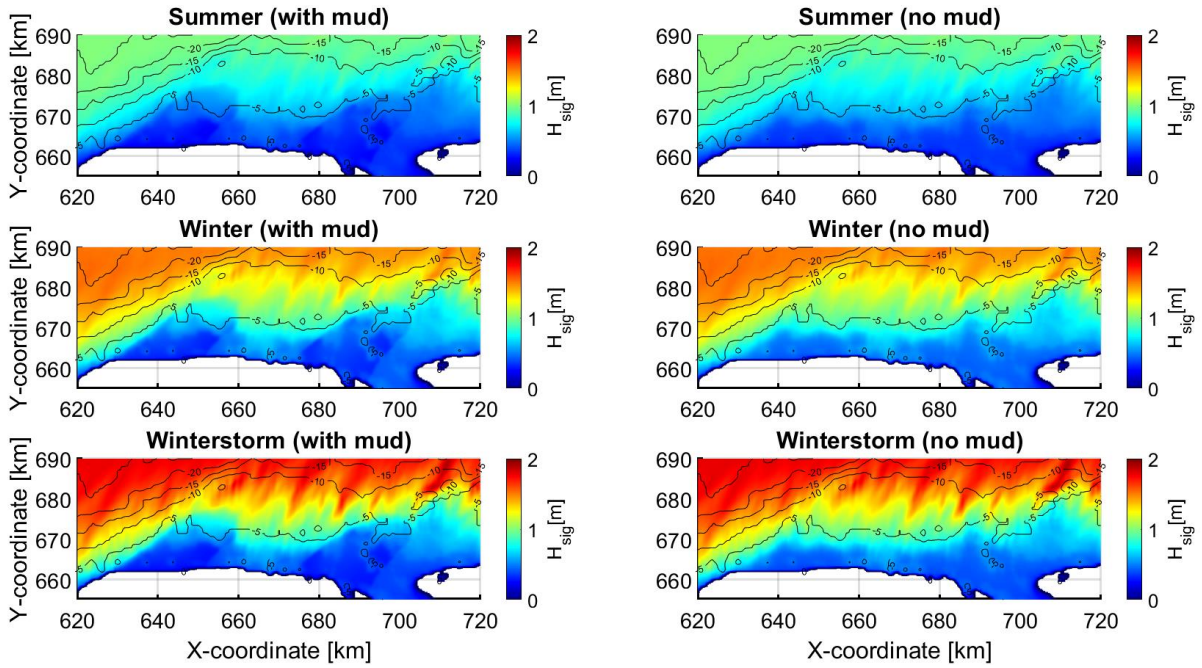

Figure 3.12: The significant wave height for the 3 main seasons investigated with the situation with mud on the left and without mud on the right. The contours of the bathymetry are included in all panels

In Figure 3.12, it can be observed that the wave height decreases at locations where mud is present. These drops in wave height correspond to the large dissipation peak at the mudbank's seaward side, illustrated in Figure 3.11. This drop-in wave height is visible in all scenarios, and the wave height nearshore is minimal when mud is present. The figure also shows that the wave height in the interbank areas is much larger than waves at the mudbanks. The bottom contours related to dissipation by bottom friction in Figure 3.11 are also related to decreasing wave heights in Figure 3.12

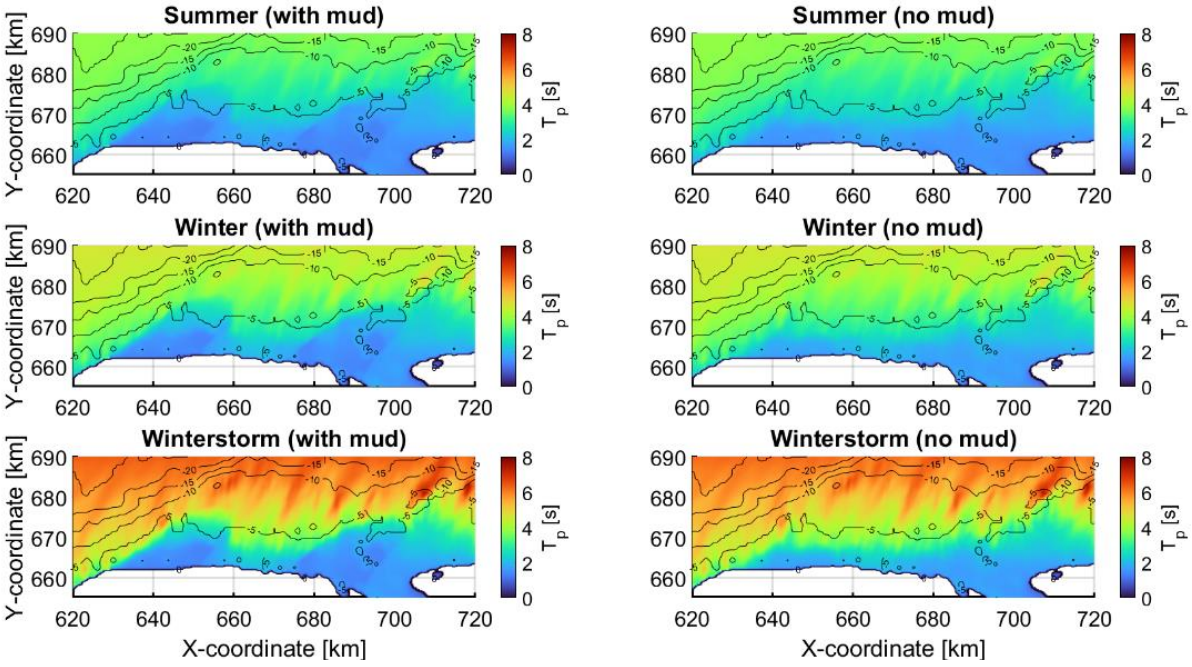

Figure 3.13: The peak wave period for the 3 main seasons investigated with the situation with mud on the left and without mud on the right. The contours of the bathymetry are included in all panels.

Figure 3.13 illustrates the peak wave period for the same three scenarios. A similar trend as in the significant wave height is visible. A substantial drop in wave period is related to the large peak in dissipation by the mud for all scenarios with mud. For the most energetic scenario, this drop in wave period is much larger compared to the lower energetic. The results from the test case are consistent with the results of the idealized 2D experiments. In Figure 3.13, the drop in wave period is very large for all scenarios. This indicates that the fluid mud efficiently damps the wave period.

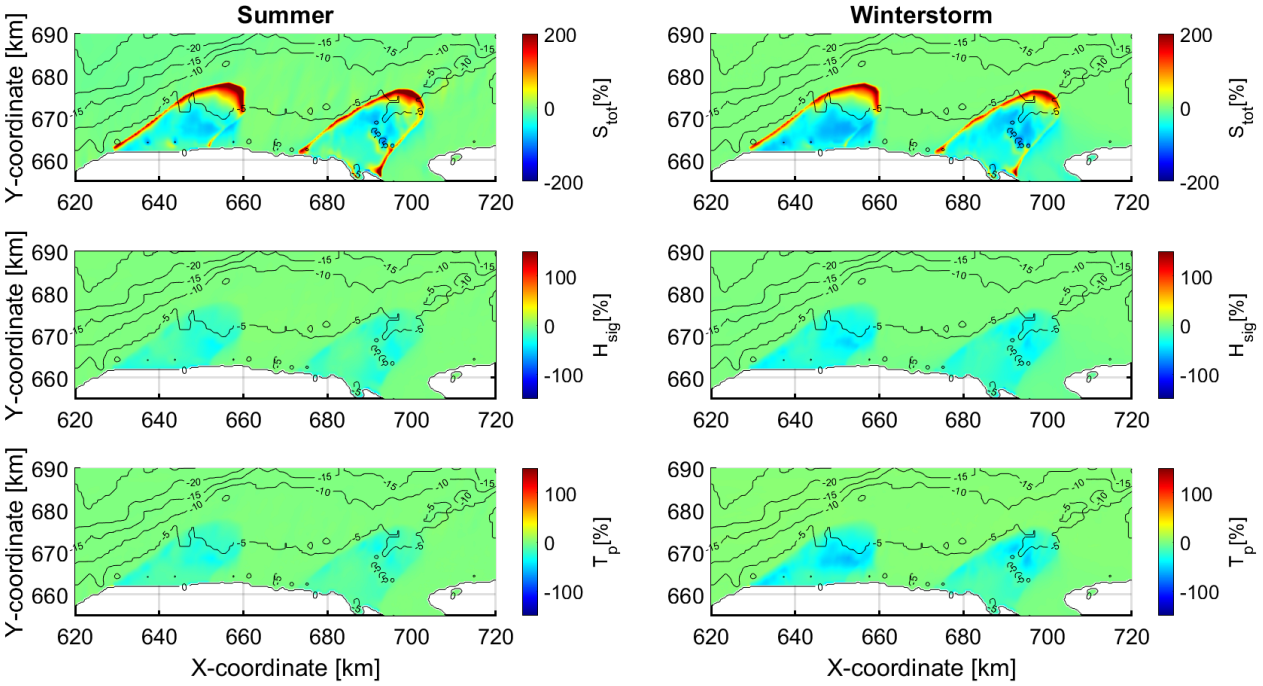

Figure 3.14: Relative differences for the summer (left) and winter storm (right) between situations with and without mud. Different parameters are: Significant wave height, Total dissipation and peak wave period. A positive percentage means that the value is higher for the scenario with mud, while a lower value means that the value without mud is higher

Figure 3.14 shows the relative differences between situations with and without mud illustrated. In this figure are two scenarios included: the summer and winter storms, and three parameters are shown: total dissipation, significant wave height and peak period. A positive percentage indicates higher dissipation for the situation with mud, and a negative percentage indicates lower dissipation for the mud-rich scenario. On the edges of the mud, the dissipation is more than 150% higher for situations with mud. This seems higher for the summer compared to the winter storm as the total dissipation at the edge of the mud seems thicker than for the winter storm. On top of the mud, the dissipation is smaller for the mud-rich scenarios compared to situations without mud. This decrease is larger for the more energetic scenarios than the less energetic summer scenario. The significant wave height declines for the summer situation by less than 50%. Interestingly, the wave height declines relatively more for the winter storm, which seems to be well over 50%. The wave period decrease is much larger for the winter storm compared to the summer. This correlates to the large drops in the wave period, shown in Figure 3.13.

The evolution of S_{tot}, H_{sig} and T_p as a function of cross-shore distance is given in Figure 3.15. In this graph, the three different scenarios are illustrated. The seaward side of the mud layer corresponds to a very strong increase in dissipation. After this increase, the dissipation becomes smaller than the situation without mud for all the scenarios. The dissipation by other factors is more significant for the situations without mud than those with mud, as the dotted line remains higher than the solid line. For all scenarios, the significant wave height declines strongly at the beginning of the mud and decreases more gradually for the remaining mudbank. All scenarios with mud reach the same height nearshore, and all scenarios without mud reach the same wave height. An almost identical result is visible for the peak period. However, the peak period becomes almost equal for both the situations with mud and without mud nearshore.

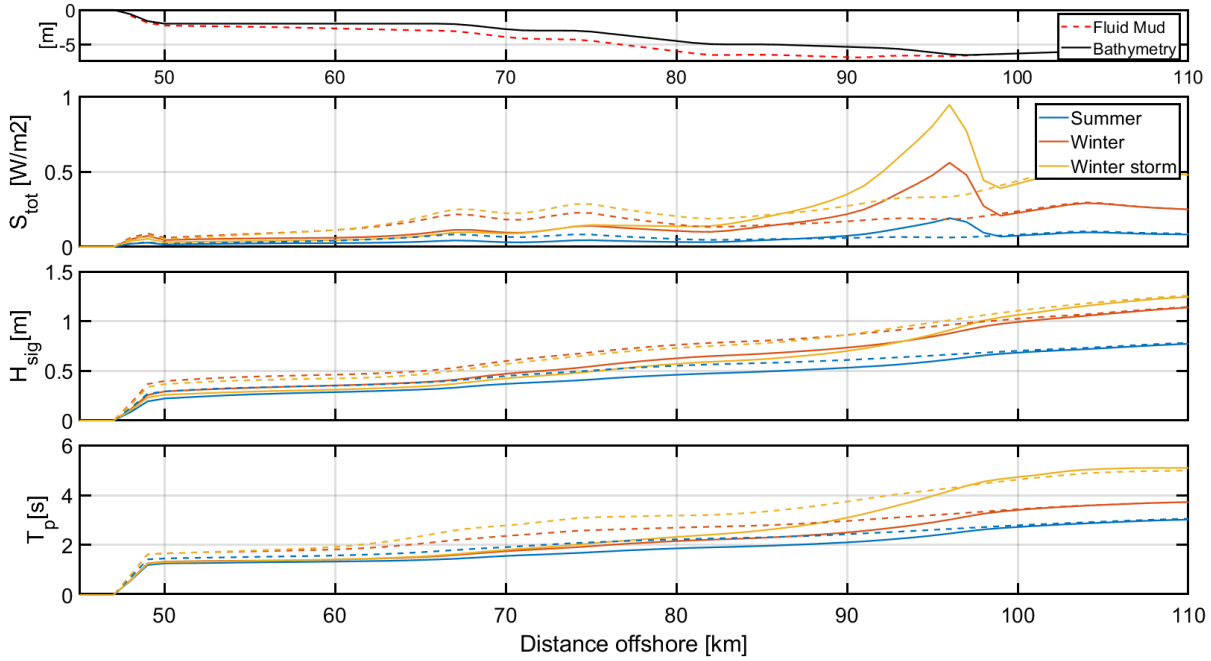

Figure 3.15: Transect perpendicular to the coast, with most offshore on the right and onshore to the left. The different panels show the total dissipation, significant wave height and peak wave period for Summer, winter and winter storm. The dotted lines indicate the same coloured scenario but then without the mud layer.

The difference in dissipation for the transect with mud and without mud is visualized for two scenarios (summer and winter storm) in Figure 3.16. In the figure, the total dissipation is split into different dissipation factors. Before the waves reach the mud, the bottom friction is the largest dissipation mechanism, combined with the whitecapping. Where the mud starts, the mud dissipation increases strongly with a high maximum, making up most of the dissipation for this part. This dissipation decreases steeply but remains significant over the remainder of the mud. For the situation without mud, the bottom friction remains the most significant mechanism, together with whitecapping (the magnitude is much smaller for whitecapping compared to bottom friction) remains of influence on the dissipation. The bottom friction almost diminishes for the situation with mud. The whitecapping increases over the mud, when present, as waves become steeper. Wave breaking does not play a role in this area for all scenarios, unrelated to mud presence.

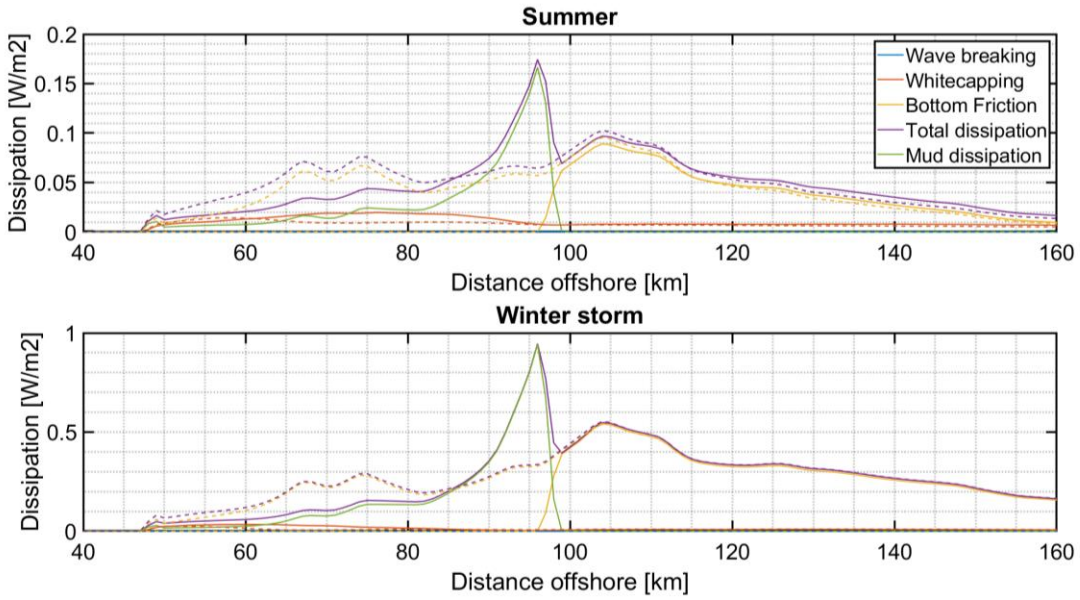

Figure 3.16: Different dissipation processes for the transect perpendicular to the coast on top of the mudbank for two scenarios: summer(a) and winter storm (b). The dotted lines indicate the same process but then for the scenario without mud.

Figure 3.17 shows alongshore variability in total dissipation, wave height and period, crossing both mudbanks at their centre. In the interbank areas (without mud), the total dissipation is more or less evenly over the whole transect, with peaks related to bathymetry features. The edges of the mud are related to high peaks in mud dissipation. In the middle of the transects with mud, the dissipation is lower than in the situations without mud. At locations with mud, the significant wave height and wave period are lower than those without mud. This is similar in the interbank areas as wave height and period are much larger here than on the mudbank.

Main findings:

1. The edge of the mud leads to a large peak in dissipation, while on the mudbank, the dissipation is lower than in the no-mud case.
2. Wave height and period at the seaward edge of the mud decrease, which is related to the peak in dissipation.
3. The interbank areas have a higher wave height and period compared to the mudbanks.
4. Dissipation by mud replaces bottom friction when mud is present. Otherwise, the bottom friction is the main dissipation source.
5. Wave breaking does not play a role at this coastline due to the low wave energy and large dissipation by other mechanisms.

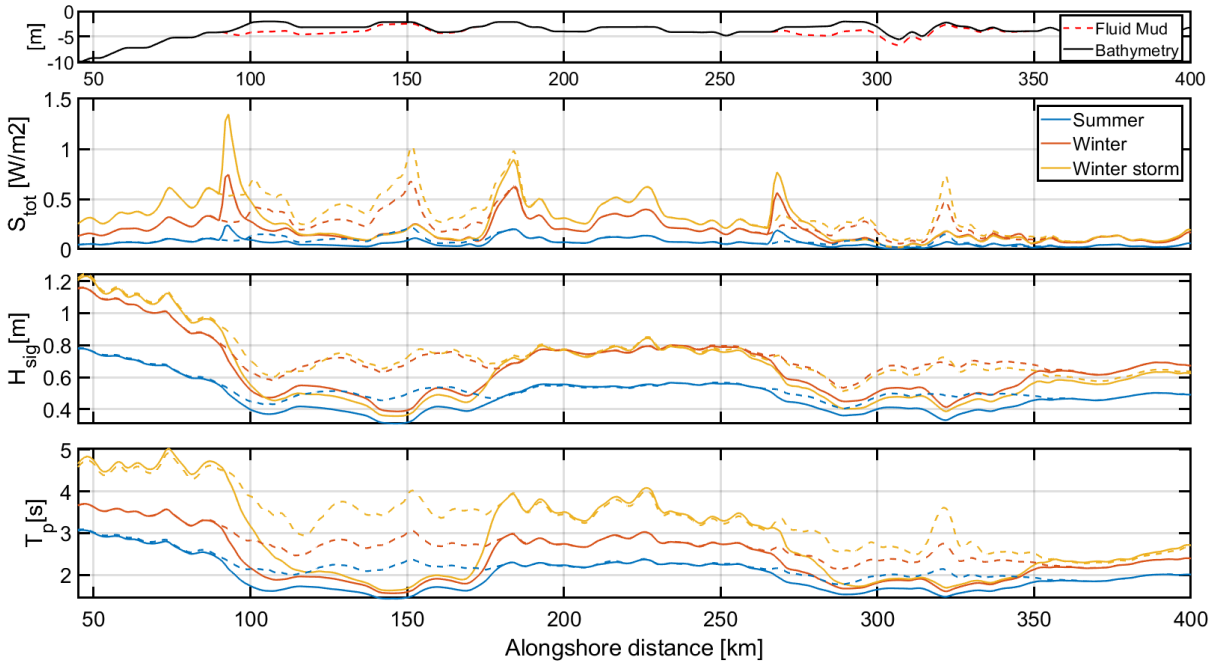

Figure 3.17: Transect along the coast over the two mudbank for the three scenarios. The dotted lines indicate similar scenarios but without the mud. The transect is indicated in Figure 2.25. In this plot are total dissipation, significant wave height and peak wave period shown respectively.

3.4.2 Different wave environments

Figure 3.18 shows the mud dissipation for a summer scenario (a) and winter scenario (d), and two scenarios in-between where only one parameter is changed (wave height and period) (see Table 2-3: All parameters for the different scenarios. All scenarios are based on three main scenarios: Summer, winter and winter storm.). The mud dissipation is the smallest in summer and largest during winter. The dissipation is more considerable for the situation where only the significant wave height was altered (c) than when only the period was changed (b). This is comparable to the results from Figure 3.19, where the wave height decreases due to the higher dissipations. The mud dissipation for the scenario where only the wave period is changed is still slightly larger than in the summer scenario, which is related to the small influence of the wave period on the dissipation.

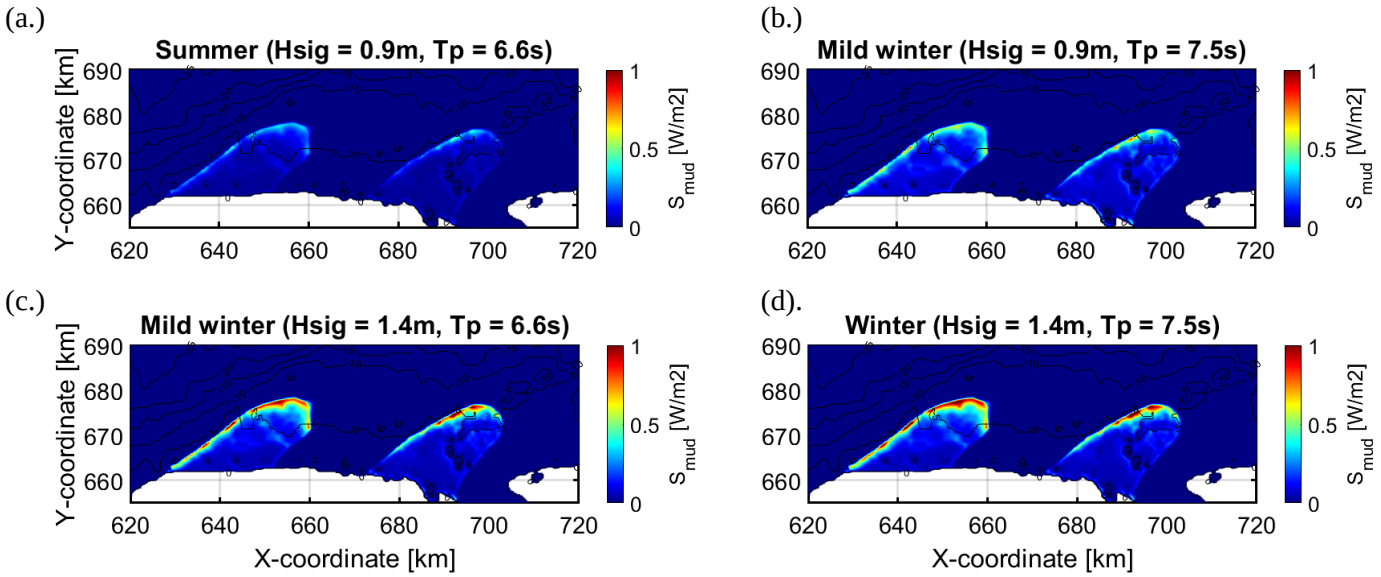

Figure 3.18: The mud dissipation of four different scenarios: Summer (a), Mild Winter #1(b), Mild Winter #2(c) and Winter(d). All their parameters are given in Table 2-3. The wave height and period are given above each panel

The significant wave height of the four different wave scenarios is given in Figure 3.19. The scenarios in this plot are related to the results in Figure 3.18. Panel b & c are intermediate scenarios between summer and winter by only changing one wave parameter (T_p and H_{sig}). As can be observed, is the initial wave height similar to the bottom two figures (c & d). The right top scenario's wave height is slightly larger than summer but smaller than the other two scenarios. It is larger than the summer, while the input is similar. This is likely caused by the wind's local energy generation as the summer wind is weaker than in the other three scenarios. The waves decrease more for the bottom panels than the top figures as the waves go from 1.4 m to less than 0.5 m. This is similar but smaller for the top right panel(b), where the dissipation seems to have the same rate, only the initial height is different.

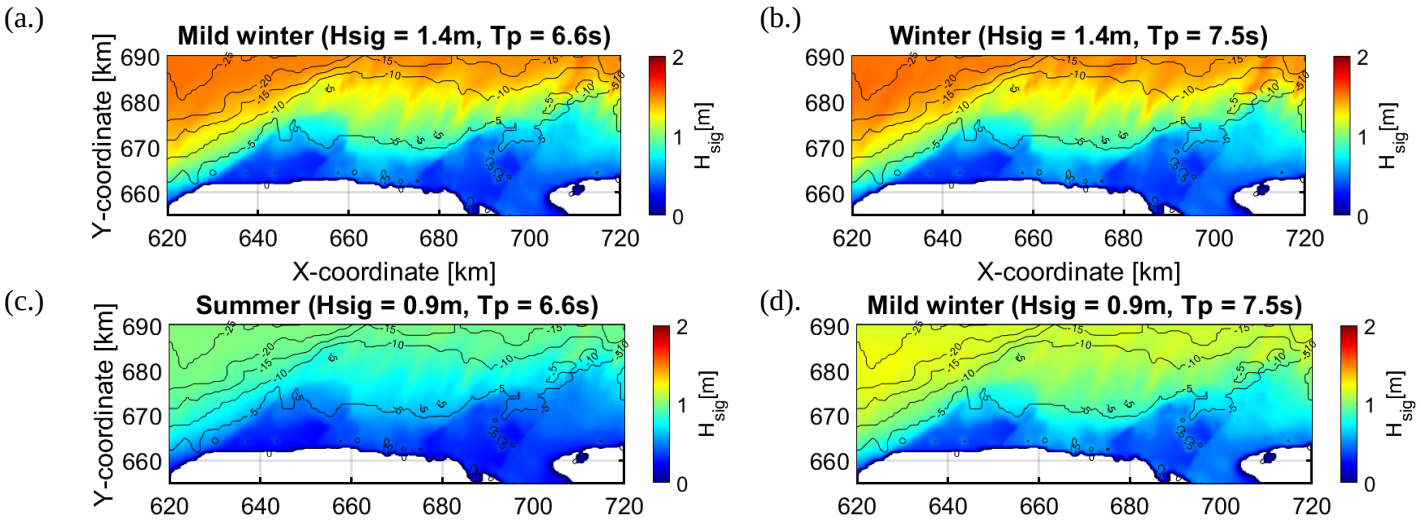

Figure 3.19: The significant wave height of four different scenarios: Summer (a), Mild Winter #1 (b), Mild Winter #2(c) and Winter (d). All their parameters are given in Table 2-3. The wave height and period are given above each panel in the figure

The total dissipation, significant wave height, and the peak period are visualized in Figure 3.20 for all different scenarios with mud. All scenarios show the same trend; when reaching the mud, the dissipation increases steeply. This is causing a steep decrease in wave period and height. Interestingly, for each intermediate step between summer-winter and winter-winter storms, the most significant change in dissipation happens for the scenario in which only the wave height is changed. So, the situation in which the period is changed is closest to the low energy situation, and the wave height scenario is closest to the high energy situation.

Figure 3.21 shows results for the alongshore transect. The total dissipation shows very large peaks at the edges of the mud. Larger peaks are found for the situations without mud at places related to bathymetry, for example, around 150 km. As seen in panel (c), at the locations with the mud, the wave height drops the most for the scenario with the highest wave height as input, except for the summer scenario, which remains the smallest over the transect. The wave period plot shows a great example of the rate of the decline induced by the mud; over the mud, the period drops from 5 s in the interbank area to 2 s on the mud for the winter storm scenario.

Main findings:

1. The wave height is related to the largest mud dissipation, similar to the 2D experiments.
2. The wave period does not influence the rate of mud dissipation, similar to the 2D experiments.
3. The most energetic scenarios lose the most energy over the mudbank. They reach further over the mudbank but will not reach the shore.
4. The winter scenarios travel far through the interbank area towards the shore.

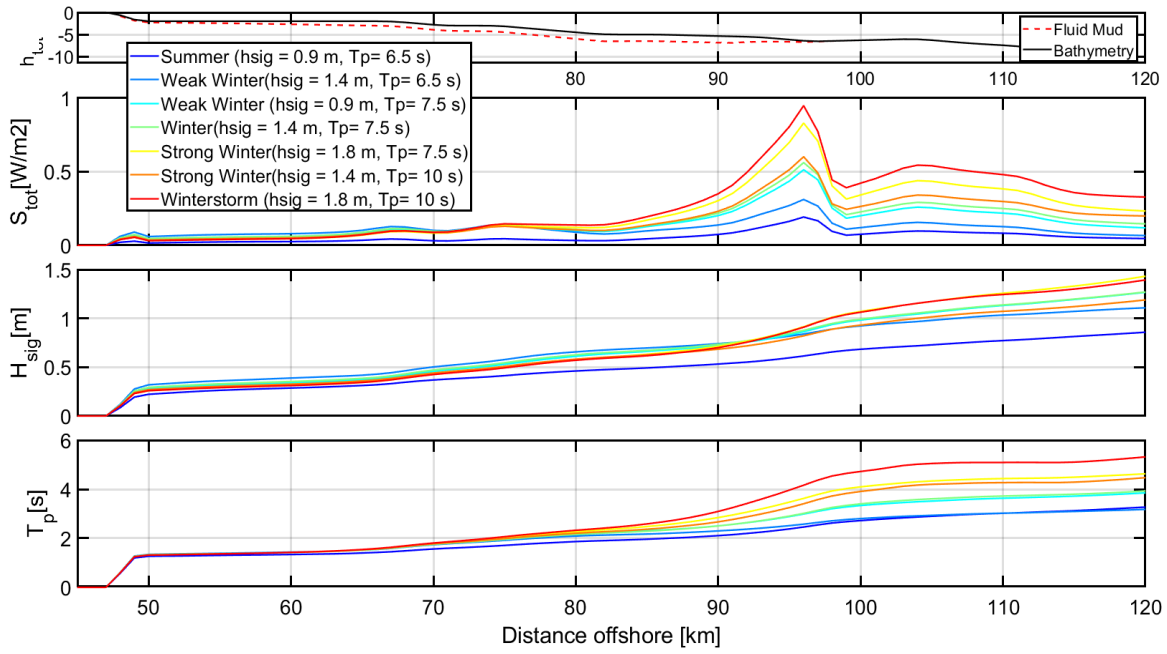

Figure 3.20: All different scenarios from summer to winter with the intermediate scenarios. Given are the significant wave height, the wave peak period and the total dissipation. The transect is perpendicular to the coast over the mudbank.

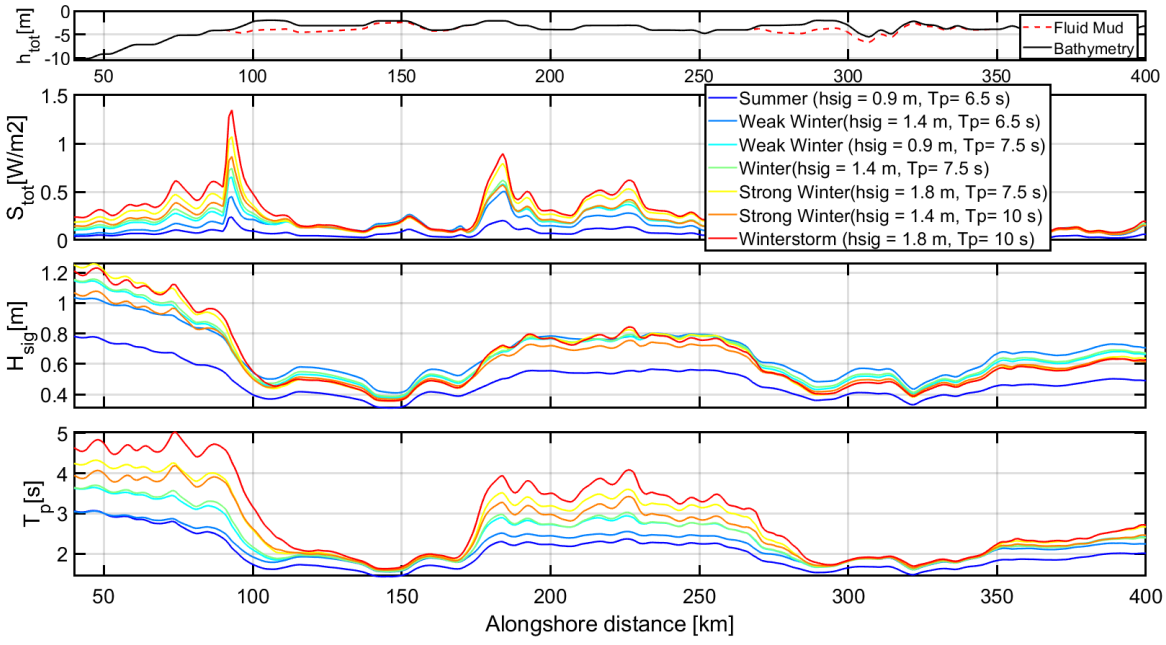

Figure 3.21: All different scenarios from summer to storm with all intermediate scenarios. Given are the Significant wave height, the wave peak period and the total dissipation. The transect is alongshore crossing both mudbanks.

3.4.3 Influence of local wind

The results for local wind in the 2D experiments showed the dependency of wind on the fetch length and lack in the accuracy of initial wave height in SWAN-Mud due to the presence of wind. For the case study, only wave energy is discussed.

For the transect perpendicular to the coast on the mudbank, the frequency of the energy density is calculated for 50 locations and visualized in Figure 3.22. These diagrams all represent the summer scenario, although the difference is made between mud and no mud; furthermore, the wind has been switched off for two tests. Contrasting the similar experiment in Section 3.3, all other dissipation processes play a role in this experiment. The top figures show that the waves are damped by bottom friction and whitecapping, causing the energy density to decrease. In the bottom left, there is no wind, so there are no wind waves. This can be seen in the lack of energy in the higher frequencies (>0.45). Significant energy dissipation happens between 0.1 and 0.4. Most energy in the range of 0.2-0.4 Hz is dissipated from 10 km to shore. The mudbanks have a length of 15 km, which coincides with this finding. When the wind is added in the right figures, the energy is larger in the lower frequencies. Where the situation without wind had a gap of around 0.4Hz, there is still some energy for situations with the wind. This energy is comparable to the energy when mud is absent, indicating that the mud does not influence the waves generated by this wind, which conforms to findings in the 2D experiments.

Main findings:

1. The results regarding the energy density correlate with those from the 2D experiments.
2. Most dissipation by the mud happens in the 0.1-0.5Hz region, and bottom friction seems to happen more in the 0.1-0.2Hz region.
3. The magnitude of mud dissipation is larger than the bottom friction.

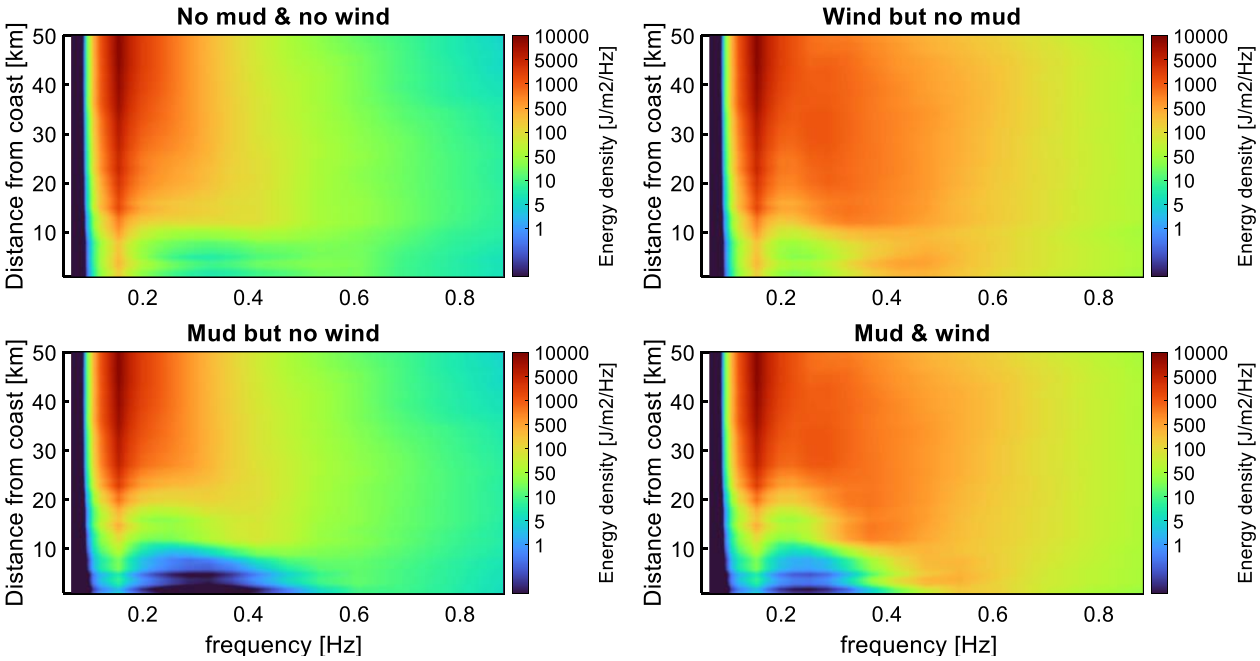

Figure 3.22: The energy density for the wave spectra measured for the transect over the length of the mudbank. Summer scenarios are used, varying in mud and wind presence

3.4.4 Different wave angles

Figure 3.23 shows wave direction for the three storm scenarios. Without mud, waves refract towards the shallower parts in the bathymetry, as can be seen in the areas 640-670 km (on the horizontal axis) and 680-670 km for all scenarios. When mud is present, the waves seem to refract less towards the coast, remain more in their original trajectory, or even bend wider to the east. The mudbanks are visible in the figures as their contours are visible due to a change in wave angle. This result is in line with the 2D experiments. The waves tend to bend further away from the coast, where the mud is present as the angle increases. For the waves with an angle of incidence of 60 and 40 degrees, this effect is smaller than the situation where waves reach the coast with a straight angle (0 degrees).

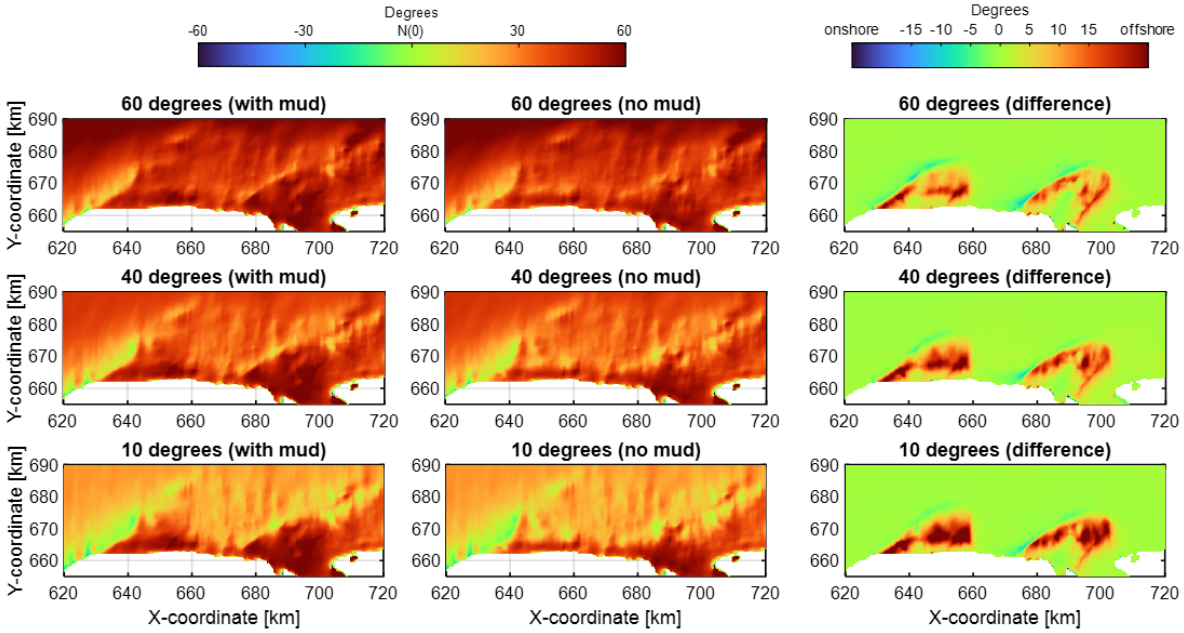

Figure 3.23: The first two columns show the wave angle for three scenarios: waves with an angle of incidence of 60, 40 and 10 degrees from the North. The first column includes mud compared to the second column without mud. The last column contains the same scenarios but then with the difference between the situation with or without mud. A positive value here means that the waves bend more offshore, so away from shore.

Figure 3.24 represents the perpendicular transect and shows the H_{sig}, T_p, S_{tot} for the three winter storms. The different scenarios reach the mud with different wave heights and periods, influencing the total dissipation. In Figure 3.24, the waves are lowest for the waves with the most western angle of incidence (60 degrees), followed by 40 degrees, which is closer to 10 degrees when reaching the mud. The same can be observed for the wave period. Further, the different storms all reach the same height and period (with mud) on the mud. The total dissipation is highest for the storms coming from the north and lowest for the storm with waves coming from 60 degrees. The trend with the high peak is similar to the tests conducted before.

Main findings:

1. The situation with waves coming mainly from the north shows higher refraction values
2. Bathymetry influences the refraction towards the shore
3. Mudbanks tend to refract the waves away from the shore
4. Storms from the north reach the shore with the highest wave height and period

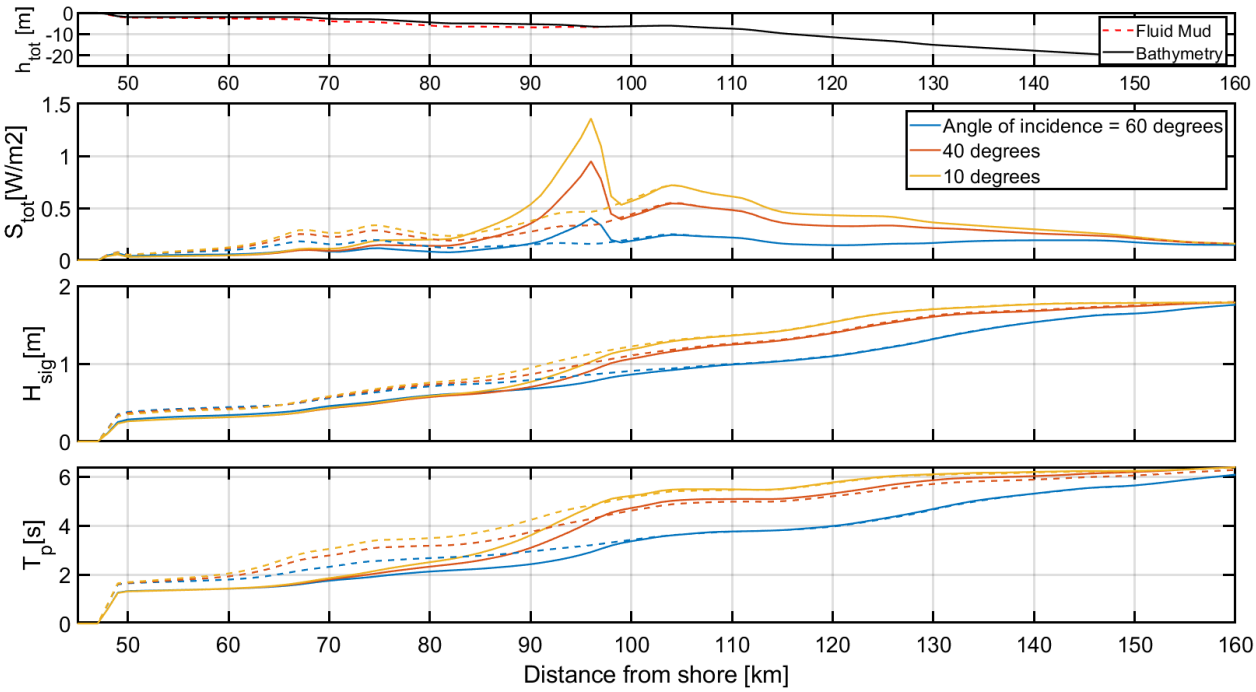

Figure 3.24: All wave parameters for the transect perpendicular on the coast. These are the total dissipation, significant wave height and peak wave period. For storms with three different angles of incidence.

4 Discussion

In this chapter, all results will be interpreted, discussed, and put into perspective with other studies. Firstly, the results from the SWAN-Mud model and the debugging efforts will be discussed. This will be followed by the idealized 1D and 2D experiments. Furthermore, the results from the case study will be put into perspective. Lastly, some recommendations are added in the last section that would be suitable to continue this research.

4.1 The SWAN-Mud model

4.1.1 Dispersion relations

The debugged model now has the correct implementation of the DELFT and DeWit dispersion relations. As shown in Figure 3.1, the results are improved over Tzampazidou (2020) and are similar to the results of Kranenburg et al. (2011), which are known to be correct due to their correlation to the analytical solution. Similar graphs for all methods can be found in the original papers (Gade, 1958; De Wit, 1995; Ng, 2000; Kranenburg, 2008); these studies show the analytical solution for each method. We see that all methods in SWAN-Mud can now correctly reproduce the imaginary part of the wavenumber.

4.1.2 Dissipation term

The new DeWit dissipation term was not originally included in SWAN-Mud and has not been used or described extensively in the literature. The method of DeWit is complicated and therefore difficult to reproduce, and the presence of many typos in the description further adds to this issue. This makes it hard to compare results for the dissipation term to other studies.

The DeWit dispersion term shows the correct pattern in Figure 3.2 (with the optimum around the thickness of the Stokes boundary layer for the imaginary part of the wavenumber). However, the results are lower than the DELFT method. This result was encountered multiple times during this study. Nevertheless, it is hard to explain these differences in dissipation. The DeWit method contains three terms that are also included in DELFT, but DELFT has two additional terms. As DELFT accounts for more viscous parameters, it could explain why this method results in values higher than the DeWit method. However, the difference is large, and more research is necessary to quantify the origin of the difference.

A significant problem during the debugging process of the DeWit method was found in the analytical solver. The method can show correct results for relatively easy experiments in 1D and 2D. When these experiments become more complicated, the solver used in SWAN-Mud could not find the correct wavenumber. Experiments become more complicated when including more and finer grid cells or more physical processes. The inclusion of wind in the SWAN-Mud calculations also results in problems with the model's accuracy, causing it to fail. The model does not reach a trustworthy accuracy as it will remain at a certain percentage. The dissipation term by DeWit thus needs to be investigated further.

4.1.3 Mud layers in SWAN-Mud

As described in the method section (2.4), the mud layer is an extension of the total depth instead of a part of the total depth (see Figure 4.1). The actual situation might not be like the situation in SWAN-Mud. The model describes the mud more as a patch of mud, which is part of the bathymetry. In the literature, the situation is described more as a bank, meaning the situation changes from the top figure of Figure 4.1 to the bottom. If the mud is implemented as a patch, the influence of shallower water depth and the bank is neglected. A situation like this could be reached by subtracting the mud layer from the bathymetry and making the water column smaller. This is done in Appendix E for the dissipation and wave height. Here, it can be observed that the differences are minor on this small scale.

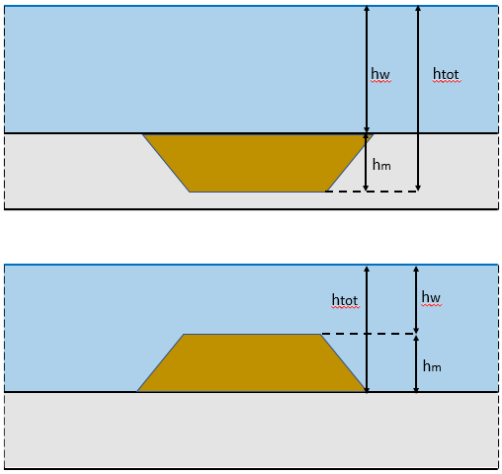

Figure 4.1: Top figure indicates how mud is implemented in SWAN-Mud, the mud here is more a mud patch. The bottom figure is how the mud is often described in literature (Chevalier et al., 2008). It is also how a mud bank is assumed to be exist in reality.

The bathymetry needs to be accurate in SWAN-Mud when trying to reproduce a mudbank. It must be known up to which depth the bathymetry is measured. If this is the top of the mud layer, the implementation of mud in SWAN makes it relatively easy to create the mud layer. If the measurements are taken up to the consolidated bottom, knowledge of the exact thickness of the mud is required, and it is already more complicated to recreate the mud layer. However, in mud-rich situations, the bathymetry data is often unreliable due to scattering of the sonars used or other reasons causing limitations, for example, the different frequencies used to reach different depths in the mud or due to the absence of field data (Carneiro et al., 2020). This makes it very complicated to create realistic mud layers in SWAN-Mud.

4.2 Mud characteristics

The first research question: **"Which characteristics of the "fluid mud" are most important for the mud-induced wave damping and why?"** can be answered with the 1D experiments supported by different modelling studies and experiments. This section is divided into the experiments with the thicknesses of the mud and water layer and a subsection regarding the mud's density and viscosity.

4.2.1 Mud & Water layer thickness

The four methods (Gade, DeWit, Ng, and DELFT) show a similar trend for the mud layer thickness with the characteristic optima. These optima could be found for all methods at different locations, confirmed by the related studies. All methods have a maximum with varying distances from the Stokes boundary layer. These differences can be found in the corresponding literature (Gade, 1958; De Wit, 1995; Ng, 2000; Kranenburg, 2008) but vary between 1.2 and 1.5 times the boundary layer. The analytical solutions for the different methods are included in these studies. The peak corresponds with the model outcome (Figure 3.3) for all different methods. This relation between the Stokes boundary layer and the peak in mud dissipation is confirmed during experiment measurements by Gade (1958). An explanation of the role of the Stokes boundary layer on the mud dissipation is given in Appendix B.

The influence of the waterlayer thickness on mud damping is not discussed at length in the literature. There is also a fundamental difference between all methods in implementing the water layer into the dispersion relation. The water layer thickness is not related to the mud layer thickness for the Gade, DeWit, and Ng methods, as these methods do not include a total water depth in the dispersion relation. The total water column is not included in the dispersion relation. The water layer thickness is computed for the DELFT method by subtracting the mud thickness from the total water column height.

Interestingly, this fundamental difference in assumptions does not influence the results in Figure 3.3. This is due to the implementation of the dispersion relations in SWAN-Mud. In the model, the water and mud layers are always independent. The results show that the imaginary wavenumber increases exponentially with the decrease in the water layer. This effect was expected as it is a similar increase as the first part of the mud layer thickness plot (Figure 3.3). If the overlying water layer is thinner, the energy has to be transferred over a shorter distance, making it easier to create a wave at the interface. This causes an increase in the rate of dissipation. Liu and Chan (2007) tested the effect of different ratios of water and mud layer thickness on the rate of mud dissipation. They found that the smaller the water layer is compared to the mud layer, the higher the dissipation rate. This is consistent with the present results in the present study.

4.2.2 Viscosity and density

As seen in the previous Subsection 3.2.1, the imaginary wavenumber's characteristic trend is also recognizable in Figure 3.4, with variations in the mud viscosity in the top graph (a) and the density in the bottom (b). It is visible that this trajectory of the imaginary wavenumber is significantly higher for mud layers with a high viscosity compared to low viscosity. The experiment shows that the mud viscosity significantly influences the mud damping of the mud. This is a result that has been discussed in different studies by, for example, Traykovski (2015), Kranenburg et al. (2011), and Borsje (2019). These papers also discuss the influence of mud density on wave damping. As shown in Figure 3.5, the trend is different for the density compared to the viscosity. The magnitude of the difference in the imaginary wavenumber is much smaller for different densities. The increase in density also leads to a decrease in imaginary wavenumber.

Kranenburg et al. (2011) found that the influence of increasing mud viscosity leads to a strong increase in mud damping, which corresponds to the findings in this thesis. Traykovski et al. (2015) confirmed these results with analytical calculations. They state that the increasing viscosity leads to more wave damping in lower wave frequencies. Although the difference in frequencies is not tested in this thesis, the overall damping shows the same result. In the study by Borsje (2019), different mud characteristics have been modelled with an older version of SWAN, where he found similar results to Figure 3.4. Siadatmousavi et al. (2012) modelled the influence of different mud viscosities on the mud damping with an older version of SWAN-Mud, using the Ng methods. Although a different method was used, similar results were found. All these studies confirm the results found regarding mud viscosity; an increase in mud viscosity leads to higher mud dissipation.

Traykovski et al. (2015) states that the influence of the density is less responsible for mud damping by the fluid mud and concludes that the influence on mud dissipation is linear dependent on the: $ratio\ of\ influence = \rho_w^2 / \rho_m$. This ratio indicates that the density of the water column has more influence on the damping than the mud density. A similar statement is made by Borsje (2019). He claims that the mud density is less of an influence than the mud viscosity. This is similar to the small range in the variation in k_i in Figure 3.4 compared to the range in k_i for the viscosity. Ng (2000, p229) concludes his study with:

"In short, the effect of mud on the wave damping is most pronounced when (i) the mud is highly viscous, (ii) the mud layer is approximately 1.5 times as thick as its Stokes' boundary layer, and (iii) the mud is not too much denser than water."

The findings in this study could confirm the third statement about mud density, as the lower mud densities give the higher values for the imaginary wavenumber. His first statement regarding viscosity is also in line with the findings in this study. The second statement is in line with the results from the previous chapter. Zhao (2006) found from a laboratory study that the larger the mud density, the smaller the dissipation by the mud. A similar statement is made by Liu and Chan (2007), who focus more on the density ratio. The wave damping rate decreases if the mud density becomes much larger than the water density. Because of the increase in density, the mud becomes heavier, and this results in an increase of inertia in the mud as a response to energy input. Furthermore, the wave periods tend to become smaller in the mud,

decreasing the effect of the waves on the mud as this decreasing wave period leads to a decrease in Stokes Boundary Layer (Torres-Freyermuth & Hsu, 2010).

From the literature and the simulation results of this thesis, it was seen that mud viscosity is more of an influence on mud dissipation than mud density. Some viscosity and density values are unrealistic in size and are only included in the sensitivity analyzes. It is important to note that a fluid mud layer is never constant in viscosity and density over the whole column. Stirring by waves causes spatial differences over the mudbank in viscosity and density. This is not included in the model. Because multiple factors influence this dissipation by the mud, it is essential to note that the increase or decrease of dissipation depends on all factors. Hence, depending on the precise location in the column and the parameters, the results might be different. Figure 4.2 from Kranenburg (2008) shows an example of this, where the imaginary wavenumber declines for some viscosities depending on the location in the parameter domain. This is caused by the increase in the Stokes boundary layer that is related to the increase of mud viscosity (Kranenburg, 2008). These changes force the maximum dissipation to happen in different parts of the wave spectra (Siadatmousavi et al., 2012). The results in Figure 3.3 and Figure 3.4 are, in essence, a transect of this large parameter domain that is interdependent on other parameters, and these results are not applicable for every situation.

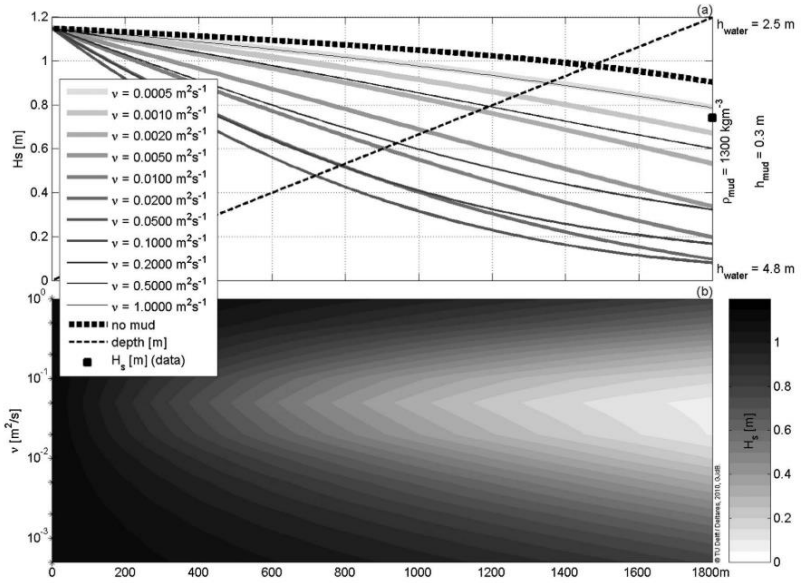

Figure 4.2: The evolution of Hs for different viscosities along a transect and different depths. The figure shows a similar response to increasing mud viscosity although the result is not identical. Measurements by Elgar and Raubenheimer (2008). Figure from Kranenburg (2008).

4.3 Wave environments

There have been different experiments and studies regarding wave damping of swell waves in literature. However, extensive modelling research is lacking. The 2D experiments were focused on answering the second research question: **"What is the influence of the wave environment on the mud-induced wave damping?"** The results are discussed in three sections for a complete coverage of the results. The case study will help support the findings of the 2D experiments and give insight into the effects of the mud in a more realistic situation and is included in the following sections.

4.3.1 Wave height & period

In Figure 3.5, the mud dissipation for different wave heights was compared to the damping for different periods. This figure shows that with an increase in wave height, the dissipation by the mud also strongly increases. In contrast, with an increase in peak wave period, the increase in dissipation stagnates beyond 7 s and remains equal. The scale of the mud dissipation is much smaller for the plot with varying wave periods compared to the wave height plot. The mud dissipation of small wave periods (<5 s) is minimal, and arguably, a minimal wave period is necessary before wave damping becomes significant. This indicates that the dissipation can be considered negligible for smaller wave periods. On the other hand, the figure with the wave periods also shows that besides the necessity of a certain wave period, the wave period only has a limited influence on the magnitude of the wave damping.

Figure 3.6 shows the integrated mud dissipation over the transect, where a similar trend can be observed. Here it is visible that the increase in significant wave height has a larger influence on the dissipation than the increase in the peak wave period. This figure also shows very little mud dissipation for the transect (Figure 3.5) when the waves have wave periods smaller than 5 seconds. In Figure 3.5f, it can be observed that the mud dissipation drops slightly beyond 12 seconds. Van Ledden et al. (2009) also found that if the period becomes large, the rate of mud damping decreases. In this study, this decline starts at a period of 14 seconds.

$$P = \frac{\rho g^2 T H^2 L}{32\pi} = \text{Wave power} \tag{51}$$

The dissipation term for mud is a function of the flux in wave energy, and the wave energy can be calculated with Equation 51. In this equation, the energy is a product of the peak wave period and the significant wave height. The wave height is squared in this equation. This would imply that the influence of the wave height on the wave energy flux is much stronger than the influence of the wave period. This can be observed in the results; the most significant dissipation happens for the highest waves instead of waves with the largest periods. However, this does not explain why the wave damping would stagnate or even decreases with an increasing wave period. A possible explanation could be the relation to Stokes boundary layer. With the increase in wave period, the wave angular frequency decreases ($\sigma = 2\pi/T$), leading to an increase in the thickness of the Stokes boundary layer: $\delta = \sqrt{2\upsilon_m/\sigma}$ (Torres-Freyermuth & Hsu, 2010). This increase in the Stokes boundary layer causes the mud thickness to lie further away from the optima (Figure 3.1) (see Appendix B), and thus causes the rate of mud dissipation to decrease

It could be argued that this cannot be described as the Stokes boundary layer thickness as this boundary layer depends on the viscosity of the water layer, while in the equation above, the layer depends on the viscosity of the mud layer. This is described in Gade (1958) as an effective Reynolds number (De Swart, personal communications, 2022).

In an experiment conducted by Hsu et al. (2013), different wave heights were tested on a fluid mud layer. This experiment confirms the model results with the increase of mud dissipation and a larger decrease in wave period and wave height with the increase of wave height. Siadatmousavi et al. (2012) separate waves in sea and swell waves based on their significant wave height. In this study, they found a similar trend: swell(high) waves are experiencing more dissipation by the mud than the sea(low) waves. They also concluded that in SWAN-Mud, there is no frequency shift over the mud from high frequencies to low frequencies, which is a process that occurs in the field (Elgar and Raubenheimer, 2008). Non-linear effects are included in SWAN-Mud, but they do not increase or vary over the mud, observed in modelling experiments in Siadatmousavi et al. (2012). An increase in these effects of the mud is not included in SWAN-Mud and may mean underestimating the dissipation of high-frequency waves, as the mud indirectly dissipates them by energy transfer.

Kranenburg et al. (2011) also state that waves with larger wave periods are more damped than waves with a low period. This means that swell waves are more damped than wind waves in practice. This is also found in the study by Gratiot et al. (2007), who also notice that swell waves are mainly damped while wind waves are not.

4.3.2 Wave direction & diffraction

In the 2D experiments, the mud is implemented as a patch. The refraction of the waves is in an unexpected direction (Figure 3.7). Although the angle is only small, the waves bend away from the mud. In Winterwerp et al. (2020), the role of refraction on the alongshore movement is discussed, and the corresponding figures are included in Subsection (Figure 2.4). This figure shows that the refraction of the waves is in the opposite direction compared to the results in Figure 3.7.

Figure 4.3 shows the result when the mud is implemented as a mudbank. This can be done as described in Subsection, this way, the water depth becomes smaller. The effects of the diffraction are very different. Here, the waves bend in the opposite direction, as in Figure 3.7. These results correspond much better with Winterwerp et al.(2020)(Figure 2.4). The results and the literature indicate that it is not the mud responsible for the refraction around the mudbank but the decrease in water depth caused by the mudbanks. The water depth becomes smaller in more realistic scenarios as the mud is collected in mudbanks. Hypothetically one could say that the influence of the decreasing water depth is more important than that of the mud damping for wave refraction. This is the reason for the onshore refraction in real mudbank situations such as Suriname and Guyana. However, experiments with different mud patches and banks should give more information about these effects as there is very little literature on this topic. Hence, no concrete conclusions can be drawn about this effect.

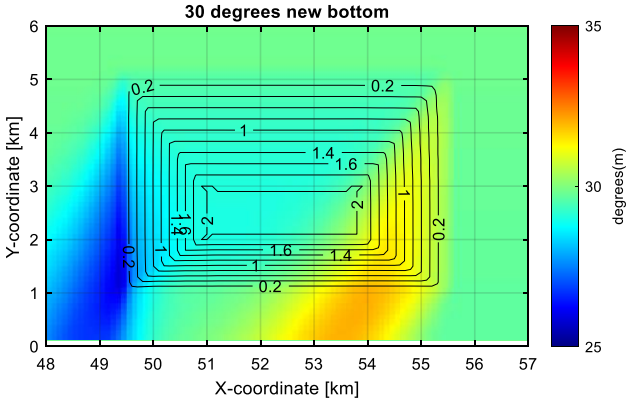

Figure 4.3: Different implementation of a mudbank with waves coming from the 30 degrees from North. It shows an exact opposite diffraction compared to Figure 3.7.

In the paper by Kaihatu et al.(2007), a 2D modelling experiment is conducted, similar to the 2D experiment in this study. This study used a phase-resolving and nonlinear frequency-domain model. This experiment found diffraction of the waves over a mud patch in the opposite direction compared to Figure 3.7, thus towards the mud patch. As this result was expected in the beginning of Kaihatu et al.(2007), it is not further explained. The reason the waves in this thesis diffract away from the mud could be caused by the functions of energy in SWAN and could be explained by focusing on the wave energy and the wave velocity, which can be calculated by dividing the wave length by the wave period ($c = \frac{\lambda}{T}$).

In SWAN, the wave period is correlated to the wave energy with equation 51 in the previous subsection. In comparison, the wave length is a function of the real part of the wavenumber when mud is present. The influence of the fluid mud on the wavenumber's real part is small, as

seen in Figure 3.1. The decrease of the real part of the wavenumber is relatively small compared to the changes in the imaginary part (which represents the dissipation by the mud, also visible in Figure 3.1). On the contrary, the wave period declines very steeply due to the mud as the wave energy decreases very steep due to fluid mud's dissipation, as seen in Figure 3.5.

Following: $c = \frac{\lambda}{T}$ can then be concluded that the wave velocity will increase due to the presence of fluid mud; this is visualized in Figure 4.4. This increase in velocity will induce the waves to diffract towards the relative slower areas without mud. However, this does not explain why the results from Kaihatu et al.(2007)show a different effect. Interestingly, Liu and Chan (2007) conclude that the wavelength decreases strongly by the fluid mud. This would strengthen the results by Kaihatu et al.(2007). Nevertheless, this is not found in this thesis. In Kranenburg (2008), this large effect of the wave length was not found either. Field measurements or laboratory experiments would be necessary to decide which effect of the fluid mud is correct.

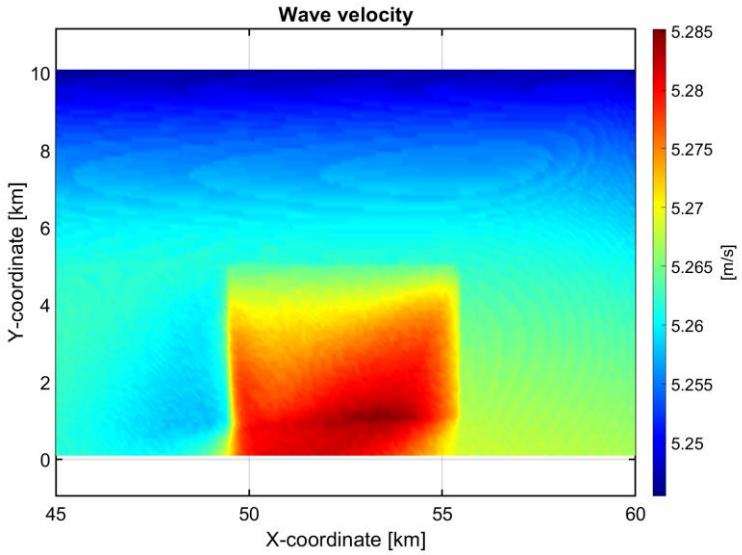

Figure 4.4: Wave velocities for the 2D experiments. Calculated by: $c = \lambda T$. In this equation is c the wave velocity [m/s], λ the wave length [m] and T the wave period [s].

4.3.3 Wave energy spectrum and the influence of wind

The Hovmöller diagram in Figure 3.10 provides the energy density along a transect over the mudbank and perpendicular to the incoming waves (north to south). The influence of the mud is most profound in the 0.1-0.2 Hz region. Especially in the plot without any influence of the wind, the nearshore part of the plot with mud loses large amounts of energy due to the wave damping. When the wind is present, the damping between 0.1-0.2 remains, and dissipation in the 0.3-0.5 Hz region can be observed. The leftover waves remain more energetic due to the input of the wind, mainly found in these higher frequencies. The damping in the region 0.3-0.5 Hz is very little, which is in line with Figure 3.9, which shows a minimal decrease of wave energy in the higher frequencies. Furthermore, it corresponds with earlier findings in Beyramzade & Siadatmousavi (2018) and Winterwerp et al. (2007). Wells & Kemp (1986) did measurements in 1986 for the Suriname coast and found the same effect of the wind on the wave spectra with mud.

4.4 Test case: Suriname

The case study contributed to the interpretation of the results of the experiments and gave more insight into Suriname's situation. The role of mudbanks in front of the coast is discussed, and the seasonality of different waves is debated. The different wave incidence angles are compared to the results in the 2D experiments. Local winds differ with the different seasons in Suriname. The influence of these local winds is compared to the 2D experiments and literature. Furthermore, the variation of the energy density over the wave spectra is discussed. In the end, the reliability of the debugged SWAN-Mud in combination with Delft3D-wave is discussed, and new or missing research is proposed.

4.4.1 Influence of the mudbanks

From the results can be concluded that the mudbanks correspond to damping of the wave height and period, while also large peaks of dissipation mark the position of the mud. The interbank areas show higher wave periods and wave height. These results correlate with field observations by Lefebvre et al. (2004). A strong decrease follows the large peak in dissipation, and eventually, the dissipation is lower on top of the mud compared to the same location for the situation without mud. In this thesis, the mudbanks are static and cannot be moved. It is unrealistic that the edge of the mudbank can maintain its position due to the wave energy reaching these parts of the mudbank. In reality, the mud edge is not sharp but fades more into the water column and disappears in the bathymetry. This means a decreasing sediment concentration at the edges. This would cause the dissipation to be lower at the seaward edge of the mudbank or a more evenly spread over the transect. This spatial difference in thickness or concentration of the mudbank is implemented in SWAN-Mud. Neither is the option to change the mudbank's edges into suspended material. Measurements of the dissipation along a transect over the mudbank are sparse. These would be necessary to confirm this large peak in dissipation or show that it is a more spread-out phenomenon with a lower peak.

Energy dissipation in similar orders of magnitude has been observed in different studies (Gade, 1958; Wells and Coleman, 1981; Wells and Kemp, 1986). In the first study by Gade (1958), field measurements measured this characteristic drop in wave height at the beginning of the mudbank. Wells and Coleman (1981) did measurements in front of the coast of Suriname and observed a drop in wave height from 0.9 meters to 0.2 meters over a length of 10 km. If we look at the transect for winter, the waves have an initial height of around 1.0 meters and drop to 0.2 meters. The measurements by Wells and Kemp (1986) have been reproduced by Winterwerp et al., (2007). This experiment used SWAN-Mud with the DeWit method but constantly calculated dissipation rates higher than in the experiment. This is possibly caused by how the mudbank is implemented in SWAN-Mud. The dissipation rate at the mudbank's seaward edge seems to be an overestimation, which could be caused by the implementation of the mud in SWAN as discussed before. This overestimation is also visible in a paper by Van Ledden et al., (2009). In this study a storm situation from 2005 was reproduced.

The total dissipation pattern for situations with and without mud is significantly different (Figure 3.11). Of course, the presence of mud causes a prominent peak, which is absent in situations without mud. Bottom friction is minimalized when mud is added to the experiment. This is caused by the protection layer of mud on top of the bathymetry. The decrease in bottom friction is partly caused by the implementation of the mud dissipation in SWAN-Mud. In the source code is defined that when the mud dissipation exceeds the bottom friction in magnitude, the bottom friction becomes zero. Not only is the difference in wave height visible for the comparison of scenarios with and without mud. The difference is also visible between the mudbank and the interbank. The interbank shows much higher wave heights and periods nearshore. This indicates possible coastal erosion in these interbank areas. This is often described in the literature by Winterwerp et al. (2007;2012; 2020) and Augustinus (2004).

Wells and Coleman (1981) observed an increase in wave period over the mud; this does not coincide with modelling the results in this study. The different experiments done with DELFT in SWAN-Mud found a decrease in wave periods over the mudbank (this was also found with Ng). If the dispersion relation by Gade is used in SWAN-Mud as is done in the thesis by Tzampazidou (2020), this increase in the wave period can also be observed. Field observations by experts do not confirm this increase in wave period. Winterwerp et al. (2007) advocates for a decrease in wave period due to mud damping. In Figure 3.22, the wave energy density shows a large decrease in low-frequency waves while the mud very little influences the high-frequency waves. Field data from Best et al. (2022) shows very small waver periods close to the coast, indicating a decrease in wave period by the mud dissipation. This strengthens the findings in this study with the DELFT method. However, more field measurements of the wave period would give more insight.

In recent work by Best et al. (2022), a measuring campaign is conducted over a mudbank for the last 3 kilometres and into the mangroves. The waves drop to 0.02 – 0.2 meters in this dataset and 2-4 seconds. This correlates to the winter scenarios; the field data is measured from November to January, which is also during winter. A future data-model comparison would be highly desirable.

4.4.2 Seasonality of the wave environment

The influence of the mud on the waves in front of the coast has been described in the previous chapter, and this chapter will focus mainly on the different waves. In the 2D experiments, it was observed that the waves with increasing periods have less influence on the rate of mud dissipation than the waves with increasing wave height. This corresponds with the results from Figure 3.18 and 3.19, as the dissipation is the highest for the most energetic scenarios, which corresponds to the findings in the 2D experiments. If we compare this to Figure 3.14, the wave height and wave period drop significantly more for the higher energetic periods. This can also be observed in Appendix F, here is a transect shown with the relative change due to the mud.

The erosion and transport of the mudbanks are not directly output from SWAN-Mud, because the mudbank is static and hydrodynamic processes are not included. Nevertheless, it is visible that the most energetic scenarios reach further over the mudbank before losing most of their energy (wave height)(see Figure 3.20). One could advocate that the fluid mud would be eroded and transported away due to the large drop in energy. Also, the possible erosion in the interbank is visible as the storms remain very high in the interbank areas and will be able to erode the intertidal part, including the trailing edge of the mudbank (Winterwerp, 2022) (see Figure 3.22). This process is also described in Winterwerp (2020) and Augustinus (2004). In these studies, it is hypothesized that the more energetic scenarios drive the movement of the mudbanks. The less energetic scenarios (summer and mild winters) do not have waves reaching far over the mud. However, they still lose a large part of the energy at the edges of the mud. As fluid mud is kept in the system by wave energy, the summer scenarios would be able to prevent the mud from settling and consolidating. This cannot be concluded as these values are not quantified, but there are indications of similar processes described in Rodrigues and Metha (2001) and Anthony (2010). However, new hypotheses regarding mudbank migration describe the mudbanks' movement as gradually and not event-driven (De Vries, personal communication, 2022). Field observations are necessary to confirm any hypotheses.

4.4.3 Wave Frequency

The plot with the wave energy for the summer scenario along the transect (Figure 3.22) contains similar results to Figure 3.10 for the idealized experiments. However, in the 2D experiments, only the dissipation by mud was accounted for, while in the test case all other dissipation terms are accounted for. The influence of the bottom friction for situations with mud is visible for the scenarios as a decrease in wave energy for the scenarios without mud. This dissipation is also mainly present in the lower frequencies but less profound in the 0.2-0.5 Hz region. The bottom friction is replaced by mud dissipation when the mud dissipation becomes more significant than the bottom friction, confirmed by checking the source code of SWAN. The mud dissipation increases so steeply that this dissipation quickly exceeds the bottom friction. Figure 3.17 also shows these results, and this is when the bottom friction becomes zero.

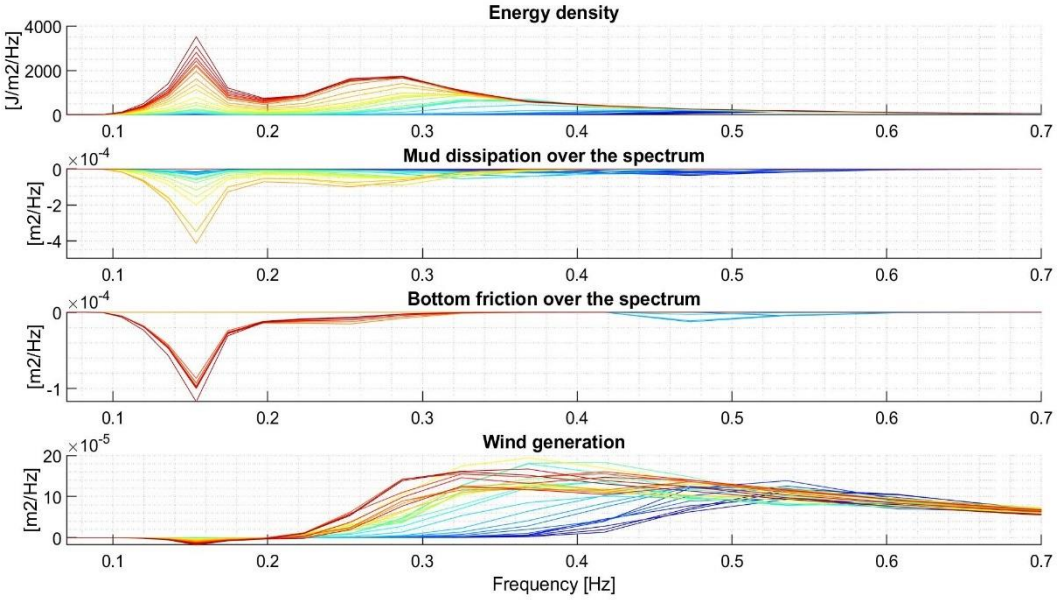

Figure 4.5: The dissipation and energy for the diagonal transect over the mudbank. The parameters are given for the wave spectra. The first graph gives the energy density of the waves, the second panel provides the dissipation by mud for the wave spectra. In the third figure the bottom friction is plotted. Wind generation is given in the last plot for the wave spectra. The colors indicate the distance from shore: red means offshore, orange the beginning of the mud layer and blue is onshore.

In Figure 4.5, the energy density of a summer scenario, including wind, is provided for the diagonal transect. The plot also contains mud dissipation and bottom friction for the wave spectra and the wind generation over the transect. The red colours indicate the offshore locations, while the blue ones mark the onshore locations. The first orange line in the mud dissipation plot marks the beginning of the mudbank. Here the mud dissipation mainly occurs between 0.1-0.2 Hz and is still profound until 0.3 Hz. This is caused by wave generation by the wind. Bottom friction only dissipates the swell waves and has almost no effect on wind-generated waves. Interesting and unexpected is that the mud still damps a part of the wind-generated waves, although it is only a small fraction. These results correspond with the results of Figure 3.22 in Suriname. However, it does not coincide with earlier experiments by Winterwerp et al. (2012), stating that higher frequency waves are not damped at all.

Contradicting, in the 2D experiments, is also advocated that a certain wave period is necessary for the dissipation by the mud. However, it is visible that in the Suriname test case, dissipation in the waves with high frequency is occurring. The dependency of this dissipation seems to be linked to the water depth, the mud's viscosity and the wave energy availability.

Siadatmousavi et al.(2012) were the first to mention the influence of the mud on waves in the frequency of 0.3 – 0.4 Hz, supporting the findings in Figure 4.5 and Figure 3.22. The decrease in water depth is expected to cause this influence. This also relates to the earlier described parameter space. If the water depth is altered, it influences different parameters, changing the dissipation rate for different frequencies. For the Suriname test case, the depth is becoming shallow towards the coast (see Figure 3.22). The result is that the smaller waves can also reach through the water depth to the mud (as explained in the 1D experiments). This could cause the dissipation of these higher frequency waves. This effect coincides with the earlier described parameter space (described in the 1D experiments).

It also coincides with the availability of energy in this region. Due to the long fetch in the Suriname test case, more energy is availably in the 0.3-0.5 Hz region compared to the 2D experiment (Figure 4.5). This is because the fetch is relatively small for this region. The energy input is also responsible for the damping in the higher frequencies. It can be observed that energy is generated in the frequencies where damping happens in Figure 4.5 (until 0.42 Hz). However, a more elaborate experiment should be conducted with the water depth and the dissipation per frequency.

4.4.4 Wave direction & diffraction

The diffraction due to the mudbanks is visible in Figure 3.23, here is visible that the waves are diffracted in a similar way as in the 2D experiments (Figure 3.7). However, not all parts of the mudbank refract in a similar way, and the response on the different angles of incidence is different for all scenarios.

Figure 3.24 shows that the wave height reaching the coast is highest for the waves coming from the north compared to the east. As concluded from the earlier experiments, these waves have the highest dissipation, directly related to the higher waves. The refraction of the waves corresponds to the refraction of the waves in the 2D experiments. In the 2D experiments, the bottom was flat without any contours. In the case study, the bottom contours greatly influence the refraction. The diffraction by the mud is more significant for the waves coming from the north, which are higher energetic when they reach the mud. This more significant diffraction is caused by the steeper drop in wave period. Appendix F shows that more energetic scenarios drop relatively more in wave period. The drop in wavelength will be similar for all scenarios as it is mainly influenced by the wavenumber. This means the diffraction by mud will be larger if the theory introduced in Section 4.3.2 is correct. Field data remains necessary to confirm this.

Figure 3.23 shows where the wave direction corresponds with the bathymetry features. Waves diffract towards the shallow parts in the bathymetry. However, the effect of the mud is recognizable in a similar fashion as in Figure 3.7. Waves are diffracted away from the mud, or the mud smooths the refraction by the bottom contours, and the waves will still refract towards

the coast. One could advocate that the influence of the decreasing water depth is more significant than the influence of the mud, as the refraction changes for the 2D experiments when the water depth is altered. This is also visible in the Suriname experiments, where parts of the bathymetry, including the mudbank's shape, are coupled to more shoreward refraction. Nevertheless, is the influence of the mud in the opposite direction of the refraction by decreasing water depth.

The bathymetry used for Suriname does not include the mudbanks used, or only segments are included. This would mean that the mudbanks implemented for the case study are partly mudbanks and partly mud patches. This is important for the interpretation of the wave direction and refraction. As stated before, the influence of this difference on dissipation is little. However, for the parts where the bathymetry includes parts of the mudbank contours, the waves still bend towards the mud, and the results look similar to the left plot of Figure 4.6 by Chevallier et al. (2008). It seems only obvious that when the mud layer is implemed as a full mudbank with accurate bathymetry the diffraction will look very identical to Figure 4.6.

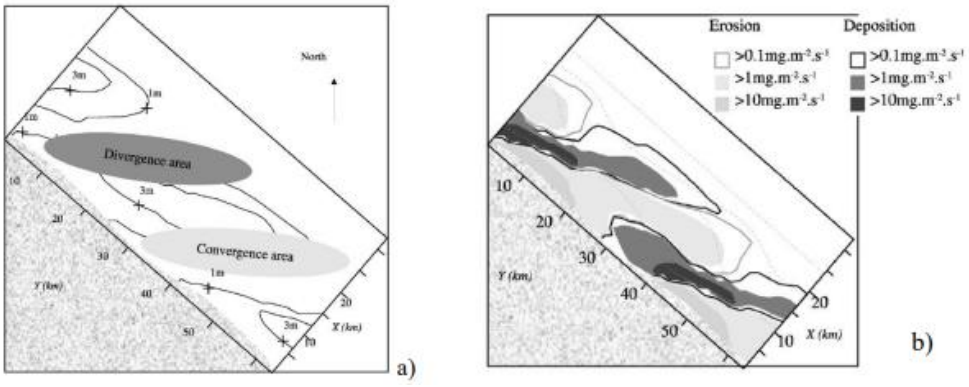

Figure 4.6: Sketch by Chevalier et al. (2008) for the divergence and convergence zones related to the mudbank and interbank area on the left. The right plot indicates areas of erosion and deposition around the mudbanks.

4.5 Further Research & Recommendations

Since the coupling between Delft3D and SWAN-Mud was made possible at the start of this study, much progress has been made in debugging the SWAN-Mud module. Now that the coupling within Delft3D-Wave is working fine, the next step would be coupling between Delft3D-Wave and Delft3D-Flow in combination with SWAN-Mud. This way, the hydrodynamic situation can be included in test cases to make them more realistic. For this, it is important to look into the static behaviour of the mud. It is of interest to include sediment transport in the model to make the mudbank dynamic. It would be complicated to include the rheologic behaviour of the mudbank as not much is known about the processes involved in the alongshore movement of the mudbanks. The flow and wave modules of Delft3d need to communicate the correct parameters, such as radiation stresses and mud layer thicknesses.

Research that would contribute to the knowledge of modelling mud dissipation would be to focus more on the dissipation over the wave spectra. The influence of changes in the 1D experiments on the damping in different frequencies would be of interest. This would help better understand some of the 2D experiments and the Suriname test case results. Measurements would be necessary to confirm the modelling results. Further research is necessary into the influence of the wind on the mud dissipation as it remains unclear why the model plots different wave heights at the fetch, different from the model input when the wind is also considered. However, this is a problem for the whole SWAN model and should be developed for the model, not only in SWAN-Mud. Not all output from SWAN-Mud is available as output in Delft3D-Wave, more explicit outputs such as dissipation for a location over the wave spectra can only be reached through SWAN-Mud stand-alone. A new solver must be implemented in SWAN-Mud to make the DeWit method work correctly. The connection between the dispersion relation, the solver, and the dissipation term is now not working optimally as the solver is designed for the DELFT method. Ideally, one solver is implemented that works optimally for both methods.

For the coast of Suriname, the lack of field measurements of wave environments is an important missing link for future research. When more modelling studies for the coast of Suriname are desired, more field data is necessary, for example, wave data of a transect over the mud layer. Also, the bathymetry data is unreliable for the coast of Suriname due to the large amount of mud in the water column. The study of Carneiro et al. (2020) describes accurate methods for measuring fluid mud, which would be of interest for further research. Furthermore, it is unclear if the bathymetry is taken from the top of the mud to the bottom of the mud or somewhere in the middle. This problem is also related to the lack of measurement of the thickness of the mudbanks and the extent of the mud into the ocean. These are problems that must be solved with an extensive field campaign. Besides accurate bathymetry, wave data over a transect would be useful, including the wave frequency. Measurements regarding the rheology of the mudbank would be of interest as well. This would need to include measurements of the different states of the mudbank (e.g. fluid mud, consolidated, suspended matter). The process of mud streaming is also discussed in Borsje (2019) and is still of interest for mudbank dynamics.

5 Conclusion

In this chapter, the research questions will be answered, the objectives reached in this study will be summarized, and lessons learned from the case study will also be provided below.

Research Question 1.

"Which characteristics of the "fluid mud" are most important for the mud-induced wave damping and why? "

The viscosity of the mud layer is the most essential variable for the mud dissipation, together with the thickness of the overlying water layer. With increasing viscosity, the mud-induced wave damping increases in orders of magnitude. The mud density has the opposite effect: the smaller the ratio between water and mud density, the larger the mud damping. This difference is relatively small compared to the viscosity. Thirdly, the mud layer shows an optimum thickness related to the Stokes boundary layer. This optimum is around 1.3 times its thickness for all implemented dispersion relations. Lastly, the increase of mud dissipation is exponential with decreasing water layer thickness. This increase is very steep and diminishes the influence of the mud thickness. It is important to note that the computations with fluid mud are complex and dependent on many parameters. These conclusions are applicable for simplified and idealized situations in the parameter range presented in this thesis. However, the effect of changing any of the parameters outside that parameter range also affects other parameters and may result in deviating effects as they are all interconnected. The results from the 1D experiments can also be seen as a transect of this parameter space.

Research Question 2.

"What is the influence of the wave environment on the mud-induced wave damping?"

The wave height has the most influence on the energy dissipation for the incoming waves, compared to the wave period, with minimal influence on the magnitude of the dissipation. However, waves with a smaller period are barely damped by the mud and can travel freely over the mud; thus, a minimal wave period is necessary for mud dissipation. The increase in mud dissipation with increasing wave period reaches an optimum beyond 8 seconds. Beyond this maximum, the mud dissipation declines in rate with very large wave periods (>12 sec). This is important for wind and swell waves as the first can grow over the mud while the mud damps the latter. More energetic waves will travel further over the mud regardless of the larger dissipation affecting them. When the mud is stored in the shape of a mudbank, the waves refract towards the mud and the shore, while the refraction by the mud is directed in the opposite direction. This implies that the effect of the water depth on the diffraction is larger than the effect of the mud layer. The wind only affects the mud by increasing the energy; however, the direct effect on the dissipation is minimal. Waves with lower frequencies are mainly damped, but the dissipation by mud extends further to higher frequencies (0.1 – 0.5 Hz) than discussed in the literature (0.1 – 0.25 Hz), which depends on the energy input. This also depends on the parameter space as the Stokes boundary layer depends on the wave period and the viscosity of the mud. The water depth has a significant influence on the dissipation by the mud and possibly on the dissipation in higher frequencies (1D experiments).

Test case: Suriname

The main objective of the test case was to support the results of the more idealized scenarios. It was also of interest to apply them to a realistic scenario, so the model's applicability is tested. In order to make this case study relevant for research in Suriname, some goals were set up. The role of the mudbanks is discussed on the coast of Suriname, and the influence of different wave environments on the dissipation of the mud is analyzed. Furthermore, the role of local winds and the influence of waves with different angles of incidence is investigated.

Only limited conclusions regarding the Suriname coastline can be drawn as field data was limited, and the bathymetry and mudbank bathymetry were unreliable. Nevertheless, it can be concluded that the mud has a considerable influence on the incoming waves and works as a protection mechanism in front of the coast, damping the incoming waves. When these banks would be absent, the incoming waves would be much higher and could induce large amounts of erosion, which corresponds with field observations in this research area. This is the same for the interbank areas. In these areas, the wave height maintains much longer and reaches the shore. Winter and winter storm scenarios would be responsible for these erosion situations. Higher energetic scenarios could cause movement of the mud as the wave height, wave period, and orbital motion reach further on the mudbank and lose a large part of their energy in this short distance. As the mud is easily transported, these higher energetic scenarios could be the drivers, as hypothesized in Augustinus (2004). The rheology of the mudbanks and sediment was out of the scope of this study and has not been investigated.

The local winds cause extra waves to reach shore when these winds are onshore as the mud does not dissipate locally generated wind waves. The local wind does influence the rate of dissipation by the mud or the bottom friction. Further research into the physical processes of the Suriname coastal zone is necessary before more conclusions can be drawn due to the lack of field data.

SWAN-Mud & Delft3d-Wave

One of the study's main objectives was debugging SWAN-Mud and testing its connection with Delft3D-Wave. After this step, it was of interest to test the new mud module in Delft3D-Wave. It can be concluded that Delft3D-Wave can model the influence of mud dissipation on incoming waves and calculate the effect on wave parameters correctly. Using Delft3D-Wave improves the usability of SWAN-Mud, which was one of the goals of this coupling. Debugging SWAN-Mud was successful for the smaller bugs caused by inconsistencies in the source code for the Gade and Ng method. Furthermore, with solving calculation errors in the dispersion relation of DELFT, the debugging of this method was successful. The DeWit method was solved only partly, the calculation errors were restored, and the dissipation term was added. The solver built for DELFT is currently used, causing the model to crash for more extensive or complicated calculations. A correct solver is necessary to solve the implicit calculations.

References

Anthony, E. J., Dolique, F., Gardel, A., Gratiot, N., Proisy, C., & Polidori, L. (2008). Nearshore intertidal topography and topographic-forcing mechanisms of an Amazon-derived mudbank in French Guiana. Continental Shelf Research, 28(6), 813–822. https://doi.org/10.1016/j.csr.2008.01.003

Anthony, E. J., Gardel, A., & Gratiot, N. (2014). Fluvial sediment supply, mudbanks, cheniers and the morphodynamics of the coast of South America between the Amazon and Orinoco river mouths. Geological Society Special Publication, 388(1), 533–560. https://doi.org/10.1144/SP388.8

Anthony, E. J., Gardel, A., Gratiot, N., Proisy, C., Allison, M. A., Dolique, F., & Fromard, F. (2010). The Amazon-influenced muddy coast of South America: A review of mud-bank-shoreline interactions. In Earth-Science Reviews (Vol. 103, Issues 3–4, pp. 99–121). https://doi.org/10.1016/j.earscirev.2010.09.008

Anthony, E. J., & Gratiot, N. (2012). Coastal engineering and large-scale mangrove destruction in Guyana, South America: Averting an environmental catastrophe in the making. Ecological Engineering, 47, 268–273. https://doi.org/10.1016/j.ecoleng.2012.07.005

Augustinus, P. G. E. F. (1978). The changing shoreline of Suriname (South America) (Doctoral dissertation, University Utrecht).

Augustinus, P. G. E. F. (2004). The influence of the trade winds on the coastal development of the Guianas at various scale levels: A synthesis. Marine Geology, 208(2–4), 145–151. https://doi.org/10.1016/j.margeo.2004.04.007

Battjes, J. A., and J. P. F. M. Janssen (1978), Energy loss and set-up due to breaking of random waves, in Coastal Engineering, 1978, pp. 569–588, Am. Soc. of Civ. Eng., New York.

Best, U., Wegen, M. Van Der, Dijkstra, J., Reyns, J., Prooijen, B. C. Van, & Roelvink, D. (2022). *Wave attenuation potential, sediment properties and mangrove growth dynamics data over Guyana's intertidal mudflats: assessing the potential of mangrove restoration works 5*. *January*, 1–24.

Bertotti, L and L. Cavaleri, 1994: Accuracy of wind and wave evaluation in coastal regions, Proc. 24th Int. Conf. Coastal Engineering, ASCE, 57-67

Beyramzade, M., & Siadatmousavi, S. M. (2018). Implementation of viscoelastic mud-induced energy attenuation in the third-generation wave model, SWAN. Ocean Dynamics, 68(1), 47–63. https://doi.org/10.1007/s10236-017-1118-4

Borsje, R. (2019). Wave-Driven Set-Up of Fluid Mud: Demak, Indonesia. Master's thesis

Bottema, M., J. P. de Waal, and H. J. Regeling (2003), Some applications of the Lake IJssel/Lake Sloten wave data set, in Coastal Engineering 2002, edited by J. McKee Smith, pp. 413–425, Am. Soc. of Civ. Eng., New York.

Cavaleri, L. and P. Malanotte-Rizzoli, 1981: Wind wave prediction in shallow water: Theory and applications. J. Geophys. Res., 86, No. C11, 10,961-10,973

Carneiro, J. C., Gallo, M. N., & Vinzón, S. B. (2020). Detection of fluid mud layers using tuning fork, dual-frequency echo sounder, and chirp sub-bottom measurements. Ocean Dynamics, 70(4), 573-590.

Chevalier, C., Froidefond, J. M., & Devenon, J. L. (2008). Numerical analysis of the combined action of littoral current, tide and waves on the suspended mud transport and on turbid plumes around French Guiana mudbanks. Continental Shelf Research, 28(4–5), 545–560. https://doi.org/10.1016/j.csr.2007.09.011

Dalrymple, R.A., Liu, P.L.-F., 1978. Waves over soft muds: a two layer model. J. Phys. Oceanogr. 8, 1121–1131

De Jong, S. M., Shen, Y., de Vries, J., Bijnaar, G., van Maanen, B., Augustinus, P., & Verweij, P. (2021). Mapping mangrove dynamics and colonization patterns at the Suriname coast using historic satellite data and the LandTrendr algorithm. International Journal of Applied Earth Observation and Geoinformation, 97, 102293. https://doi.org/10.1016/j.jag.2020.102293

Deltares (2021) Delft3D 3D/2D modelling suite for integral water solutions - User Manual Delft3D-WAVE – Version 3.07

Deng, B. Q., Hu, Y., Guo, X., Dalrymple, R. A., & Shen, L. (2017). Numerical study on the dissipation of water waves over a viscous fluid-mud layer. Computers and Fluids, 158, 107–119. https://doi.org/10.1016/j.compfluid.2017.04.015

De Waal, J. P. (2002). Wave growth limit in shallow water. In Ocean Wave Measurement and Analysis (pp. 560-569).

Dewaelheyns Ph, Etneo L (2007) Modellering van de stromingen voor de kust van Suriname. MSc thesis, Dept. of Civil Engineering, KU Leuven (in Dutch)

De Wit, P.J., & Kranenburg, C.V. (1993). Liquefaction and Erosion of China Clay Due to Waves and Current.

De Wit, P. J. (1995). "Liquefaction of cohesive sediment by waves." Ph.D. dissertation, Delft Univ. of Technology, Netherlands.

De Wit, P. J., & Kranenburg, C. (1997). The wave-induced liquefaction of cohesive sediment beds. Estuarine, Coastal and Shelf Science, 45(2), 261–271. https://doi.org/10.1006/ecss.1996.0184

De Wit, P. J., & Kranenburg, C. (1996). On the effects of a liquefied mud bed on wave and flow characteristics. Journal of Hydraulic Research, 34(1), 3–18. https://doi.org/10.1080/00221689609498761

Doyle, E. H. (1973, April). Soil-Wave Tank Studies Of Marine Soil Stability. In Offshore Technology Conference. OnePetro.

Eldeberky, Y. (1996), Nonlinear transformations of wave spectra in the nearshore zone, Ph.D thesis, 203 pp., Delft Univ. of Technol., Delft, Netherlands.

Eldeberky, Y., and J. A. Battjes (1996), Spectral modeling of wave breaking: Application to Boussinesq equations, J. Geophys. Res., 101, 1253–1264.

Elgar, S., & Raubenheimer, B. (2008). Wave dissipation by muddy seafloors. 35, 1–5. https://doi.org/10.1029/2008GL033245

Einstein, HA, 1941. The viscosity of highly concentrated underflows and its influence on mixing. Transactions Twenty-Second Annual Meeting American Geophysical Union. Part 1, section of Hydrology Papers, National Research Council, Washington, DC. pp. 597- 603

Eisma, D., & Van der Marel, H. W. (1971). Marine muds along the Guyana coast and their origin from the Amazon Basin. Contributions to Mineralogy and Petrology, 31(4), 321-334.

ERA-5 (2022), website: https://www.ecmwf.int/en/forecasts/datasets/reanalysis-datasets/era5

Froidefond, J. M., Lahet, F., Hu, C., Doxaran, D., Guiral, D., Prost, M. T., & Ternon, J. F. (2004). Mudflats and mud suspension observed from satellite data in French Guiana. Marine Geology, 208(2–4), 153–168. https://doi.org/10.1016/j.margeo.2004.04.025

Froidefond, J.-M., M. Pujos and X. Andre´. 1988. Migration of mudbanks and changing coastline in French Guiana. Mar. Geol., 84, 19 –30.

Gade, H.G., 1958. Effects of a non-rigid, impermeable bottom on plane surface waves in shallow water. J. Mar. Res. 16, 61–82.

Gardel, A., Gensac, E., Anthony, E., Lesourd, S., Loisel, H., Marin, D., & du Littoral Côte, U. (2011). Journal of Coastal Research SI 64 pg-pg ICS2011 (Proceedings) Poland. Journal of Coastal Research, Special Issue, 64.

Gardel, A., & Gratiot, N. (2005). A satellite image-based method for estimating rates of mudbank migration, French Guiana, South America. Journal of Coastal Research, 21(4), 720–728. https://doi.org/10.2112/03-0100.1

GEBCO. Computers Geosciences. URL https://www.gebco.net/data and products/gridded bathymetry data/.

Gensac, E., Gardel, A., Lesourd, S., & Brutier, L. (2015). Morphodynamic evolution of an intertidal mudflat under the influence of Amazon sediment supply - Kourou mudbank, French Guiana, South America. Estuarine, Coastal and Shelf Science, 158, 53–62. https://doi.org/10.1016/j.ecss.2015.03.017

Gensac, E., Martinez, J. M., Vantrepotte, V., & Anthony, E. J. (2016). Seasonal and inter-annual dynamics of suspended sediment at the mouth of the Amazon river: The role of continental and oceanic forcing, and implications for coastal geomorphology and mudbank formation. Continental Shelf Research, 118, 49–62. https://doi.org/10.1016/j.csr.2016.02.009

Geyer, W. R., Hill, P. S., & Kineke, G. C. (2004). The transport, transformation and dispersal of sediment by buoyant coastal flows. Continental Shelf Research, 24(7–8), 927–949. https://doi.org/10.1016/j.csr.2004.02.006

Gratiot, N., & Anthony, E. J. (2016). Role of flocculation and settling processes in development of the mangrove-colonized, Amazon-influenced mud-bank coast of South America. *Marine Geology*, *373*, 1–10. https://doi.org/10.1016/j.margeo.2015.12.013

Gratiot, N., Gardel, A., & Anthony, E. J. (2007). Trade-wind waves and mud dynamics on the French Guiana coast, South America: Input from ERA-40 wave data and field investigations. *Marine Geology*, *236*(1–2), 15–26. https://doi.org/10.1016/j.margeo.2006.09.013

Guo, J. (2002). “Simple and explicit solution of the wave dispersion relation.” Coastal Eng., 45, 71–74

Hasselmann, K., 1960: Grundgleichungen der Seegangsvoraussage, Schiffstechnik, 1, 191−195

Hasselmann, K., 1962: On the non-linear transfer in a gravity wave spectrum, part 1. General theory, J. Fluid Mech., 12, 481-500

Hasselmann, K., T.P. Barnett, E. Bouws, H. Carlson, D.E. Cartwright, K. Enke, J.A. Ewing, H. Gienapp, D.E. Hasselmann, P. Kruseman, A. Meerburg, P. Muller, growth and swell decay during the Joint North Sea Wave Project (JONSWAP), Dtsch. D.J. Olbers, K. Richter, W. Sell and H. Walden, 1973: Measurements of wind−wave Hydrogr. Z. Suppl., 12, A8

Hersbach, H., Bell, B., Berrisford, P., Biavati, G., Horányi, A., Muñoz Sabater, J., Nicolas, J., Peubey, C., Radu, R., Rozum, I., Schepers, D., Simmons, A., Soci, C., Dee, D., Thépaut, J-N. (2019): ERA5 monthly averaged data on single levels from 1979 to present. Copernicus Climate Change Service (C3S) Climate Data Store (CDS). (Accessed on 17-11-2021), 10.24381/cds.f17050d7

Holthuijsen. L, Waves in oceanic and coastal waters. Cambridge University Press., 2007. doi: 10.1017/ CBO9780511618536.

Hsu, W. Y., Hwung, H. H., Hsu, T. J., Torres-Freyermuth, A., & Yang, R. Y. (2013). An experimental and numerical investigation on wave-mud interactions. *Journal of Geophysical Research: Oceans*, *118*(3), 1126–1141. https://doi.org/10.1002/jgrc.20103

Inglis, CC and Allen, FH, 1957. The regimen of the Thames estuary as affected by currents, salinities and river flow. Proceedings Institution of Civil Engineers London, 7:827-868.

Jaramillo, S., Sheremet, A., Allison, M. A., Reed, A. H., & Holland, K. T. (2009). Wave-mud interactions over the muddy Atchafalaya subaqueous clinoform, Louisiana, United States: Wave-supported sediment transport. *Journal of Geophysical Research: Oceans*, *114*(4). https://doi.org/10.1029/2008JC004821

Kaihatu, J. M., Sheremet, A., & Holland, K. T. (2007). A model for the propagation of nonlinear surface waves over viscous muds. *Coastal Engineering*, *54*(10), 752–764. https://doi.org/10.1016/j.coastaleng.2007.05.003

Kaihatu, J. M., & Tahvildari, N. (2012). The combined effect of wave-current interaction and mud-induced damping on nonlinear wave evolution. *Ocean Modelling*, *41*, 22–34. https://doi.org/10.1016/j.ocemod.2011.10.004

Komen, G.J., Cavaleri, L., Donelan, M., Hasselmann, K., Hasselmann, S. and P.A.E.M. Janssen, 1994: Dynamics and Modelling of Ocean Waves, Cambridge Uni- versity Press, 532 p.

Kranenburg, W. M., Winterwerp, J. C., de Boer, G. J., Cornelisse, J. M., & Zijlema, M. (2011). SWAN-Mud: Engineering Model for Mud-Induced Wave Damping. *Journal of Hydraulic Engineering*, *137*(9), 959–975. https://doi.org/10.1061/(asce)hy.1943-7900.0000370

Kranenburg, W. M. (2008). Modelling wave damping by fluid mud: Derivation of a dispersion equation and an energy dissipation term and implementation into SWAN.

Lade, P. V., & De Boer, R. (1997). The concept of effective stress for soil, concrete and rock. Geotechnique, 47(1), 61-78.

Lefebvre, J. P., Dolique, F., & Gratiot, N. (2004). Geomorphic evolution of a coastal mudflat under oceanic influences: An example from the dynamic shoreline of French Guiana. *Marine Geology*, *208*(2–4), 191–205. https://doi.org/10.1016/j.margeo.2004.04.008

Liu, K., & Mei, C. C. (1989). Effects of wave-induced friction on a muddy seabed modelled as a Bingham-plastic fluid. *Journal of Coastal Research*, *5*(4), 777–789.

Liu, P. L. F., & Chan, I. C. (2007). A note on the effects of a thin visco-elastic mud layer on small amplitude water-wave propagation. *Coastal Engineering*, *54*(3), 233–247. https://doi.org/10.1016/j.coastaleng.2006.08.015

Maa, P.-Y. (1986). "Erosion of soft mud beds by waves." Ph.D. dissertation, Coastal and Oceanographic Engineering Dept., Univ. of Florida, Gainesville, FL.

Maa, J.P.-Y., Metha, A.J., 1990. Soft mud response to water waves. J. Waterw. Port Coast. Ocean Eng. 116, 634–650

Mastenbroek, C., G. Burgers, and P.A.E.M. Janssen, 1993: The dynamical coupling of a wave model in a storm surge model through the atmospheric boundary layer, J. Phys. Oceanogr., 23, 1856-1866

Mathew, J., and M. Baba (1995), Mudbanks of the Southwest Coast of India. 2. Wave-Mud Interactions, J. Coastal Res., 11(1), 179–187

McAnally, W. H., Friedrichs, C., Hamilton, D., Hayter, E., Shrestha, P., Rodriguez, H., Sheremet, A., & Teeter, A. (2007). *Management of Fluid Mud in Estuaries, Bays, and Lakes. I: Present State of Understanding on Character and Behavior ASCE Task Committee on Management of Fluid Mud*. https://doi.org/10.1061/ASCE0733-94292007133:19

Mehta, A. J. (1991). Understanding fluid mud in a dynamic environment. *Geo-Marine Letters*, *11*(3–4), 113–118. https://doi.org/10.1007/BF02430995

Mei, C.C., 1983: The applied dynamics of ocean surface waves, Wiley, New York, 740 p

Nedeco (1968) Surinam transportation study: report on hydraulic investigation. Netherlands Engineering Consultants, The Hague, p 293

Nedeco (1972) Report on sea defence studies. Netherlands Engineering Consultants, The Hague

Ng, C.-O. (2000). Water waves over a muddy bed: a two-layer Stokes' boundary layer model. In *Coastal Engineering* (Vol. 40). www.elsevier.comrlocatercoastaleng

Nichols MN, 1984-1985. Fluid mud accumulation processes in an estuary, *Geo-Marine Letters* 4:171-176.

Owen, MW, 1976. Problems in the modeling of transport, erosion, and deposition of cohesive sediments. In: Goldberg, ED, McCave, IN, O'Brien, JJ, Steele, JH (Eds.), *The sea, vol. 6.* Wiley, New York. pp. 515-537

Plaziat, J. C., & Augustinus, P. G. E. F. (2004). Evolution of progradation/erosion along the French Guiana mangrove coast: A comparison of mapped shorelines since the 18th century with Holocene data. *Marine Geology*, *208*(2–4), 127–143. https://doi.org/10.1016/j.margeo.2004.04.006

Rogers, W. E., and Holland, K. T. (2009). "A study of dissipation of wind- waves by mud at Cassino Beach, Brazil: Prediction and inversion." Cont. Shelf Res., 29(3), 676–690.

Proisy, C., Gratiot, N., Anthony, E. J., Gardel, A., Fromard, F., & Heuret, P. (2009). Mudbank colonization by opportunistic mangroves: A case study from French Guiana using lidar data. *Continental Shelf Research*, *29*(3), 632–641. https://doi.org/10.1016/j.csr.2008.09.017

Rodriguez, H. N., and Mehta, A. J. (2001). "Modeling muddy coast re- sponse to waves." J. Coastal Res., SI27, 137–148.

Ross, M.A., 1988. Vertical structure of estuarine fine sediment suspensions. Technical Report. Coastal and Oceanographic Engineering Department, University of Florida, Gainesville.

Ross, M. A., & Mehta, A. J. (1989). On the Mechanics of Lutoclines and Fluid Mud, pp.51-62 Coastal E. *Journal of Coastal Research*, *5*, 51–62.

Sakakiyama T, Bijker EW (1989) Mass transport velocity in mud layer due to progressive waves. J Waterw Port Coast Ocean Eng 115 (5):614–633

Shemdin, P., K. Hasselmann, S.V. Hsiao and K. Herterich, 1978: Non−linear and linear bottom interaction effects in shallow water, in: Turbulent Fluxes through the Sea Surface, Wave Dynamics and Prediction, NATO Conf. Ser., V, 1, 347−372

Sheremet, A., Jaramillo, S., Hsu, S.F., Allison, M.A., Holland, K.T., 2011. Wave-mud interactions over the muddy Atchafalaya subaqueous clinoform, Louisiana, United States: wave processes. J. Geophys. Res. 116 http://dx.doi.org/10.1029/ 2010JC006644. C06005. http://dx.doi.org/10.1029/2010JC006644

Sheremet, A., & Stone, G. W. (2003). Observations of nearshore wave dissipation over muddy sea beds. *Journal of Geophysical Research: Oceans*, *108*(11). https://doi.org/10.1029/2003jc001885

Suhayda, J. N. 1984 Interactions between surface waves and muddy bottom sediments. *Lecture Notes on Coastal and Estuarine Studies 14*, 401–428.

Siadatmousavi, S. M., Allahdadi, M. N., Chen, Q., Jose, F., & Roberts, H. H. (2012). Simulation of wave damping during a cold front over the muddy Atchafalaya shelf. *Continental Shelf Research*, *47*, 165–177. https://doi.org/10.1016/j.csr.2012.07.012

Simpson, M. C., Scott, D., New, M., Sim, R., Smith, D., Harrison, M., ... & Overmas, M. (2012). An overview of modelling climate change impacts in the Caribbean region with contribution from the Pacific Islands.

Solaun, K., Alleng, G., Flores, A., Resomardono, C., Hess, K., & Antich, H. (2021). State of the Climate Report: Suriname.

SWAN (2009). SWAN, User manual - Cycle III version 40.72AB. Tech. rep., Delft University of Technology

SWAN (2014) SWAN, Scientific and technical documentation – Cycle III version 41.31AB, Tech. rep., Delft University of Technology

Temmink, R. J., Lamers, L. P., Angelini, C., Bouma, T. J., Fritz, C., van de Koppel, J., ... & van der Heide, T. (2022). Recovering wetland biogeomorphic feedbacks to restore the world's biotic carbon hotspots. Science, 376(6593), eabn1479.

Torres-Freyermuth, A., & Hsu, T. J. (2010). On the dynamics of wave-mud interaction: A numerical study. *Journal of Geophysical Research: Oceans*, *115*(7), 1–18. https://doi.org/10.1029/2009JC005552

Toorman. E, Anthony. E, Augustinus. P, Gardel. G, Gratiot. N, Homenauth. O, Huybrechts. N, Monbaliu. J, Moseley. K (2018). Interaction of mangroves, coastal hydrodynamics, and morphodynamics along the coastal fringes of the guianas. http://www.springer.com/series/8795

Traykovski, P., Trowbridge, J., & Kineke, G. (2015). Mechanisms of surface wave energy dissipation over a high-concentration sediment suspension. *Journal of Geophysical Research: Oceans*, *120*(3), 1638–1681. https://doi.org/10.1002/2014JC010245

Tzampazidou .M.E, H.E, de Swart Smits, H. B., de Vries, J., Nnafie, A., & de Jong, S. (2020). Modelling waves and currents in muddy coastal areas, with a focus on the Suriname coastal zone. *Master's Thesis*

Van Der Westhuysen, A. J., M. Zijlema, and J. A. Battjes (2007), Nonlinear saturationbased whitecapping dissipation in SWAN for deep and shallow water, Coastal Eng., 54, 151–170.

Van Der Westhuysen, A. J. (2010). Modeling of depth-induced wave breaking under finite depth wave growth conditions. *Journal of Geophysical Research: Oceans*, *115*(1), 1–19. https://doi.org/10.1029/2009JC005433

Van Ledden, M., Vaughn, G., Lansen, J., Wiersma, F., & Amsterdam, M. (2009). Extreme wave event along the Guyana coastline in October 2005. *Continental Shelf Research*, *29*(1), 352–361. https://doi.org/10.1016/j.csr.2008.03.010

Van Prooijen B. C., van Maren D. S., Chassagne C., and Winterwerp J. C.. CIE4308: Fine sediment dynamics. Lecture notes, 2017

WAMDI group, 1988: The WAM model − a third generation ocean wave prediction model, J. Phys. Oceanogr., 18, 1775−1810

Wells, J. T., & Coleman, J. M. (1981). *PHYSICAL PROCESSES AND FINE-GRAINED SEDIMENT DYNAMICS, COAST OF SURINAM, SOUTH AMERICA I*. http://pubs.geoscienceworld.org/sepm/jsedres/article-pdf/51/4/1053/2808393/1053.pdf?casa_token=x9soblakTJUAAAAA:meW7KezcSUw0PtznziC4sPzMPotFc2I_MH5JrQ0JQunqupaMstZKdTdCu7APnKe1MMP-

Wells, J. T., & Kemp, P. (1986). Interaction of Surface Waves and Cohesive Sediments: Field Observations and Geologic Significance. *Estuarine Cohesive Sediments Dynamics*, 43–65. https://link.springer.com/chapter/10.1007/978-1-4612-4936-8_3

Wetlands International (2016) Website article: Building with Nature concept successfully introduced in Suriname - Wetlands International

Whitham, G.B., 1974: Linear and nonlinear waves, Wiley, New York, 636 p

Winterwerp, J. C. (2001). Stratification effects by cohesive and noncohesive sediment. Journal of Geophysical Research: Oceans, 106(C10), 22559-22574.

Winterwerp, J. C., Graaff, R. F. d., Groeneweg, J., & Luijendijk, A. P. (2007). Modelling of wave damping at Guyana mud coast. *Coastal Engineering*, *54*(3), 249–261. https://doi.org/10.1016/j.coastaleng.2006.08.012

Winterwerp, J. C., de Boer, G. J., Greeuw, G., & van Maren, D. S. (2012). Mud-induced wave damping and wave-induced liquefaction. *Coastal Engineering*, *64*, 102–112. https://doi.org/10.1016/j.coastaleng.2012.01.005

Winterwerp, J. C., D. S. van Maren, T. van Kessel, C. Chassagne, and B. C. van Prooijen. Fine sediments in the marine environment – from fundamentals to modeling. World Scientific, 2019.

Winterwerp, J.C., T. Albers, E. J. Anthony, D. Friess, A. Gijón Mancheño, K. Moseley, A. Muhari, S. Naipal, J. Noordermeer, A. Oost, C. Saengsupavanich, S.A.J. Tas, F.H. Tonneijck, T. Wilms, C. van Bijsterveldt, P. van Eijk, E. van Lavieren and B.K. van Wesenbeeck, 2020. *Managing erosion of mangrove-mud coasts with permeable dams – lessons learned, Ecological Engineering*, 158, 106078, https://doi.org/10.1016/j.ecoleng.2020.106078

Winterwerp, J. C., Van Kessel, T., van Maren, D. S., & Van Prooijen, B. C. (2022). *Fine Sediment in Open Water: From Fundamentals to Modeling*.

Wong T, Kroonenberg S, Augustinus P (2017). Geologie en landschap van Suriname. Stichting LM Publishers, Volendam, the Netherlands, 198p (in Dutch)

Zhao, Z. D., Lian, J. J., & Shi, J. Z. (2006). Interactions among waves, current, and mud: Numerical and laboratory studies. *Advances in Water Resources*, *29*(11), 1731–1744. https://doi.org/10.1016/j.advwatres.2006.02.009

Personal communications

Job de Vries, February 2022

Huib de Swart, April 2022

Appendix A

Standard SWAN dissipation terms

S_{wind} is the first term and is the primary influence in the generation of waves. This wave input is described in Equation A.1, which includes exponential growth and linear growth.

$$S_{wind}(\sigma,\theta) = A + BE(\sigma,\theta) \tag{A.1}$$

The wind is included as a source in the energy balance because it is the generator of waves. In SWAN, the wind input is described as a resonance mechanism (Philips, 1957) and a feedback mechanism (Miles, 1957). This results in both an exponential term (A) and a linear growth term (B). These terms depend on wave frequency and direction and wind speed and direction. Wind and waves interact as there is friction on the water surface which creates drag, and this causes waves to generate. Part A is represented by Cavaleri & Malanotte-Rizzoli's (1981) expression, where a filter from Tolman (1992) is included. For B, there are two options included in the model; one defined by the WAMDI group (1988) and one from the WAM Cycle 4 (Komen et al., 1994). This corresponding combination of equations is solved with iterative procedures defined by Mastenbroek et al. (1993). The exact equations and formulations in the wind calculations are not further discussed in this thesis as it is out of the scope of this research.

There are three terms for energy dissipation in the source-sink balance of the standard SWAN model: dissipation by depth induced wave breaking, dissipation due to bottom friction, and dissipation by whitecapping (Komen et al., 1994). The last term in the equation accounts for non-linear wave interactions. All these terms will be explained shortly in this chapter. For the SWAN-Mud extension of SWAN, an additional dissipation term is introduced: Dissipation by the (fluid) mud layer. This will be explained more elaborated in the next chapter.

Bottom friction is induced by the orbital motion of waves that extends to the bottom of the shore, a sandbank, or reef. Wave energy is redistributed by scattering and compression of this orbital motion, and waves dissipate their energy. This is very elaborated explained by Shemdin et al. (1978). Multiple models are included in the SWAN model to define the bottom friction accurately. Included is JONSWAP (Hasselmann et al., 1973), which is an empirical model, an eddy-viscosity model of Madsen et al. (1988), and last of all, a drag model of Collins (1972). Dissipation by bottom friction is expressed by a formulation from Bertotti and Cavaleri (1994) with Equation A.2. C_b is the bottom friction coefficient, which depends on the bottom orbital motion.

$$S_{ds,b} = -C_b \frac{\sigma^2}{g^2 sinh^2 kd} E(\sigma,\theta) \tag{A.2}$$

This bottom friction becomes dominant when the waves reach the shore and start to shoal. After the shoaling, the waves start to break, and wave energy dissipates because of depth-induced wave breaking. This is included in the source/sink term as S_{br}. The standard formulation of Battjes and Janssen (1978) is included in the SWAN. This formula is given in Equation A.3 and includes a term for a maximum wave height per depth and a mean frequency. In SWAN, a depth induced breaker fraction (Q_h) is determined (Eldeberky and Battjes, 1995). H_m is the maximum wave height, given in Equation A.4, which is a modified Miche expression (Battjes and Janssen, 1978).

$$D_{tot} = -\frac{1}{4}\alpha_{BJ} Q_h \bar{f} {H_m}^2 \tag{A.3}$$

$$H_m = 0.88 k_p^{-1} \, tanh\left(\gamma_{BJ} k_p d / 0.88\right) \tag{A.4}$$

Non-linear wave-wave interactions were discovered in the 1960s by Philip (1960) and Hasselman(1960, 1962). These interactions include quadruplets, which are between four waves, and triads, the interaction between three different waves. These two processes are most important in deep and intermediate waters, where waves exchange and redistribute energy over the spectrum. Deepwater quadruplets transfer wave energy from the spectral peak to the higher frequencies as they "flatten the curve". The triads transfer energy from the lower to higher frequencies in shallow water, leading to higher harmonics (Eldeberky, 1996)).

Whitecapping is included in the source/sink formula as S_{wc}. Whitecapping is the process where waves collapse when they grow too steep for the wave to maintain itself. This process depends on the wind as the growth of the waves is wind-driven (Van der Westhuysen et al., 2007). This whitecapping term is thus related to the wind growth term and thus is wind indirectly not only a source for the energy balance but also a sink. Van der Westhuysen et al. (2010) states that whitecapping is the dominant dissipation term in deep waters, as was analyzed from multiple SWAN experiments. The bottom friction becomes more dominant over the intermediate depths, and whitecapping becomes of less influence. This is all diminished by the magnitude of the depth-induced wave breaking, the most dominant energy sink for the smaller depths (De Waal, 2002; Bottema et al., 2003; Holthuijsen et al., 2008). This is observed for sandy coasts, while SWAN's application is limited without SWAN-Mud for mud coasts. More explanation of all dissipation terms included in SWAN can be found in the SWAN process description (SWAN, 2009) and SWAN manual (SWAN, 2011).

Appendix B

Explanation of the optimal mud layer thickness and relation to the Stokes boundary layer.

In essence is the layer that is described by De Wit(1995) as the Stokes boundary layer is not accurate. Because the Stokes boundary layer is related to the viscosity of the water, while the layer described in Gade(1958) the viscosity of the mud layer includes instead. (De Swart, personal communications, 2022)

The aim of this section is to provide an explanation for the fact that dissipation of wave energy by mud reaches a maximum when the mud layer has a thickness H_{mud} that is of order $\sqrt{\frac{2\nu_m}{\omega}}$). Following Gade58, the ratio $H_{mud}/\sqrt{\frac{2\nu_m}{\omega}}$ is called the effective Reynolds number of the (wave) disturbance. The reason for this naming will be given at the end of this Appendix. The optimum in imaginary wavenumber is found when the effective Reynolds number is slightly larger than 1 as is given in Figure B.1. In this figure by Gade(1958) is the imagery wavenumber given as function of the effective Reynolds number.

The layer described by Gade is an effective Reynolds number: $H_{mud}/\sqrt{\frac{2\nu_m}{\omega}} \sim 1$

The dissipation is defined by $D \equiv \overline{p_1 w_1}$ at the interface, while 1 indicates the waterlayer. The kinematic condition at the water surface is described as: $w_1 = \mathrm{d}\xi/\mathrm{d}t$ at the same time is: $p_1 \sim \eta$ as it is the pressure at the free surface. Meanwhile when there would be no mud in the column, a progressive wave can be described with $p \sim \eta$.

When the mud layer and the waterlayer are coupled, a small phase difference is found between p_1 and η which is described by Gade (1958) as ϕ.

From this it follows that the dissipation is

$$D \sim \overline{\eta \frac{d\xi}{dt}}$$

Now in order to have $D \neq 0$, a phase difference needs to be present between η and $\frac{\mathrm{d}\xi}{\mathrm{dt}}$, which is described by Gade as $\phi' - \frac{\pi}{2}$

Now assume $H_{mud} >> \sqrt{\frac{2\nu}{\omega}}$.

The two layers are very strongly coupled, meaning that the phase difference ϕ between the interface and the free surface reaches zero. Consequently η and $\frac{d\xi}{dt}$ will tend towards 90 degrees out of phase, resulting in $D \to 0$.

It is interesting here that the amplitude at the interface is of the order of the amplitude of the free surface, but there is no dissipation. In terms of Reynolds number will the layer behave turbulent.

Now consider $H_{mud} \ll \sqrt{\frac{2\nu}{\omega}}$.

In this case the inertia in the mud layer is negligible with respect to the viscous terms. As a consequence, ξ is 90 degrees out of phase with η, so that η and $\frac{d\xi}{dt}$ are in phase. However, even in this case, we find that $D \to 0$, since the amplitude of ξ approaches zero. The reason is that the mud layer is so thin that the divergences in mass transport approach zero, so there is no possibility of free surface variations. In terms of Reynolds number will the mud layer behave laminar

Therefore, the most significant dissipation is to be expected when $H_{\mathrm{mud}} \sim \sqrt{\frac{2\nu}{\omega}}$.

The dynamics in the mud layer will be governed by the ratio of inertial and viscous terms. This ratio is an effective Reynolds number, and its expression is

$$Re_{eff} = \frac{\frac{\partial u_2}{\partial t}}{\nu_{mud}\frac{\partial^2 u_2}{\partial z^2}} \to \frac{u_2\omega}{\nu_{mud}\frac{u_2}{H_{mud}^2}} = \frac{H_{mud}^2}{\frac{\nu}{\omega}}$$

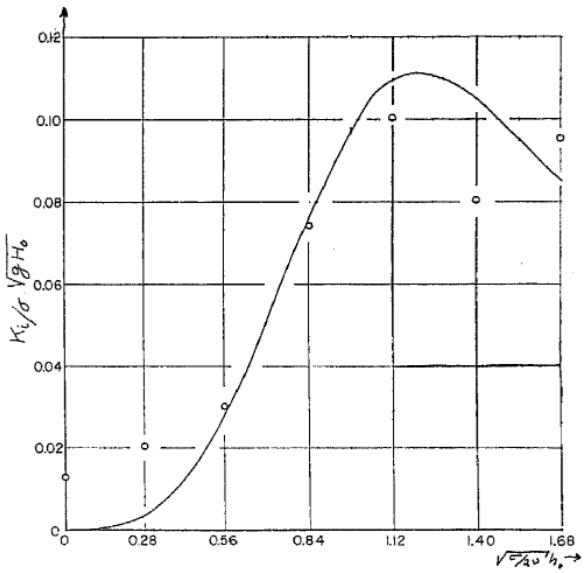

Figure 4. Imaginary part of the dimensionless parameter $k/\sigma\sqrt{gH_0}$ versus the Reynolds number $\sqrt{\sigma/2\nu}\,h_0$. The circled points are results from a separate wave tank experiment.

Figure B.1: Showing a figure from Gade(1958) with the relation between the Reynolds number and the rate of dissipation

Appendix C

This appendix contains two experiments, one is the reproduction of the DeWit method in SWAN-Mud and the Analytical solution of DeWit made in SWAN-Mud.

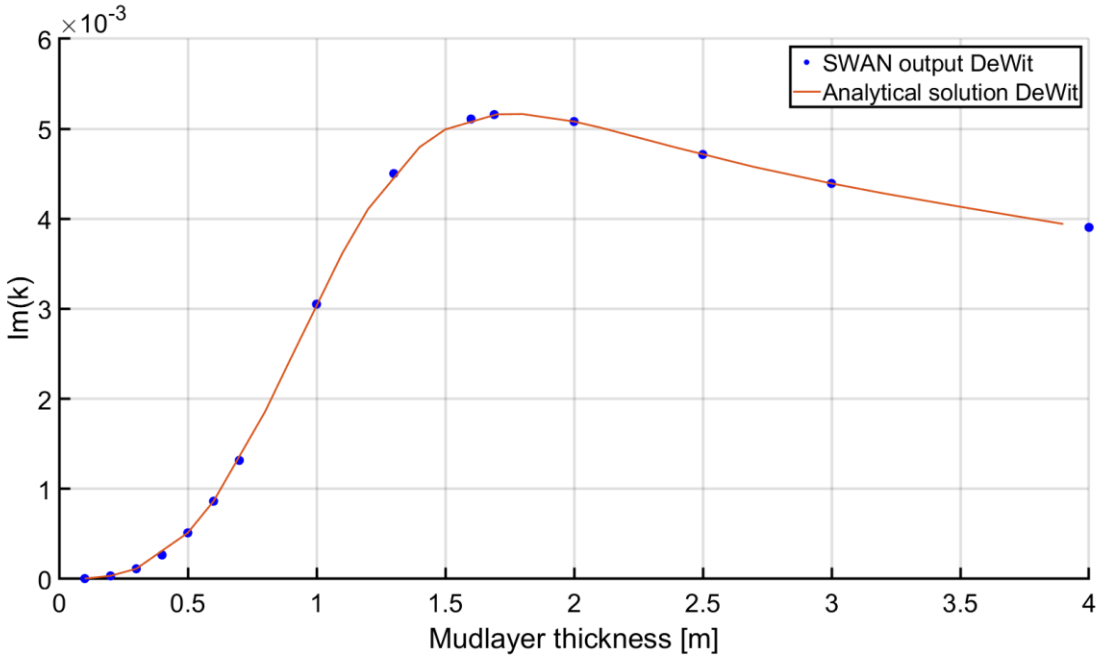

Figure C.1: The analytical solution done made in Wolfram Mathematica in orange to compare the output of the SWAN-Mud method by DeWit, the correlation is obvious.

Appendix D

Wind and wave roses for Suriname from ERA-5

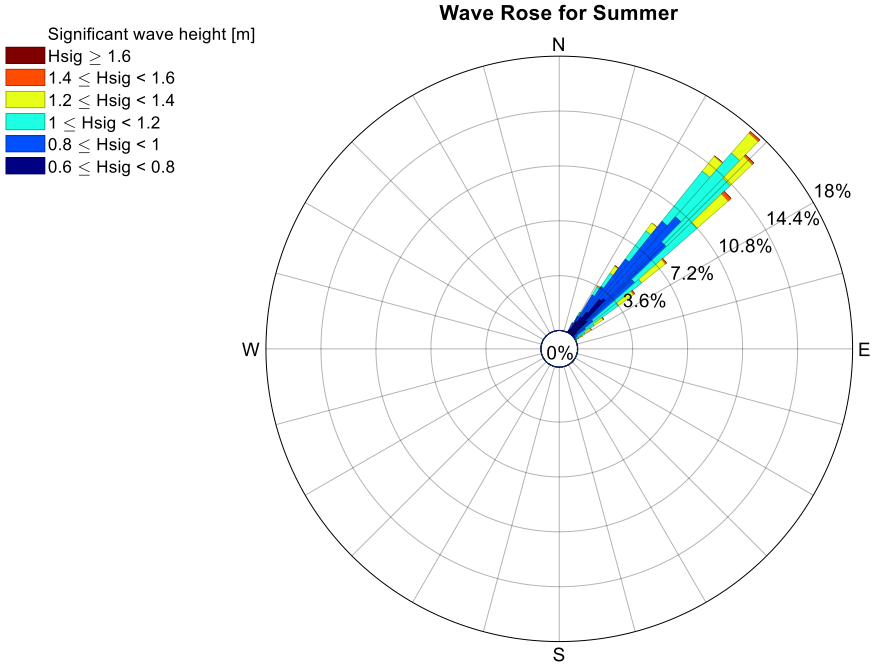

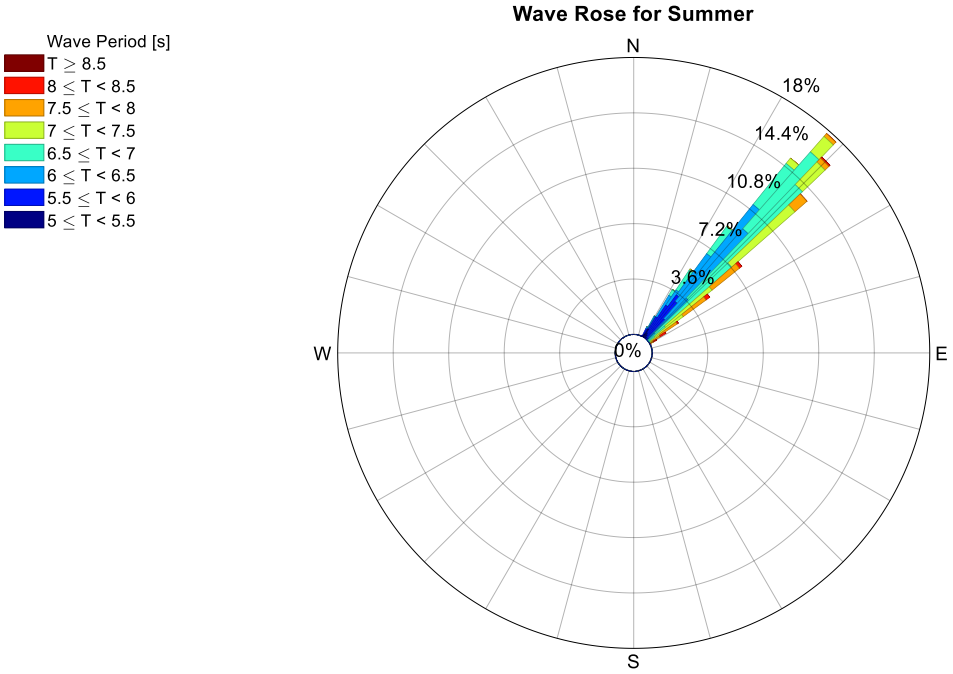

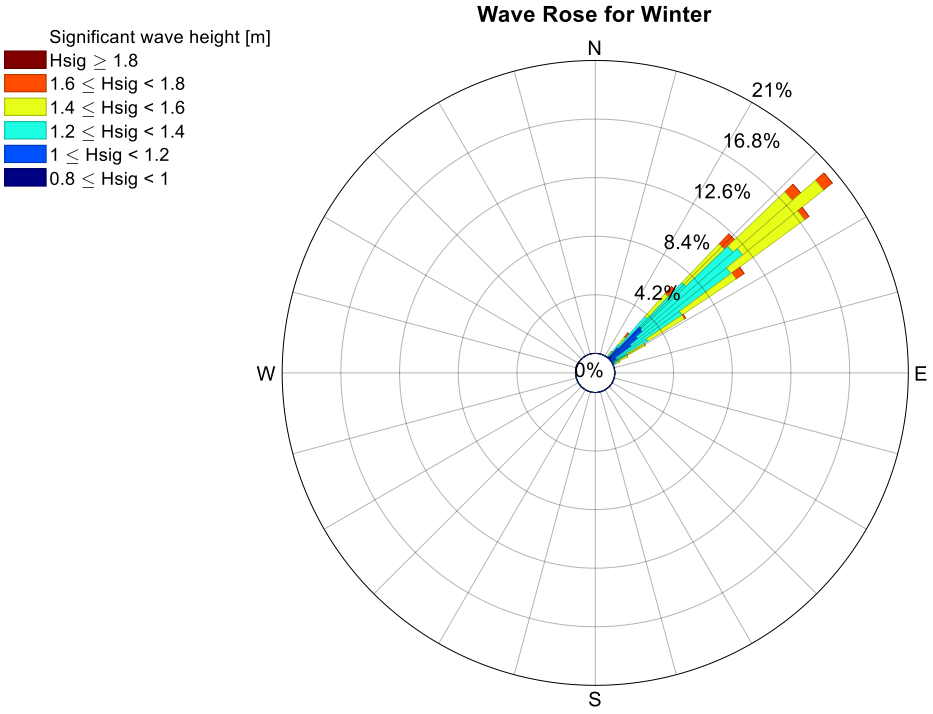
Wave Rose for Winter
Significant wave height [m]
Hsig ≥ 1.8
1.6 ≤ Hsig < 1.8
1.4 ≤ Hsig < 1.6
1.2 ≤ Hsig < 1.4
1 ≤ Hsig < 1.2
0.8 ≤ Hsig < 1
N
21%
16.8%
12.6%
8.4%
4.2%
W
E
0%
S

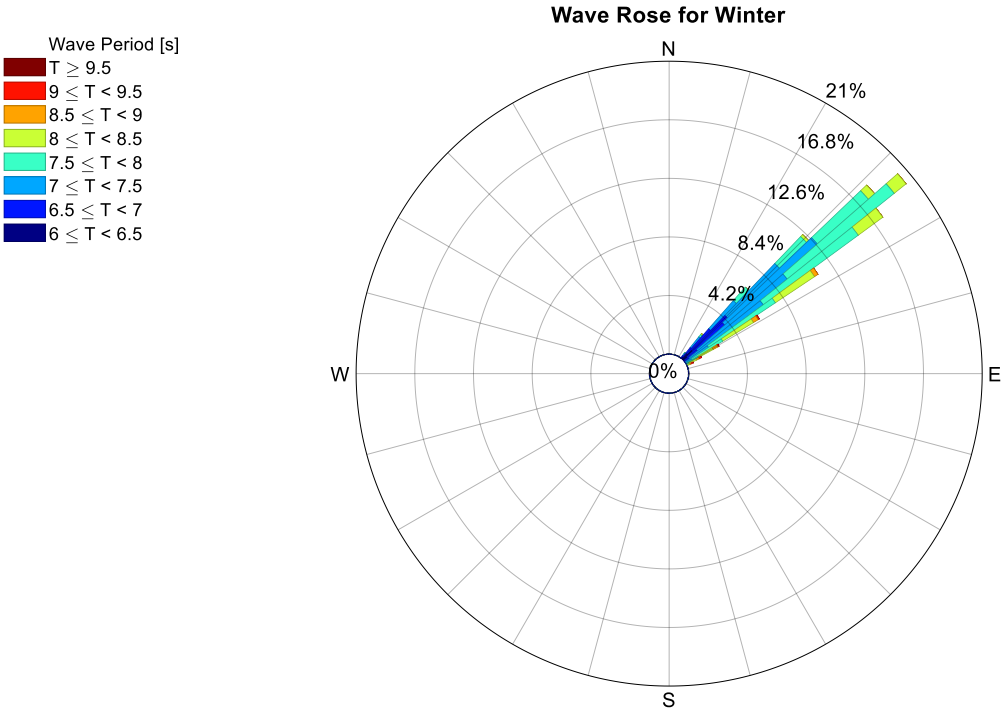
Wave Rose for Winter
Wave Period [s]
T ≥ 9.5
9 ≤ T < 9.5
8.5 ≤ T < 9
8 ≤ T < 8.5
7.5 ≤ T < 8
7 ≤ T < 7.5
6.5 ≤ T < 7
6 ≤ T < 6.5
N
21%
16.8%
12.6%
8.4%
4.2%
W
E
0%
S

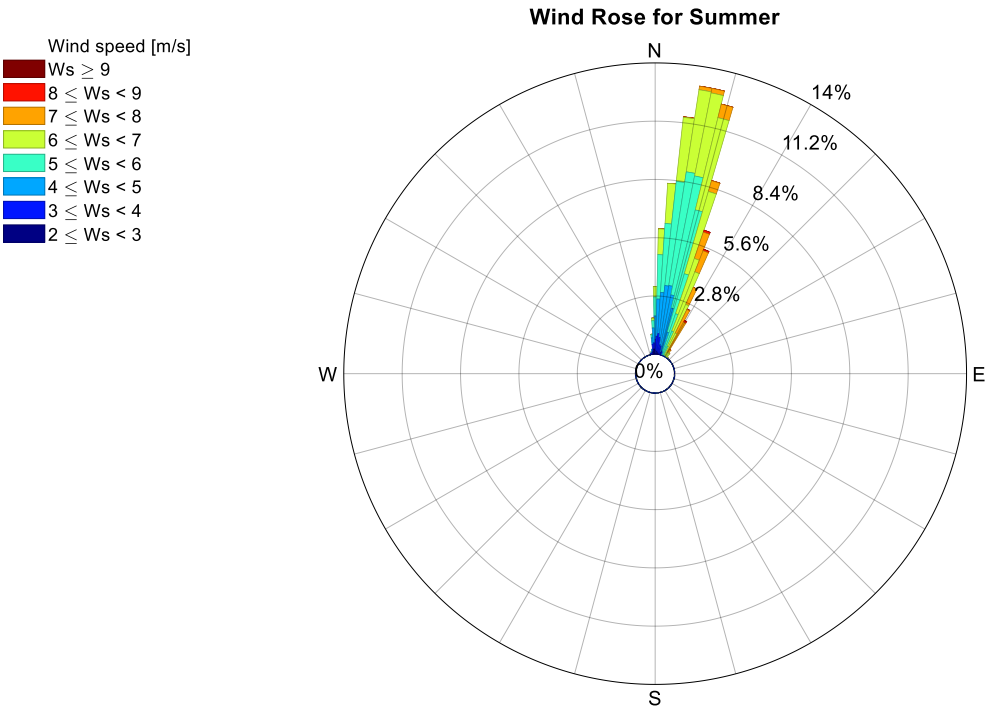
Wind Rose for Summer
Wind speed [m/s]
Ws ≥ 9
8 ≤ Ws < 9
7 ≤ Ws < 8
6 ≤ Ws < 7
5 ≤ Ws < 6
4 ≤ Ws < 5
3 ≤ Ws < 4
2 ≤ Ws < 3
N
E
S
W
14%
11.2%
8.4%
5.6%
2.8%
0%

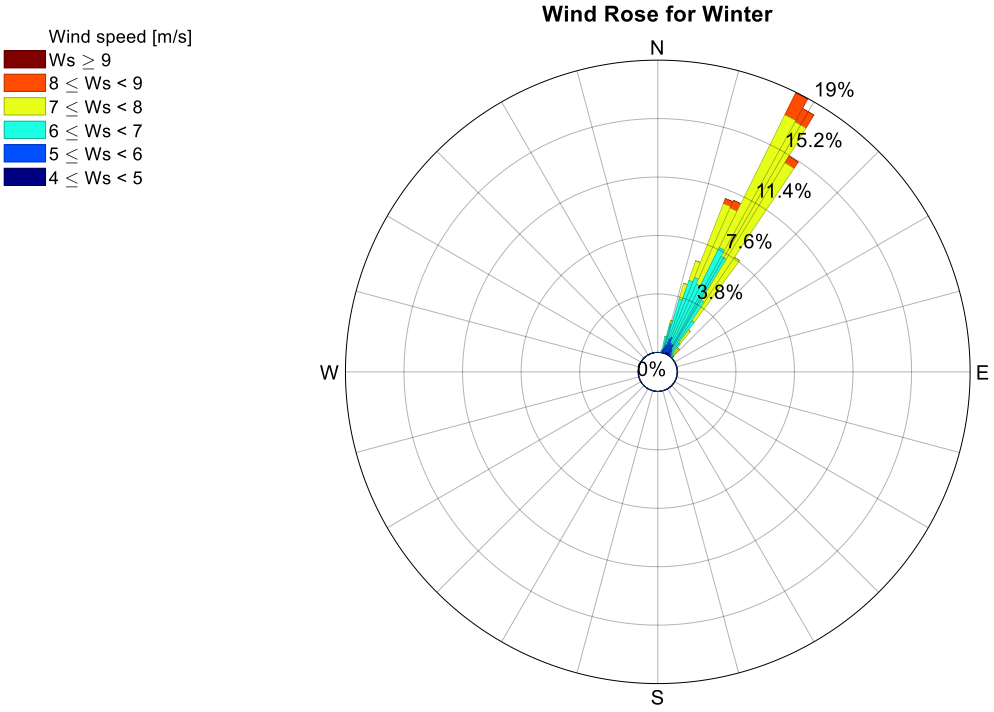
Wind Rose for Winter
Wind speed [m/s]
Ws ≥ 9
8 ≤ Ws < 9
7 ≤ Ws < 8
6 ≤ Ws < 7
5 ≤ Ws < 6
4 ≤ Ws < 5
N
E
S
W
19%
15.2%
11.4%
7.6%
3.8%
0%

Appendix E

Difference in bathymetry for dissipation

The “old” scenarios are the scenarios where the mud is implemented as a mudpatch while the “new” have a mudbank implemented. The degree is the angle of incidence for the waves in a 2D experiment. The difference in the height of the peak in the dissipation is not very large. A difference between the two implementations can be found further over the mudbank where the two deviates. This is also similar in the wave heights of the different experiments.

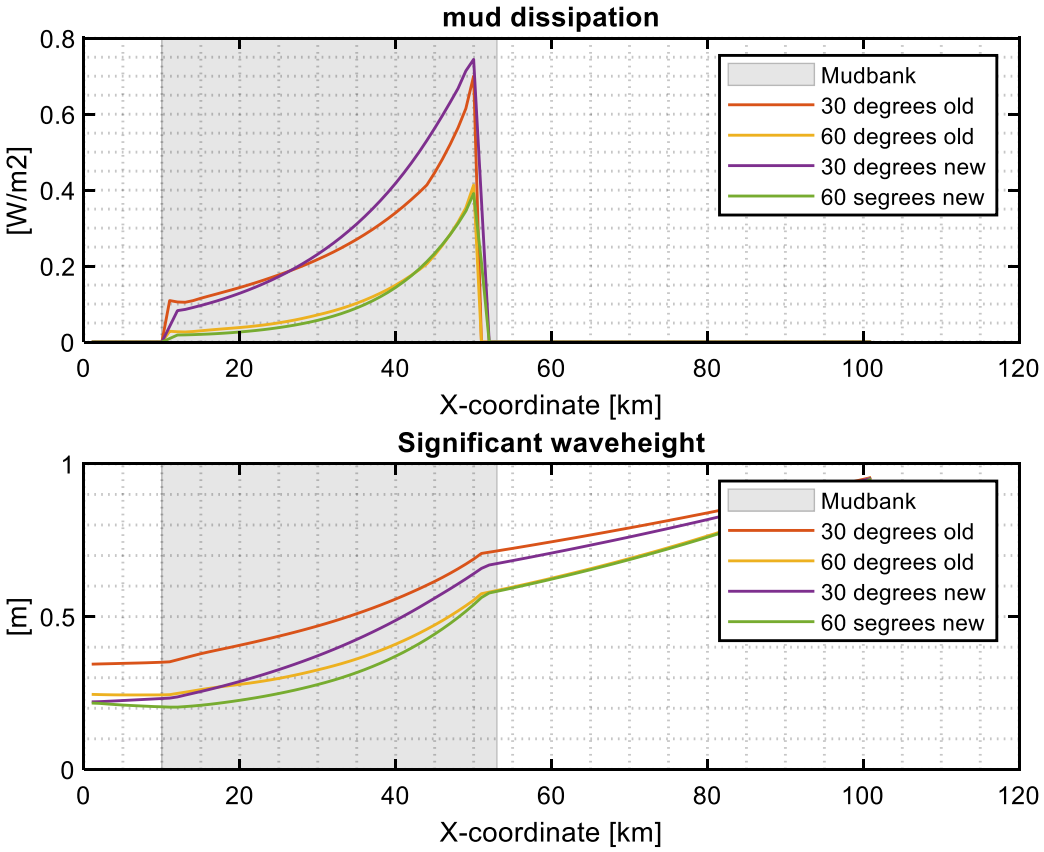

Figure E.1: Difference in Mud dissipation (top panel) and wave height (bottom panel) between the mudbank implemented as mudpatch (old) and as mudbank (new). The grey area marks the beginning of the mud.

Appendix F

Relative change between mud and no mud scenarios

The relative change over the perpendicular transect is given in Figure E.1 for all scenarios. This difference is between the situation with and without mud. A positive change means the output is higher for the situation with mud (for example, the dissipation). When negative, it means it is lower for the situation with mud (for example, wave height or period). Most important is the difference between the different scenarios. The relative change in significant wave height is highest for the highest energetic waves, decreasing until summer. Here the drop is most significant for the intermediate situations with the largest wave height, followed by scenarios with the larger period. This is similar for the wave period, but the differences are substantial between the winter storm and the summer when reaching further on the mud. The total dissipation does not show many differences in the peak between the different scenarios. Further, the summer has the smallest value on the mud, and the winter storm the largest. However, this difference is not very large.

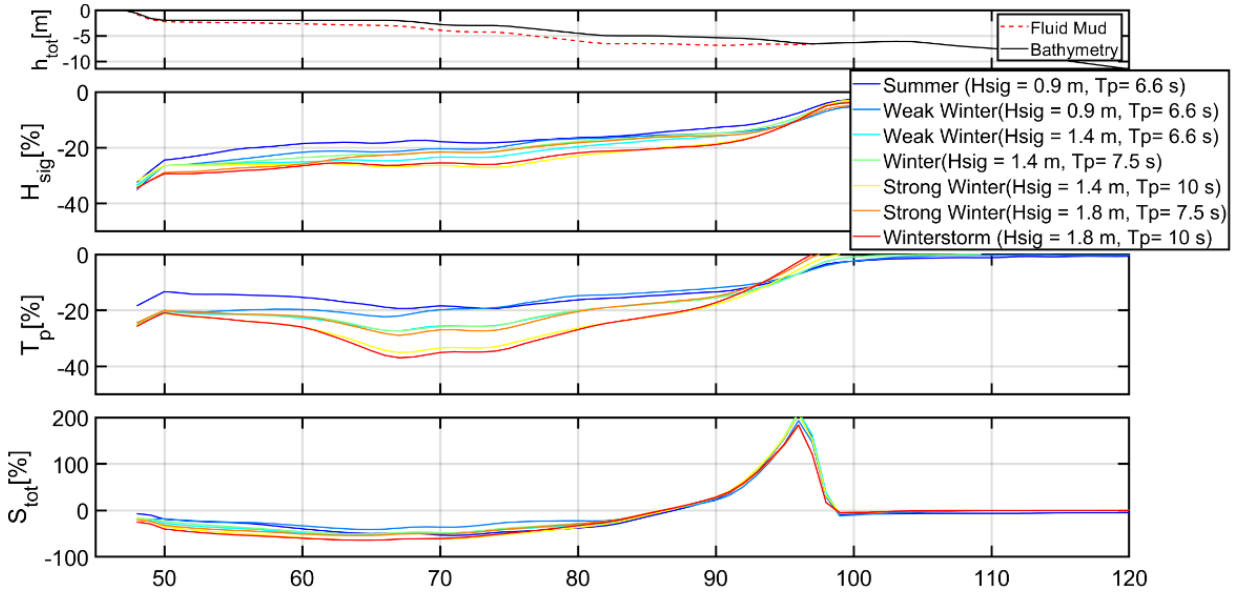

Figure F.1: The relative change for the scenarios with and without mud. All the scenarios discussed differ only in one parameter, these are given in the legend. The direction is for the summer is: for the other scenarios it is: The wind is coming from 78 degrees with 5.5 m/s for the summer, 60 degrees with 7.0 m/s for all winter scenarios and 60 degrees and 7.0 m/s for the winter storm.